

October 25, 2018

Hard probes of short-range nucleon-nucleon correlations

J. Arrington^a, D. W. Higinbotham^b, G. Rosner^c, M. Sargsian^d

^a*Physics Division, Argonne National Lab, Argonne, IL 60649*

^b*Thomas Jefferson National Accelerator Facility, Newport News, VA 23606*

^c*University of Glasgow, Glasgow, G12 8QQ, Scotland, UK*

^d*Florida International University, Miami, FL 33199*

Abstract

One of the primary goals of nuclear physics is providing a complete description of the structure of atomic nuclei. While mean-field calculations provide detailed information on the nuclear shell structure for a wide range of nuclei, they do not capture the complete structure of nuclei, in particular the impact of small, dense structures in nuclei. The strong, short-range component of the nucleon-nucleon potential yields hard interactions between nucleons which are close together, generating a high-momentum tail to the nucleon momentum distribution, with momenta well in excess of the Fermi momentum. This high-momentum component of the nuclear wave-function is one of the most poorly understood parts of nuclear structure.

Utilizing high-energy probes, we can isolate scattering from high-momentum nucleons, and use these measurements to examine the structure and impact of short-range nucleon-nucleon correlations. Over the last decade we have moved from looking for evidence of such short-range structures to mapping out their strength in nuclei and examining their isospin structure. This has been made possible by high-luminosity and high-energy accelerators, coupled with an improved understanding of the reaction mechanism issues involved in studying these structures. We review the general issues related to short-range correlations, survey recent experiments aimed at probing these short-range structures, and lay out future possibilities to further these studies.

Key words: Nucleon-Nucleon Correlations, Tensor Correlations, Short-Range Correlations

1. Introduction

Despite a fairly detailed understanding of the rich structure of the nucleon-nucleon strong interaction, its implications for the dynamics of atomic nuclei are not yet fully understood. Bulk properties of medium and heavy nuclei follow from the rather general characteristics of nuclear forces such as nucleons being fermions and nuclear forces being short-range and having a repulsive core.

Because of these characteristics, nuclei demonstrate degeneracy of the Fermi system with clear identification of the Fermi momentum, k_{Fermi} , for quantities such as momentum or kinetic energy distributions of bound nucleons [1]. Refinements of such approximations within the framework of Bethe-Goldstone [2] or Nuclear Shell [3] models require, but are not very sensitive to, the short-range properties of the nucleon–nucleon (NN) interaction. Therefore, these models provide limited ability to investigate the structure of nuclear matter beyond saturation density, where one approaches the expected transition from nucleonic to quark-gluon degrees of freedom. As such, the experimental evidence for short-range correlations within the context of these models is rather indirect.

Simple shell model calculations make predictions for the momentum distribution and occupation number (or spectroscopic factor) for each nuclear shell. Early measurements found that while such mean-field calculations provide extremely successful descriptions of the energy and momentum distribution of nucleons in these shells, they do not correctly predict the occupancy of the shells. In the early 70s, with the advent of high-quality, medium-energy $A(e,e'p)X$ experiments on various nuclei, several observations were made which suggested significant strength of the nuclear spectral function beyond the single shell excitations. For example, the apparent violation of the Koltun sum rule [4] in proton knock-out experiments [5] was clearly attributed to the high energy excitation part of the nuclear spectral function [6] while no correlation effects were found in the momentum distributions corresponding to the fixed nuclear shells [7]. More comprehensive measurements of the proton knock-out reactions [8, 9] show that the spectroscopic factor, basically the ratio of the observed strength within a given shell to the expected strength, is less than one. The observed strength is typically $\sim 30\text{--}40\%$ below the shell-model expectation for measurements in many nuclei and looking at several nuclear shells. Even the most advanced Hartree-Fock calculations, which include long-range correlations, significantly overestimate the strength observed in the nuclear shells. A very plausible explanation for this discrepancy is the presence of strong short-range NN interactions. The repulsive core and tensor components of the NN force yield hard interactions that can excite nucleons outside of the low-lying shells. Thus, the nucleons are removed from the relatively low excitations associated with the nuclear shells and moved to higher energies and momenta, where there is little or no strength in the mean-field calculations.

To understand why the independent particle shell model can yield detailed and precise predictions for the nucleon distributions yet fail to predict the absolute strengths, one needs only to consider modern nucleon momentum distributions. At lower nucleon momenta, the distributions shown in Fig. 1 clearly show the characteristics of a degenerate Fermi system with broad momentum distribution, falling off rapidly at momenta approaching k_{Fermi} . In stark contrast to this behavior, the high-momentum tail has a much less rapid falloff which is similar for all nuclei from deuterium to nuclear matter. This universality of the high momentum tails strongly argues against the role of the collective or mean-field effects. Indeed, the mean-field calculations dramatically underestimate the strength at $k > k_{Fermi}$, falling short by several orders of magnitude at high

momenta, as shown in Fig. 1. This universality of the high momentum tails can be easily understood if they are generated via the short-range part of the two-nucleon potential, and are thus independent of the shell model component of the momentum distribution.

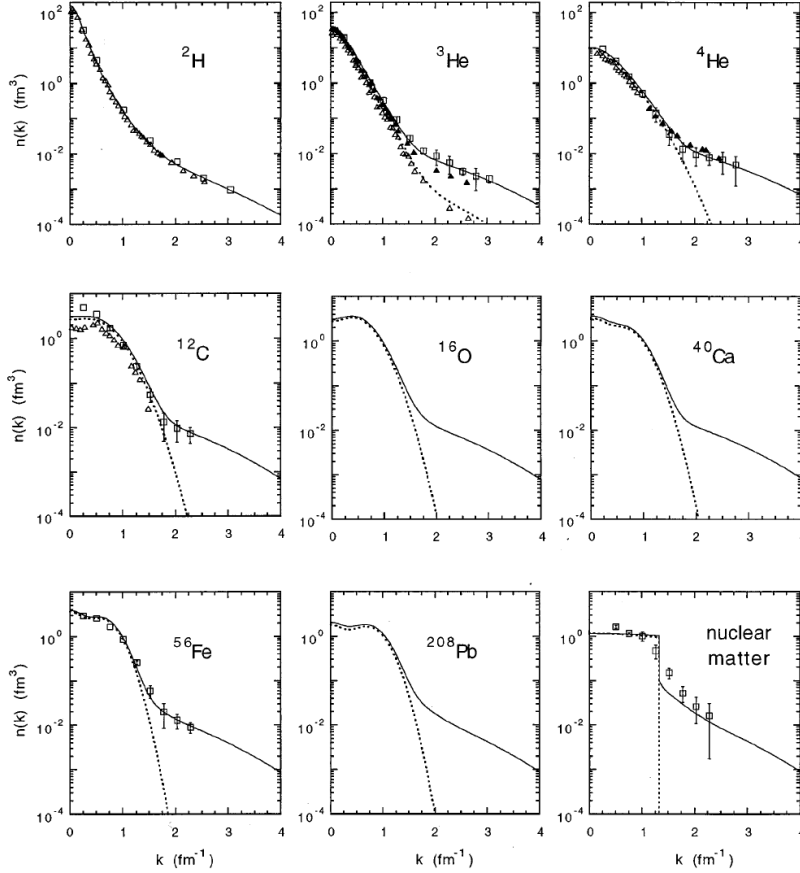


Figure 1: Nucleon momentum distributions $n(k)$ (solid lines) along with the momentum distribution for nucleons in an average potential (dotted lines) for various nuclei are shown. The deuteron distribution was calculated in [10] using the Paris potential [11]. Also shown are distributions for ${}^3\text{He}$ [12], ${}^4\text{He}$ [13], ${}^{12}\text{C}$ [14], ${}^{16}\text{O}$ [15], ${}^{40}\text{Ca}$ [14], ${}^{56}\text{Fe}$ [16], ${}^{208}\text{Pb}$ [17], and infinite nuclear matter [18]. The open squares represent the results obtained within the y -scaling analysis of inclusive data from Ref. [19] and the open and full triangles represent the values obtained from exclusive experiments on ${}^2\text{H}$ [20, 21], ${}^3\text{He}$ [22, 23, 24], ${}^4\text{He}$ [25, 26] and ${}^{12}\text{C}$ [27]. Figure reprinted with permission from Ref. [10]

Note that we often describe these two-body short-range correlations as excitations in the nucleus where two nucleons undergo a hard interaction and end up in a configuration with large relative momenta but a small total momentum. However, these are excitations relative to a theoretical mean-field ground state

of the nucleus are not related to any real excited states of the nucleus; they are a contribution to the true nuclear ground state. When trying to probe these configurations in high-energy reactions, the goal is to take a “snapshot” of the configuration of the nucleons, and so the SRCs are often described as static configurations, treating the nucleons as though they were simply an isolated pair of high-momentum nucleons, analogous to the high-momentum part of the deuteron momentum distribution. However, such configurations are components of the nuclear ground wave function, with these *virtual* excitations responsible for generating most of the high-momentum nucleons.

The above scenario naturally suggests that if the two-body NN interaction is responsible for the high-momentum tail of the nuclear momentum distribution, then one expects the shape of the distribution beyond the Fermi momentum to be essentially identical for all nuclei,

$$n_A(k) = a_2(A, Z) \cdot n_2(k) \quad \text{for } k > k_{Fermi} , \quad (1)$$

neglecting the small center-of-mass momentum of the SRC. In this case, $n_2(k)$ represents the momentum distribution generated by the two-body interaction and $a_2(A, Z)$ yields the relative strength in the high-momentum tails which is related to the probability of finding these high-momentum two-nucleon configurations, or two-nucleon short-range correlations (2N SRCs) in the nucleus relative to the two-nucleon system.

In this scenario, the NN SRC represents a pair of nucleons where each nucleon has a large momentum (exceeding k_{Fermi}) but the total momentum of the pair is very small, i.e. a pair of nucleons with large, back-to-back momenta. In the case of an iso-singlet SRC, one expects the high-momentum part of the distribution to look much like the high-momentum tails in the deuteron, which is an iso-singlet nucleon pair with zero total momentum.

The short-range NN attraction is dominated by the tensor interaction, which yields high momentum iso-singlet $(np)_{I=0}$ pairs but does not contribute to the iso-triplet channel $(pp, nn, np)_{I=1}$. Therefore, one expects the two-body distribution to be identical to the deuteron distribution, $n_2(k) = n_D(k)$, and the ratio of scattering cross sections between a heavy nucleus A and the deuteron to yield $a_2(A, Z)$. The value of a_2 can then be interpreted as the relative probability of finding NN SRCs in the nucleus A compared to the deuteron.

This simple picture should break down at momenta where the central repulsive core of the NN potential dominates, as the SRCs will no longer be dominated by deuteron-like configurations. Additionally, as one goes to extremely high momenta, inclusion of three-nucleon configurations may become important. At even higher momenta, where the nucleon kinetic energy is comparable with the excitation energies of nucleon, non-nucleonic degrees of freedom may also need to be taken into account.

Extensive theoretical investigations of the impact of nucleon correlations in the structure of nuclei have been performed using a variety of methods. See, for example the review of Ref. [28] as well as several more recent works [29, 30, 31, 32, 33, 34, 35]. Detailed calculations employing the Green’s function Monte

Carlo method using various 2N and 3N interactions have been used to study the structure and impact of correlations in light nuclei [36, 37, 38].

To probe the high momentum tail experimentally one needs to deal with several issues which follow mainly from the fact that the momentum distribution of the nucleon is not an experimental observable. As a result, one needs to identify the appropriate observables which are most relevant for characterization of bound nucleons in the high momentum tail.

The second problem one faces is finding a probe that is able to distinguish genuine j -Nucleon ($j = 2, 3, \dots$) SRCs from j -body processes involving long range interactions. The most efficient solution of this problem is to study the SRC using a probe with large momentum transfer, q , and energy transfer, q_0 . Most of these measurements utilize single nucleon knock-out reactions, so one must choose kinematics which minimize contributions from more inelastic scattering processes. The optimal approach depends on the reaction mechanism, and the kinematic requirements are detailed in Section 4.

Prior to the high-energy experiments reviewed herein, the effects of short-range and tensor correlations were seen in valence knock-out experiments where, as mentioned above, the strength of the $A(e, e'p)(A-1)$ cross sections is over-predicted by independent particle models by 30-40% [8]. Also, experiments which probed the continuum of the $A(e, e'p)$ reaction found peaks in the missing momentum spectra [24, 26]. The most straightforward interpretation of those peaks is that a large fraction of the continuum strength arises from the breaking of an initial-state correlated pair with large relative and small center-of-mass momenta [8]. Such an interpretation is consistent with calculations that include nucleon-nucleon short-range correlations such as Muther and Dickhoff [39].

These initial indications of the importance of short-range correlations, missing strength relative to mean-field expectations and peaks in the missing momentum distribution, did not cleanly isolate SRCs or provide direct information that could elucidate the structure of SRCs. High energy scattering experiments, aimed at isolating scattering from high-momentum nucleons, provide a more direct way to probe SRCs in nuclei. Over the last decade, several such high energy nucleon knock-out experiments were performed which provided significant advances in our understanding of short-range nucleon correlations in nuclei. In this work we review these experiments, emphasizing their impact on our understanding the dynamics of short-range correlations.

2. The Origin and the Features of Short-Range Correlations in Nuclei

Already in the 1950s, it was observed the nucleons in nuclei exhibit collective behavior in response to the absorption of specific probes such as real photons or pions. These effects were understood on the basis of the simple observation that a free nucleon cannot absorb a real photon below the pion production threshold and must couple to other nuclear constituents for photon absorption to take place. Based on the experimental fact that the real photon has a large absorption cross section on the iso-triplet pn system it was observed in Refs. [40, 41] that the photo-absorption cross section will scale as $L \frac{NZ}{A} \sigma_{\gamma d}$, where constant

L was called as Levinger factor and $\sigma_{\gamma D}$ represents the photon-deuteron absorption cross section. However this two-nucleon or “quasi-deuteron” regularity of the photo-absorption cross section was a property of the nuclear response rather than its ground state wave function. These “quasi-deuterons” will not be observed, for example, in scattering by virtual photons or by real photon above the pion-production threshold.

When we discuss short-range correlations in this work, we are referring to properties of the ground state wave function of the nucleus which should contribute to scattering by any probe with sufficiently high resolution power. The universality of nuclear momentum distributions discussed in the introduction defines the framework within which we define the short-range nucleon correlations in nuclei. The short-range correlations are baryonic configurations in nuclei which are defined by local properties of NN interaction rather than by the mean field nuclear properties that are generated by the superposition of the long-range parts of the NN potentials.

The sensitivity of SRCs to the properties of the NN interaction follows from the singularity theorem which states that if a two-body short-range potential behaves like $V_{NN}(k) \sim k^{-n}$, with $n > 1$ at large relative momenta, then the nuclear wave function of the nucleon with momentum $k^2 \gg 2M|\epsilon_B|$ is expressed through this potential in the following form:

$$\Psi_A(k_1, k_2, k_3, \dots, k_{A-1}) \sim \frac{V_{NN}(k_1)}{k_2^2} f(k_3, \dots, k_{A-1}), \quad (2)$$

where $\vec{k}_2 \approx -\vec{k}_1$ and $f(k_3, \dots, k_{A-1})$ is a smooth function of the momenta of spectator nucleons. Such a relation can be obtained both from Lipman-Schwinger equation [42] and its relativistic generalizations such as the Bethe-Salpeter and Weinberg equations [43, 44] using any Yukawa or exchange-type NN interaction. Eq. (2) defines certain key properties of SRCs as well as the conditions of their localization:

- (a) The momentum distribution of the nucleons in the correlated pair is directly related to the NN potential. It will therefore reflect the dynamical as well as spin/isospin structure of the NN interaction at short distances
- (b) The 2N SRCs are associated with finding two high-momentum nucleons in a nucleus with large relative momentum and a small total momentum, i.e. $\vec{k}_1 \approx -\vec{k}_2$.
- (c) Isolation of 2N SRCs in nuclei will require probing nucleon with momentum $k > k_{Fermi}$ as well as excitation energies $\sim k^2/(2M)$ which far exceed energies relevant to the nuclear shells.

In the momentum range $300 < k < 600$ MeV/c, where V_{NN} is dominated by the tensor interaction, 2N SRCs should dominantly be in an iso-singlet state ($I = 0$). Thus, one expects that the nuclear momentum distributions at $k > k_{Fermi}$ should be nearly identical to the deuteron ($I = 0$) distribution: $n_2(k) = n_D(k)$,

and the ratio of scattering cross sections between a heavy nucleus A and the deuteron should be related to the probability of finding NN SRCs in the nucleus A relative to the deuteron.

The dominance of the deuteron-like simple picture should break down at momenta where the central repulsive core of the NN potential dominates. This is expected to occur for $k > k_{max} \sim 800$ MeV/c - the characteristic momenta at which one expects that the isospin-independent repulsive core will dominate in the NN interaction.

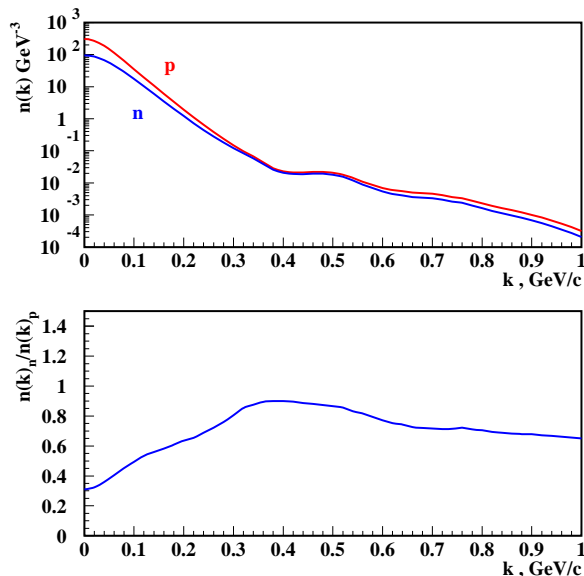


Figure 2: Proton and neutron momentum distributions in ${}^3\text{He}$ (top), and their ratio (bottom) as a function of momentum.

The above discussed features are seen in Fig. 2, in which momentum distribution of the proton and neutron are compared for ${}^3\text{He}$ nucleus. For $k \leq 300$ MeV/c, dominated by the long range NN interaction, the average n/p ratio is approximately equal to 0.5, which is simply the ${}^3\text{He}$ N/Z ratio. For $300 \text{ MeV}/c \lesssim k \lesssim 600 \text{ MeV}/c$, the n/p ratio is close to unity, as expected if the high-momentum distribution was generated exclusively by iso-singlet pairs. The n/p ratio diminishes at even larger momenta as the repulsive core of the NN central interaction begins to dominate. The calculation uses a realistic ${}^3\text{He}$ wave function calculated based on Argonne v18 (Av18) NN potential [45]. Other potentials yield nearly identical results at low momentum but show some differences for $k > 300$ MeV/c.

Condition (b) provides a qualitative definition for NN SRCs, in that they appear as a pair of high-momentum ($k > k_{Fermi}$), nearly back-to-back nucleons. This provides an important condition for experimental identification of 2N SRCs which should show a strong *angular correlation* between the constituents of the

2N SRCs. Such correlations can be explored in triple-coincidence experiments in which both nucleons from the SRC are detected, as discussed in detail in section 8.

Finally, condition (c) predicts new kind of correlation between the excitation energy of the residual nucleus and the internal momentum of the 2N SRCs. As a result, nuclear excitations relevant to short-range correlations significantly exceed the excitation energies characteristic to the nuclear shells.

Based above discussion of the characteristics of NN SRCs the following “definitions” will be used throughout the text:

- The measurements we present use the kinematics to isolate scattering from high-momentum nucleons based on the Plane-Wave Impulse Approximation (PWIA). If the value of the reconstructed initial nucleon momentum exceeds the characteristic Fermi momentum of the nucleus, then we infer that the nucleon is in a short-range two-nucleon configuration.
- The NN SRC is typically assumed to be *at rest*, meaning that the two nucleons have no total momentum relative to the center-of-mass of the nucleus.
- The residual nucleus is considered to be “highly excited” when the excitation energy of the residual ($A-1$) nucleus significantly exceeds the energies characteristic to the nuclear shells. This corresponds to the situation where the probe interacts with a high-momentum nucleon whose momentum is balanced by a single nucleon, as opposed to the case where the residual system is an ($A-1$) nucleus where the momentum is shared more evenly among the spectator nucleons.

While these are the basic assumptions used in high-energy studies of SRCs, we can test or go beyond these approximation in the analysis of such experiments. In the sections summarizing recent experimental results, we will typically begin with these simplifying approximations and then emphasize the ways in which we can go beyond this simplest picture of SRCs.

3. Main Approaches of Probing Short-Range Correlations in Nuclei

This section details the desired requirements for a complete and detailed investigation of SRCs in both light and heavy nuclei. Some of these are universal, applying to all hard probes, while others are reaction dependent.

- I. *Instantaneous interaction involving a nucleon from the SRC*: One should have a clear way of identifying events in which the high energy probe interacts with the correlated nucleon and instantaneously removes it from the SRC. The requirement that the process is instantaneous is necessary to be able to reliably infer information on the spectral functions or momentum distributions from the measured observables.

- II. *Struck and spectator nucleons from SRC are distinguishable:* The ability to distinguish which nucleon is knocked out by the virtual photon and which one is a spectator from the SRC is essential for mapping out the dynamical mechanism of pre-existing SRCs in the ground state wave function of the nucleus. For example, the measurement of the momentum and energy correlations between two detected nucleons will allow for the extraction of relative and center-of-mass momentum distribution of 2N SRCs, provided that one clearly can identify the spectator and struck nucleons in the reaction.
- III. *Separation of two- and three-nucleon SRCs:* SRC studies should allow unambiguous separation of signatures for two- and three- nucleon correlations. This will require specific reactions and kinematic conditions which enhance either two-, three- or many-nucleon correlations.
- IV. *Long-range two-nucleon effects are suppressed:* Because the momentum distribution is dominated by the low-momentum components, long-range two-step processes such as meson exchange currents (MECs) and intermediate state resonance contributions will significantly alter the SRC picture unless they are suppressed by kinematics or other dynamical conditions. Typically, this means operating at higher Q^2 values, to suppress final state interactions and meson exchange contributions, and at relatively low energy transfer or missing energy, to suppress inelastic or intermediate state resonance contributions.
- V. *Final state interaction effects are small or well understood:* The major problem in SRC studies is the final state interaction (FSI) effects between particles in the final state. Hadronic FSIs do not diminish with an increase of the transferred momentum and energy of the reaction, but do enter into the eikonal regime. The eikonal regime (or “regime of geometrical optics”) has several important characteristics which follow from the high energy and small angle scattering nature of the FSIs. One key consequence is the approximate conservation of the $p_- = E - p_z$ components of the four-momenta of scattered particles [46]. Because of this, one still can extract information about the high momentum component of the nuclear wave function, even in the presence of large FSI.

Another important property of the eikonal regime of FSIs comes from the fact that rescattering is localized in the direction almost transverse to the direction of the fast moving particle and that the distance the fast particle travels before rescattering decreases with increasing virtuality of the particle. As a result, deeply bound nucleons knocked out from the SRC propagate a short distance, comparable to the size of the SRC, before rescattering. This implies that the bulk of the rescattering takes place between the nucleons in the SRC [44], and thus a very large component of the FSI is also dependent only on the structure of the two-body system, and therefore independent of the nucleus in which the SRC appears.

This plays an critical role in preserving important kinematical correlations between struck and spectator nucleons, even when FSI effects are sizable.

- VI. *Improved understanding of relativistic and bound-nucleon effects:* Nucleons in SRCs are characterized by large momenta and binding energies. This increases significantly the effects due to the relativistic motion of the nucleon as well as possible modification of the nucleon structure due to the large binding effects. The comprehensive exploration of the dynamics of SRCs requires an understanding of the reaction dynamics and nucleon modification effects of deeply bound nucleon in the short-range correlations. Thus the program of SRC studies should proceed in parallel with studies of reaction dynamics and nuclear medium modification effects.
- VII. *Detailed studies of few-body nuclei:* Due to a certain degree of factorization between the short and long range interactions in nuclei (similar to Eq. (1)), the above discussed reaction dynamics, relativistic and binding effects can be studied using few nucleon systems: ^2H , ^3He and ^3H . Therefore, systematic studies of the lightest nuclei should be an integral part of the program to understand SRCs.
- VIII. *Comparisons of different SRC observables and reactions:* SRCs can be studied in electroproduction reactions with different degrees of complexity, including inclusive $A(e,e')$, semi-inclusive $A(e,e'N)$, and triple-coincidence $A(e,e'NN)$ reactions for both polarized and unpolarized processes. In each case, one deals with specific observables relevant to the SRC dynamics. The assumed universality of the short-range interaction implies that there should be clear consistency and relationship among all observables measured in these reactions. This helps to demonstrate a reliable separation of initial-state SRC structure and reaction-dependent corrections related to meson exchange and resonance contributions in the scattering.

4. SRC Kinematics

4.1. General kinematical considerations for SRC Studies

The above conditions will drive the restrictions on momentum and energy transfers in reactions aimed at probing SRCs. While the exact kinematic requirements depend on the reaction, one can make some general estimates for the different classes of reactions. Condition (I), the desire to have a nucleon from the SRC removed instantaneously, can be achieved if the energy and momentum transfer scales are much larger than the excitation energy scale characteristic to the nuclei in general and the SRC in particular. This can be achieved by requiring [44, 43]

$$q_0 \gg V_{NN}, \quad q \gg m_N/c, \quad (3)$$

where V_{NN} is the characteristic potential of the NN interaction. In this case the residual system after the nucleon is removed from the SRC can be considered

intact at the time of the interaction and therefore a spectral function can be introduced for the reaction which will reflect the direct properties of SRCs.

Condition (IV), the suppression of long-range two-body interactions is generally achieved by requiring

$$Q^2 \gg m_{meson}^2 . \quad (4)$$

In some cases, such as for reactions close to the deuteron threshold or in elastic scattering [47], exchange currents are expected to be important even at large Q^2 values. In principle, they are also important in hard break-up reactions, although they are more naturally described by the quark-exchange diagrams [48] due to large masses produced in the intermediate states. However, it is rather well established that for the reactions we will discuss in the context of SRC studies, meson exchange currents significantly diminish for $Q^2 \gg m_{meson}^2$. Above $Q^2 = 1 \text{ GeV}^2$, long-range meson exchange current contributions are suppressed with respect to the direct production from SRC by an additional factor of Q^{-4} [46, 49], and are already a small correction in the kinematics relevant to SRC studies at $Q^2 \geq 1 \text{ GeV}^2$ [46, 49].

Contributions from intermediate state resonances are still important at these Q^2 values, especially contributions from Δ -isobars which, due to the large magnetic transition form-factor, have sizable contribution in electroproduction reactions close to the pion threshold for $Q^2 \leq 4 \text{ GeV}^2$ [50, 51]. For moderate momentum transfers ($1 \text{ GeV}^2 \leq Q^2 \leq 4 \text{ GeV}^2$), where the $\gamma N \rightarrow \Delta$ transition is comparable with $\gamma N \rightarrow N$, a suppression of these contributions can be achieved by working at low energy transfer, thus keeping away from the inelastic threshold. A convenient parameter for identifying the closeness to the threshold is the Bjorken variable $x = \frac{Q^2}{2m_N q_0}$, where we use the nucleon mass in the denominator, even though we are scattering from a heavier target. This leads to a kinematically allowed region of $0 < x < M_A/M_N$, rather than $0 < x_A < 1$, where x_A is defined using the mass of the nucleus. Defined this way, quasi-elastic scattering from low-momentum nucleons corresponds to $x \approx 1$ for all nuclei, while inelastic processes (with larger values of q_0) occur at smaller values of x . Choosing to probe high-momentum nucleons on the $x > 1$ side of the quasi-elastic peak yields a significant suppression of IC contributions.

Figure 3 demonstrates how requiring $x > 1$ and Q^2 above 1–2 GeV^2 allows one to select large internal momenta associated with the two-nucleon correlations. For $p_{min} > k_{Fermi}$, there is almost no contribution from the mean-field part of the nucleon momentum distribution in the PWIA, allowing for isolation of high-momentum nucleons associated with SRCs. Note that p_{min} corresponds to an initial nucleon with momentum parallel to the momentum transfer and assumes no excitation of the residual (A-1) nucleus. Accounting for transverse momentum and excitation of the spectator nucleus, one expects that the true momenta probed will be well above p_{min} . The requirements that the scattering selects high-momentum nucleons and suppresses MEC and IC contributions, together with Eq. (3), set the necessary kinematic conditions: an energy transfer of at least 0.5 GeV, and Q^2 of 1–2 GeV^2 or higher, while working at $x \gtrsim 1$ to minimize intermediate resonance contributions.

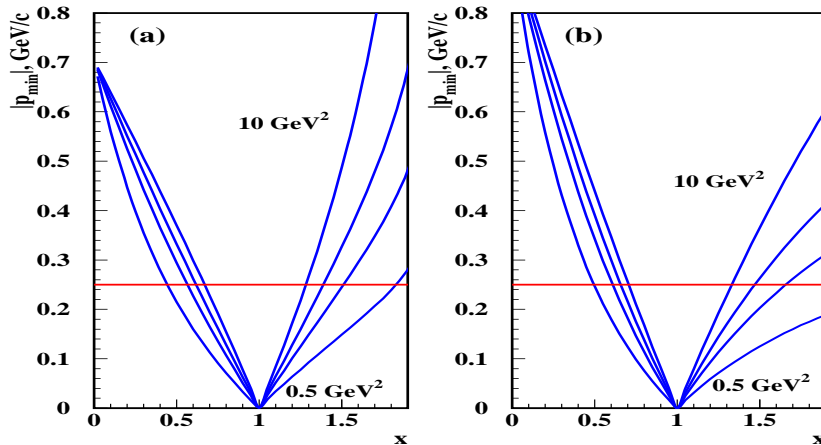


Figure 3: The minimum momentum for scattering from a nucleon in deuterium (left) and gold (right) as a function of x and Q^2 for quasi-elastic $\gamma + 2N \rightarrow N + N$ scattering for Q^2 values of 0.5, 1.5, 3, and 10 GeV^2 . For heavy nuclei, the minimum momentum for a given x and Q^2 value is somewhat smaller, as the heavier recoil system requires less kinetic energy to balance the momentum of the struck nucleon. This, combined with the larger Fermi momentum for heavy nuclei, means that slightly higher x or Q^2 values are required to fully suppress scattering from nucleons associated with the mean-field structure. Figure adapted from Ref. [44]

Condition (III) requires the ability to separate two-nucleon and three-nucleon SRCs. This can be achieved in a rigorous way by defining the parameter α_i :

$$\alpha_i = A \frac{E_i - p_{i,z}}{E_A - p_{A,z}} = A \frac{E_i^{lab} - p_{i,z}^{lab}}{m_A}, \quad (5)$$

where p_A is the four-momentum of the nucleus A and $p_i \equiv (E_i, \vec{p}_i)$ is the initial four-momentum of the struck nucleon. Note that $m_i^2 \equiv p_i^2 = E_i^2 - \vec{p}_i^2 \neq m_N^2$, which reflects the off-shellness of the nucleon. The parameter α_i is invariant under boosts in the z direction [52, 53, 54] and in the infinite momentum frame it describes the momentum fraction of the nucleus carried by the interacting nucleon. The parameter α_i is analogous to Bjorken- x which describes the fractional momentum of the quark constituents in deep inelastic scattering. The definition of α_i is such that on average, each quark carries a momentum fraction $\alpha_i \approx 1$. To have $\alpha_i > 1$ requires the sharing of the momentum of at least two nucleons, while $\alpha_i > 2$ must involve at least three nucleons. This property can be used to separate scattering from different SRCs, since for

$$j - 1 < \alpha_i < j, \quad (6)$$

the reaction will involve at least j nucleons, allowing one to distinguish interactions with $j = 2, 3, \dots$ nucleons. Another important property of α_i is that in the eikonal regime, discussed as part of condition (V), this quantity is nearly

unaffected by final state interactions. Therefore, the experimentally extracted α_i distribution function is Lorentz boost invariant largely insensitive to FSI.

We can further elaborate the properties of α_i by applying energy-momentum conservation for the nucleon knocked out from the nucleus. Using the kinematic relation for the produced final mass in γ^*N interaction, $W_N^2 = (p_i + q)^2$, one obtains

$$\alpha_i = x \left(1 + \frac{2p_{i,z}}{q_0 + |q|} \right) + \frac{W_N^2 - m_i^2}{2m_N q_0}, \quad (7)$$

where $p_{i,z}$ is the rest-frame longitudinal momentum of the initial nucleon along the direction of the transferred momentum q . For quasi-elastic scattering, $W_N = m_N$, yielding a simplified expression for α_i . One can see from the above equation that for any given values of nucleon initial momentum and Q^2 one can find solution for $x > 1$ such that α_i will satisfy the SRC selection rule of Eq. 6.

This is very important for at least two reasons. First, the possibility of probing at $x > 1$ kinematics will significantly suppress the Δ -isobar contribution and secondly at sufficiently large Q^2 when according to Eq. (7), $\alpha_i \approx x$, and so the $x > j - 1$ kinematics will allow us to select j -nucleon SRCs in the quasi elastic region. The latter is significant for SRC studies in inclusive reactions in which only Bjorken- x can be reconstructed (see Sec. 4.2).

The above considerations are largely independent of the specific reaction being used to probe SRCs. We now discuss in more detail the requirements, separating the further discussion of the ideal conditions for sensitivity to SRCs according to the complexity of the electro-nuclear reactions used to probe the SRCs. We discuss three main types of the reactions: *inclusive* $A(e, e')X$, *semi-inclusive* $A(e, e'N)X$ and *triple-coincidence* $A(e, e', NN)X$ reactions. For all three cases we consider only the quasi-elastic scattering in which case one nucleon is knocked out from the SRC in the elastic γ^*N interaction and the residual nuclear system consists only of nucleons.

4.2. Kinematics of Inclusive Reactions

Because of the requirements discussed in the previous section, the cross sections involved in quasi-elastic scattering studies of SRCs are suppressed by both the relatively large Q^2 values required and the fact that one is sampling from the high momentum tail of the nucleon momentum distributions. Because of this, the first attempts to isolate SRC contributions in high- Q^2 reactions, and the only attempts to isolate 3N SRCs to date, involved inclusive measurements where only the scattered electron is detected. This maximizes the cross section while still allowing for isolation of the SRC contributions through selection of appropriate kinematics.

Note that α_i (Eq. (5)) depends on the initial nucleon momentum, $p_{i,z}$, which cannot be fully reconstructed in inclusive scattering. However, it follows from Eq. (7) that $x \rightarrow \alpha_i$ in the limit where q_0 and $|q|$ are much larger than $|p_{i,z}|$ and $W_N^2 - m_i^2$. Since x is defined only by the kinematics of the initial and scattered electron, one can use x in place of α_i to isolate scattering from high-momentum nucleons. Because of the kinematic condition that scattering at

$x > j - 1$ requires that at least j nucleons be involved, one can attempt to isolate 2N correlations by requiring x to be sufficiently larger than one, and 3N SRCs when sufficiently above $x = 2$.

Extremely high Q^2 values are not required for this to be an effective way of separating 2N and 3N configurations. The kinematic limit for scattering from a proton at rest is $x = 1$ for all Q^2 values and scattering at $x > 1$ must involve at least *two* nucleons. For x slightly above unity, the “multi-nucleon” contributions are dominantly quasi-elastic scattering from a single nucleon which has a non-zero momentum, $k < k_{Fermi}$, due to its interaction predominantly in the mean field of the residual nucleus. The threshold in x for which one is sensitive only to nucleons with $k > k_{Fermi}$ depends on Q^2 (see Fig. 3). Similarly, for $x > m_D/m_N \approx 2$, at least *three* nucleons must be involved in the reaction, and configurations where the three nucleons all have large momenta are expected to become dominant at some value of x well above $x = 2$, the limit for contributions from an at-rest 2N SRC.

Based on Fig 3, one would expect that inclusive $A(e,e')$ reactions measured at $Q^2 \gg m_N^2$ and $x \gtrsim 1.4$ should allow us to probe the nucleon in 2N and higher order correlations. At lower Q^2 values, where the above approximations are not as good, the onset of 2N SRC dominance will require somewhat larger values of x . While α_i cannot be reconstructed in inclusive scattering, one can estimate $p_{i,z}$ from the inclusive kinematics under the assumption that one is interacting with one of the nucleons in an at-rest 2N SRC. Making this assumption, one obtains

$$\alpha_{2N} = 2 - \frac{q_- + 2m_N}{2m_N} \left(1 + \frac{\sqrt{W^2 - m_N^2}}{W^2} \right), \quad (8)$$

where $W^2 = 4m_N^2 + 4m_N\nu - Q^2$. The quantity α_{2N} , sometimes called α_{tn} , is equal to α_i to the extent that the two-body approximation is valid and the transverse momentum of the initial nucleon can be neglected. This allows for a comparison of the onset of 2N SRC dominance as a function of x and α_{2N} , where the onset in α_{2N} should be Q^2 -independent if the 2N SRC picture is correct. For multi-nucleon SRCs, there is not a unique prescription for determining $p_{i,z}$, as it depends on the distribution of relative momentum of the nucleons in the SRC. A 3N SRC in a symmetric configuration, where all three nucleons have similar momentum, will provide a different spectator system than a linear configuration where the momentum of one nucleon is balanced by two nucleons splitting the momentum in the opposite direction. Thus, examination of the onset of scaling for $x > 2$ using different models of the microscopic structure of the 3N SRCs may allow for an evaluation of these models, providing insight into the structure of these multi-nucleon correlations.

4.3. Final-State Interactions in Inclusive Reactions

While the cross section for hadronic interaction of the struck nucleon with the rest of the nucleus can be large, the inclusive scattering cross section factorizes from later hadronic interactions, and only specific FSI contributions are expected to impact the inclusive cross sections at $x > 1$ and high Q^2 . Here we

present a brief discussion of the current state of understanding of FSI in this kinematical region.

It is well established that there are large FSI contributions at low Q^2 values [55, 19] which provide a clear breakdown of the scaling picture for QE scattering in the PWIA (discussed in Sec. 5). It was generally argued that for inclusive scattering, FSI contributions would vanish when the spatial resolution of the probe is small and the ejected nucleon has a large momentum. This was a consequence of the factorization of the initial interaction of the probe with the nucleon from the later rescattering of the struck nucleon, as discussed in more detail in Refs. [56, 19]. Additional studies provided more detailed predictions that FSI would be small at sufficiently large Q^2 [57, 58], although there were still questions, e.g. the possible further suppression of FSI for high-momentum nucleons because of the impact of the nucleon virtuality in the rescattering [58, 59, 60]. Some more recent calculations [61, 62] show FSI contributions that become very small by $Q^2=3-4 \text{ GeV}^2$, suggesting that the more recent inclusive data [63, 64] reach sufficient Q^2 values that these effects do not interfere with the extraction of SRCs from high- Q^2 inclusive measurements. In addition, these high- Q^2 inclusive measurements show no indication of Q^2 dependence, as presented in Secs. 5 and 6, suggesting small contributions from FSI.

While these arguments were used as justification for analysis of inclusive measurements in the PWIA, there are still some questions as to the applicability of the impulse approximation. First, this relies on the electron being insensitive to interactions of the struck nucleon once it is “far” from the location of the interaction (far in terms of the wavelength of the probe and the final-state proton). However, in scattering from a pre-existing SRC, one is selecting cases where the struck nucleon is very close to another nucleon, and thus FSIs may not vanish, but may be localized within the SRCs [57, 65, 44]. In this case, the FSI within the SRC may decrease slowly with Q^2 , making it difficult to verify the lack of FSI contributions by examining the onset of scaling from the Q^2 dependence of the data. However, if the FSI are contained within the SRC, and the SRCs in nuclei have the same deuteron-like structure as the high-momentum tails in the deuteron, then the ratio of nuclear cross sections should still yield a relative measure of the presence of high-momentum nucleons in nuclei.

In addition, some calculations of FSI were not consistent with the prediction that the effects should become small (or localized within the SRC) at large Q^2 . Calculations by Gurvitz and Rinat [66, 67, 68] and Correlated Glauber Approximation (CGA) calculations by Benhar and collaborators [69, 70, 71, 72] indicated significant FSI even at relatively large Q^2 values. For some of the earlier calculations, questions were raised about the consistency of the real and imaginary potentials used [57] and the sensitivity of the calculations to the inclusion of the N-N correlation function¹. The calculations of Benhar, *et al.*,

¹The correlation function encodes the fact that the short-range repulsive core of the NN potential significantly suppresses the probability for another nucleon to be found very close

include significant color transparency effects which reduce the FSI contributions at large Q^2 , but such large color transparency effects appear to be ruled out in $A(e,e'p)$ experiments [73, 74, 75, 76] at the range of Q^2 considered in Ref. [69]. It would be beneficial to have updated versions of the CGA calculations, including both the A and Q^2 dependence of FSI effects. This would allow for evaluation of the results against existing measurements of absolute cross sections and ratios for a variety of nuclei and a significant range of x and Q^2 values [77, 63, 64].

It has been argued [44, 78] that the CGA calculations yield an overestimate of the inclusive final-state interactions because they do not include inelastic diagrams needed to restore unitarity. Details of this argument are presented in Sec. 4.3.1. However, because the quantitative effect of these diagrams has not been fully evaluated, it is not yet clear whether the issue of unitarity provides an explanation for the large FSI results in the CGA calculations. Therefore, it is important to remember that the inclusive measurements are typically analyzed under the assumption that FSI are small or at least cancel in the ratio, as discussed in Sec. 6, and this remains a critical assumption in the examination of the inclusive results.

4.3.1. Inelastic Processes and their Impact on Final-State Interactions

In inclusive scattering, where only the scattered electron is detected, one cannot kinematically ensure pure quasi-elastic scattering. Indeed the threshold of Q^2 at which inelastic processes can happen is defined from the condition

$$(q + M_A)^2 \geq (M_A + m_\pi)^2, \quad (9)$$

where q is the four-momentum of the virtual photon M_A and m_π are masses of the target nucleus and pion. From Eq. (9) one obtains the threshold value of Q^2 for inelastic processes as:

$$Q^2 \geq Q_{thr}^2 = \frac{2M_A m_\pi + m_\pi^2}{\frac{M_A}{m_N x} - 1} \quad (10)$$

The inelastic threshold is shown in Figure 4. For $Q^2 \gtrsim 2 \text{ GeV}^2$, the inelastic processes is relevant for all nuclei in the range $1.3 < x < 1.5$ where one expects to be able to study contributions from SRCs.

In this case, one must include the inelastic scattering diagrams in the form of Fig. 5(c)² in addition to the quasi-elastic scattering diagrams (Fig. 5(a) and 5(b)). Models in which only quasi elastic (Fig. 5(b)) channels are included in the FSI diagram may become increasingly inaccurate at large Q^2 .

The direct calculation of the diagram of Fig. 5(c) is practically impossible, due to an increasing number of inelastic channels involved in the scattering. The high energy approach to this problem is based on the fact that at sufficiently high energies, in which eikonal approximation is valid, the FSI can be

to the struck nucleon [70]

²Note that in this case inelastic contributions from the PWIA diagrams are strongly suppressed due to large virtuality involved in the inelastic γN vertex at $x > 1$.

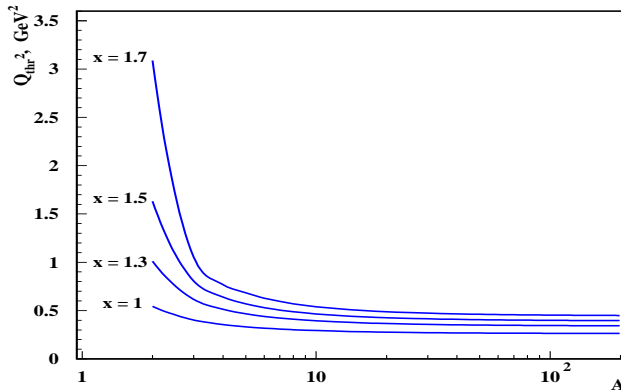


Figure 4: The dependence of the threshold value of Q^2 for inelastic processes in inclusive $A(e, e')X$ reactions to the mass number of nuclei, A at different values of Bjorken x .

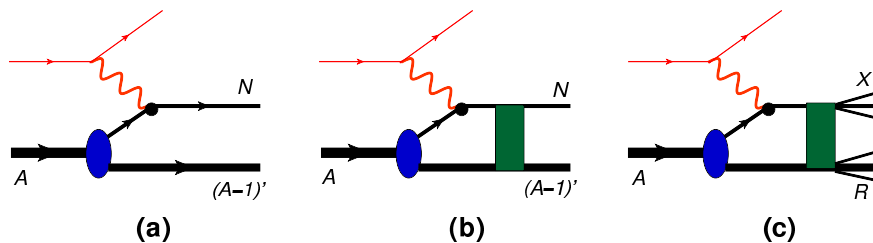


Figure 5: Diagrams contributing to inclusive $A(e, e')X$ reactions: (a) plane wave impulse approximation, (b) elastic and (c) inelastic final state interaction contributions.

expressed through the sequential diffractive elastic and inelastic rescatterings of nucleons in the nuclei, for which one can apply the optical theorem in the form $Im\{f_{NN}^{el}(t=0)\} = \sigma_{NN}^{tot}$ with $f_{NN}^{el}(t) = \sigma^{tot}(i + \alpha)e^{\frac{B}{2}t}$. Such an approach within Regge theory of diffractive scattering for inclusive processes was discussed in Ref. [79], which resulted to well known Abramovsky-Kanchelly-Gribov (AGK) cutting rules. Similar rules have been discussed within eikonal approximation by Bertocchi and Treleani [80] for inclusive hadron-nucleus scattering. They demonstrated that including only elastic rescattering amplitudes (Glauber theory) in the inclusive scattering violates the unitarity condition for the nuclear scattering amplitude, which is restored with the inclusion of the inelastic rescatterings. The main essence of these cutting rules is that, because of the unitarity relations between inelastic and elastic NN scattering amplitudes, it is necessary to account for the cancellations between rescattering amplitudes.

The qualitative aspects of the application of AGK type cutting rules can be seen from Fig. 6, in which the inclusive cross section is defined by the sum of the four terms, where Fig. 6(b) represents the interference between PWIA

and elastic rescattering amplitude and in the eikonal regime is predominantly destructive. The main effect of the application of AGK rules in the sum of the terms in Fig. 6 is that the sum of the squares of elastic (c) and inelastic (d) terms cancels half of the interference term (b) resulting to the net contribution of diagrams as given in Fig. 7. The latter is related to the imaginary part of the forward nuclear Compton scattering [81].

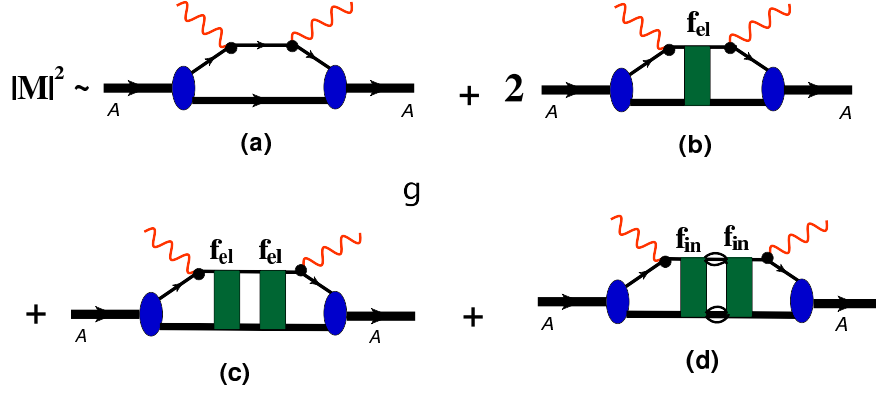


Figure 6: The main terms contributing to the cross section of inclusive $A(e, e')X$ cross section in quasi-elastic kinematics.

The above discussion illustrates the potential importance of maintaining unitarity through the inclusion of inelastic rescattering diagrams and also shows that inclusion of only the elastic rescatterings in the FSI (Glauber theory) can overestimate the final state interaction contribution. This is seen in Ref. [69] where authors used the correlated Glauber approximation to calculate the cross section of inclusive $A(e, e')X$ scattering. While they obtained reasonably good description of the data at small Q^2 , their FSI calculation significantly overestimated the data at large Q^2 (where according to Fig. 4 inelastic processes become important). In Ref. [69] the agreement with the data is achieved only after the inclusion of a large color transparency effect.

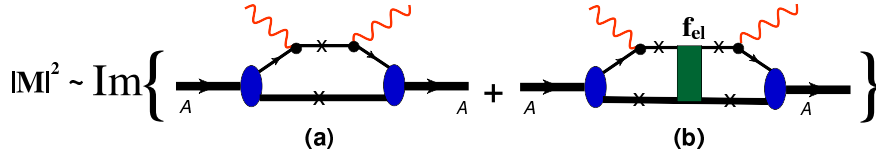


Figure 7: The imaginary part of the forward nuclear Compton scattering amplitude.

As mentioned above, the FSI in the inclusive $A(e, e')X$ reaction can be calculated through the imaginary part of the forward nuclear virtual Compton scattering amplitude (Fig. 7). Ref. [44] used these amplitudes to analyze the

space time properties of the final state interaction at $x > 1$. This analysis (Sec. 3.4 of Ref. [44]) demonstrated that the distance the knocked-out nucleon propagates before the rescattering in the amplitude of Fig. 7(b) is inversely proportional to the initial longitudinal component of the nucleon $|p_{iz}| \sim |p_{min}|$, where the dependence of p_{min} on x and Q^2 is given in Fig. 3. This suggests that already at 300 MeV/c, the reinteraction distances are $\lesssim 1$ fm, indicating that at least the first rescattering will take place within the 2N SRC. So while FSI between nucleons in the SRC may survive at high Q^2 , these very short-distance interactions within the SRC should be identical for scattering from a deuteron or from a deuteron-like pair within a heavy nucleus. This situation naturally explains the persistence of the scaling in the ratios of inclusive cross sections measured for nuclei A and the deuteron or ${}^3\text{He}$. However, a full, quantitative evaluation of FSI has not yet been performed, although numerical estimates are in progress [81].

4.4. Kinematics of semi-inclusive $A(e, e'N)$ reactions

We now examine the semi-inclusive $A(e, e'N)$ reaction with kinematics chosen such that the struck nucleon, with momentum \vec{p}_N , is detected in coincidence with the scattered electron. The goal is to isolate the single nucleon knock-out channel where only the $(A-1)$ spectator nucleons are undetected and the initial kinematics of the struck nucleon can be reconstructed in the PWIA. Clean identification of the nucleon as being struck requires a large momentum transfer such that the final nucleon momentum is much larger than the momentum of any of the spectator nucleons in the residual nucleus. This is achieved by requiring

$$\vec{p}_N = \vec{p}_i + \vec{q} \gg k_{Fermi} . \quad (11)$$

where \vec{p}_i will represent the initial momentum of the struck nucleon within the PWIA picture of the scattering.

For further discussion we start with the "standard" definition of the kinematics of knock-out $A(e, e'N)$ reactions (e.g. [8, 9, 27]) by introducing missing momentum p_m and missing energy E_m of the reaction as follows:

$$\vec{p}_m = \vec{q} - \vec{p}_N , \quad E_m = E_R - T_{A-1} , \quad (12)$$

where $T_{A-1} = \frac{p_m^2}{2m_{A-1}}$ is the center of mass kinetic energy of the residual $A-1$ nucleus. The above definition was justified from the point of view of the shell-model studies. Indeed applying the energy and momentum conservation for the reaction $\gamma^* + A \rightarrow N + (A-1)^*$ one obtains

$$E_m = E_{A-1} - T_{A-1} - m_{A-1} + E_\alpha , \quad (13)$$

with E_{A-1} , and m_{A-1} being the total energy and ground state mass of the recoil $(A-1)$ nucleus, while E_α is the removal energy of the knocked-out nucleon. It follows from the above equation that for the situation in which the $(A-1)$ nucleus is in its ground state the missing energy, E_m , equals to the removal energy of the nucleon from the particular shell- α .

However, for semi-inclusive reactions aimed at studies of SRC structure of the nucleus the above definition of the missing energy, E_m , is somewhat inconvenient. The major reason is the fact that the structure of the residual $A - 1$ nucleus is more complex and strongly depends on whether 2N or 3N SRCs are probed³. For this reason much more relevant quantity is the recoil nuclear energy, E_R [44] which is related to E_m through:

$$E_R = E_m + T_{A-1} = q_0 - (\sqrt{m_N^2 + p_N^2} - m_N), \quad (14)$$

and represents more natural variable describing SRCs, as shown below.

In the PWIA, it is straightforward to relate the four momentum of the initial nucleon $p_i \equiv (E_i, \vec{p}_i)$ to missing momentum and residual nuclear energy as follows:

$$\vec{p}_i = -\vec{p}_m \quad \text{and} \quad E_i = m_N - E_R. \quad (15)$$

Using these variables, we define the *necessary* condition for probing SRCs as

$$|p_m| = |q - p_N| > k_{Fermi}, \quad (16)$$

as this corresponds to scattering from a nucleon with $p_i > k_{Fermi}$ in the PWIA. This condition is not *sufficient*, since it is derived within PWIA and final state interactions could significantly alter the actual relation between p_m and p_i .

Another observation that can be drawn from the PWIA picture is the relation between p_m and E_R (or E_m)⁴. If one assumes that the interaction took place with 2N SRCs which are well factorized from the mean field of (A-2) nucleus, one obtains for the quasi-elastic kinematics the relation

$$E_R \approx \sqrt{m_N^2 + p_m^2} - m_N, \quad (17)$$

i.e. the kinetic energy associated with the recoil of the correlated nucleon. Thus p_m and E_R (or E_m) will be correlated quantities if the SRC is probed in the interaction. Note, however, that this correlation arises from a purely kinematical condition, so any two-body current (such as meson exchange currents or Δ -isobar contributions) may induce similar correlations. To enhance the role of the 2N SRCs in the observation of $p_m - E_R$ correlations, the additional conditions on Q^2 and x discussed in Sec. 4.1 should be imposed.

4.5. Kinematics of triple-coincidence $A(e,e'NN)X$ reactions

Triple-coincidence measurements, while adding additional complexity, also have the potential to provide more comprehensive information about the structure of SRCs. In such experiments, one couples the semi-inclusive single-nucleon

³For example in the case of the knockout of the nucleon from 2N SRC the residual (A-1) system consists predominantly of slow (A-2) nucleus and fast nucleon that was in correlation with the struck nucleon.

⁴The missing momentum p_m and energy E_m (or E_R) are in general independent kinematical variables for A(e,e'p) reactions.

knock-out measurement of a high-momentum nucleon with detection of the spectator nucleon from the initial state SRC. We start with same kinematic requirements as for the case of semi-inclusive $A(e,e'N)$ scattering from a nucleon in an SRC (Eqs. 11 and 16). In addition, we detect another nucleon with a recoil momentum $p_r \approx -p_i$, which we identify as the recoil nucleon from the 2N SRC.

This is convenient experimentally, because while one is potentially interested in a large region of initial nucleon momenta, these should all be found in a relatively narrow cone around the momentum transfer for sufficiently large $|q|$. Once these kinematic conditions are satisfied, several signatures can be explored to study SRCs.

The first step is to identify events consistent with pre-existing SRCs. In the PWIA, there should be a strong correlation between initial momentum of the struck nucleon (p_i) and recoil momentum (initial and final momentum p_r in the PWIA) if both were in the SRC prior to the scattering:

$$\vec{p}_m \approx -\vec{p}_i \approx \vec{p}_r , \quad (18)$$

where these momenta are equal for an at-rest SRC, where the entire missing momentum is carried by the spectator nucleon from the SRC. If the SRC has a non-zero net momentum, one can reconstruct the initial momentum of both nucleons in the PWIA, in principle allowing for a measure of the momentum distribution of the pair in the nucleus. Similarly, the SRC picture predicts a correlation between missing energy of the reaction and the kinetic energy of the recoil nucleon. This correlation is a generalization of Eq. (17) which yields:

$$E_R \equiv q_0 - T_p \approx T_r , \quad (19)$$

where T_p , T_r are the kinetic energies of struck and recoil nucleons.

The above two correlations also yield a relation between light-cone momentum fractions of initial struck nucleon α_i and recoil nucleon α_r :

$$\alpha_i + \alpha_r \approx 2 , \quad (20)$$

which is a statement of the condition that 2N SRC carries a fraction of approximately $2/A$ of the light cone momentum of the nucleus A , as expected for a two-nucleon system whose total momentum is small. One important advantage of Eq. (20) as compared to Eqs.(18,19) is that while latter relations are strictly speaking correct only within the PWIA, the former survives the FSI in the eikonal regime.

Perhaps the most interesting advantage of the triple-coincidence experiments is the possibility to study the isospin-dependence of the SRCs by detecting different possible final states: pp, pn, nn. Generalizing these reactions to the case in which the recoiling system represents a baryonic resonance, such as Δ -isobar, one can use these reactions to gain access to the non-nucleonic components of SRCs [82, 78].

Many of the detailed studies possible in a triple-coincidence reaction rely on small final-state interactions, although the approximate conservation of α_i in the eikonal regime leave some information intact even in the presence of large FSIs. These issues will be discussed in more detail in Sec. 8.

5. Studies of the Deuteron

The deuteron plays a special role in SRC studies. The measurement of the momentum distribution is necessary for identification of the iso-singlet component of 2N SRCs in nuclei, which is expected to be a universal feature in the high-momentum tail of all nuclei (Eq. (1)). As the simplest nucleus, the deuteron also provides an ideal testing ground for many issues related to details of the reaction mechanism: meson exchange contributions (MECs), isobar contributions (ICs), final state interactions (FSIs), as well as modification of the properties of nucleons due to their off-shellness.

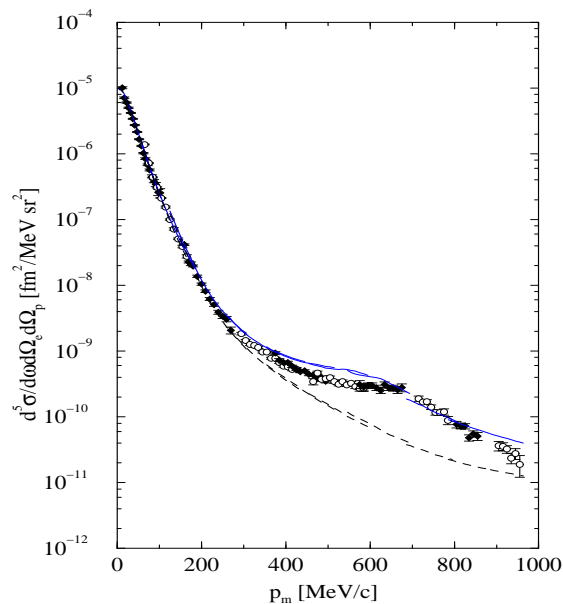


Figure 8: The p_m dependence of the $D(e,e'p)n$ differential cross section [83] at $Q^2 = 0.13 - 0.33 \text{ GeV}^2$. Dashed line is PWIA contribution, solid line is PWIA+MEC+IC [84]. Figure reprinted with permission from Ref. [83]

Extensive measurements of single nucleon knockout, both inclusive and coincidence, have been made to probe the low-momentum region and high-momentum tails of the deuteron momentum distribution. For nucleon momenta above $\sim 250 \text{ MeV}/c$, calculations of the cross sections showed growing sensitivity to the choice of nucleon-nucleon potential in exactly the region where correlations are expected to dominate the momentum distribution. It was thus expected that measurements at large values of missing momentum would allow one to study the details of the short-range part of the nucleon-nucleon potential.

In 1981, Saclay measured the $D(e,e'p)n$ reaction with a 500 MeV electron beam [20] and extracted a momentum distribution up to $\approx 300 \text{ MeV}/c$. The sub-GeV beam energies that were available meant that subsequent experiments

at higher p_m were forced to make measurements in the $x_B < 1$ region, near the Δ resonance. So while these experiments were able to measure missing momenta out to 950 MeV/c, the cross section for p_m above 400 MeV/c was dominated by meson exchange and isobar currents [83] and it was not possible to extract information about the underlying distribution (see Fig. 8).

The situation is somewhat improved when exploring polarization observables in the deuteron electrodisintegration reaction. For example, the NIKHEF polarized $D(e,e'p)n$ measurements [85] shown in Fig. 9 provide information on the structure at high p_m , with reduced sensitivity to FSI and MEC. While these play a role, the change of sign provided a clear demonstration of the importance of including both the S and D wave components of the deuteron. However, a detailed description of the data still requires contributions due to isobar and meson exchange currents.

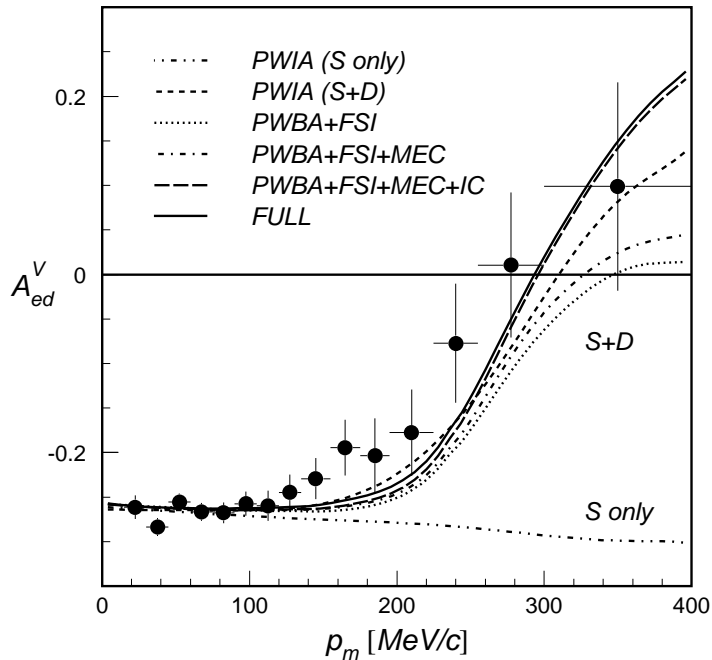


Figure 9: Spin correlation parameter A_{ed}^V as function of missing momentum for the $\bar{D}(e, e'p)n$ reaction at $Q^2 = 0.21 \text{ (GeV/c)}^2$ [85]. The short-dashed and dot-dot-dashed curves are PWIA predictions with and without inclusion of the D -wave, respectively. The other curves are calculations [86, 87] including additional contributions, folded over the detector acceptance. Figure reprinted with permission from Ref. [85]

The first high-energy studies involving the deuteron were the studies of inclusive high- Q^2 reactions at SLAC in late 1970s, 1980s and early 90s [88, 89, 90]. These experiments for the first time probed $x > 1$ kinematics. The most comprehensive high Q^2 inclusive electron-deuteron scattering measurements for

$x > 1$ were performed in Hall C at Jefferson Lab. Cross sections for the inclusive $D(e,e')$ reaction were taken over a range of x and Q^2 using a 4 GeV electron beam in 1996 [91, 63, 92] and the kinematics significantly extended in a subsequent measurements at 6 GeV [93, 94, 64]. These inclusive measurements extract the deuteron momentum distribution by means of y -scaling analysis [95, 96, 97, 57, 98, 64]. This analysis assumes the dominance of quasi-elastic scattering and involves reconstructing the minimum initial momentum of the struck nucleon (y) consistent with the kinematics of the scattering. The minimum initial momentum can be obtained from energy conservation assuming that the momentum is entirely along the direction of the transferred momentum q , and that the residual (A-1) nucleus is left in an unexcited state:

$$q_0 + m_d = \sqrt{m_N^2 + (q + y)^2} + \sqrt{m_N^2 + y^2} . \quad (21)$$

We obtain the y -scaling function, $F(y, Q^2)$, by dividing out the elastic e-N cross section:

$$F^{exp}(y, Q^2) = \frac{\frac{d\sigma}{dE'_e d\Omega}}{\sigma_{ep} + \sigma_{en}} , \quad (22)$$

where σ_{eN} is the elastic scattering cross section off the bound nucleon.

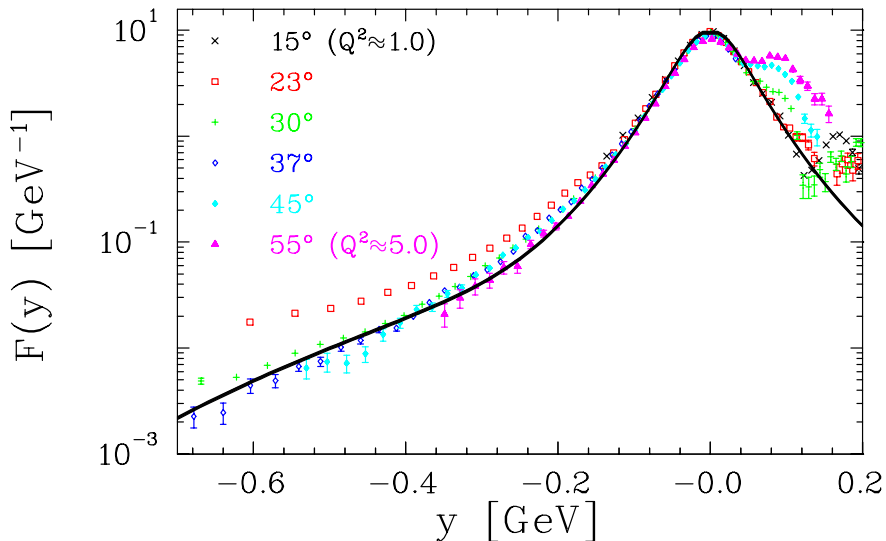


Figure 10: Scaling function $F(y)$ for deuteron from Ref. [91, 99] for scattering at $E=4.045$ GeV and $15^\circ \leq \theta \leq 55^\circ$. The solid line represents the expected $F(y)$ based on the calculation of the deuteron momentum distribution using the Av14 NN potential. Note that the inelastic contribution for $y \geq 0$ has been subtracted using a model. Figure adapted from Ref. [99]

In the scaling limit, $F(y, Q^2) \rightarrow F(y)$ if the assumptions of the scaling analysis are valid: quasielastic scattering, PWIA (no final-state interactions), and low excitation of the final spectator system. Inelastic scattering is suppressed

by going to low energy transfer, corresponding to $x > 1$, while for the deuteron, the final spectator system is a single nucleon where there are no options for low energy excitations. The observation of scaling in the data, shown in Fig. 10, supports the assumptions of the y -scaling analysis suggesting that FSI, which are expected to fall rapidly with Q^2 , are small.

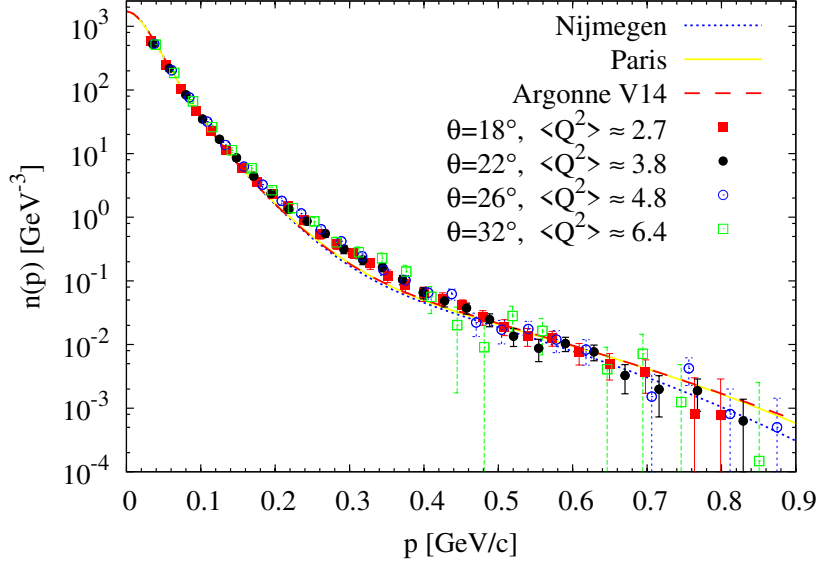


Figure 11: Deuteron momentum distribution, $n(p)$, as extracted from inclusive scattering at $x > 1$ from JLab E02-019 [64]. The different symbols show the data sets corresponding to different scattering angles, and thus different Q^2 values, and the curves are calculations based on three different NN potentials. Figure adapted from Ref. [64].

In the PWIA picture of quasi-elastic scattering, the above extracted scaling function can be directly related to the nucleon momentum distribution, as the cross section is simply a convolution of the e-N elastic cross section and the momentum distribution of the nucleons in the nucleus:

$$F(y) \approx 2\pi \int_{|y|}^{\infty} n(p) p dp \quad , \quad n(p) \approx \frac{-1}{2\pi p} \frac{dF(p)}{dp} . \quad (23)$$

The relation between the scaling function and the momentum distribution can be understood in a simple picture. The kinematics of the scattering set the minimum initial nucleon momentum that can contribute to the cross section (y). While the inclusive cross section is an integral that involves all momenta above y , it is dominated by momenta close to y , due to the rapid falloff of the nucleon momentum distribution. So the main difference between the cross section at kinematics corresponding to y_1 and $y_2 = y_1 + \delta y$ is the loss of the

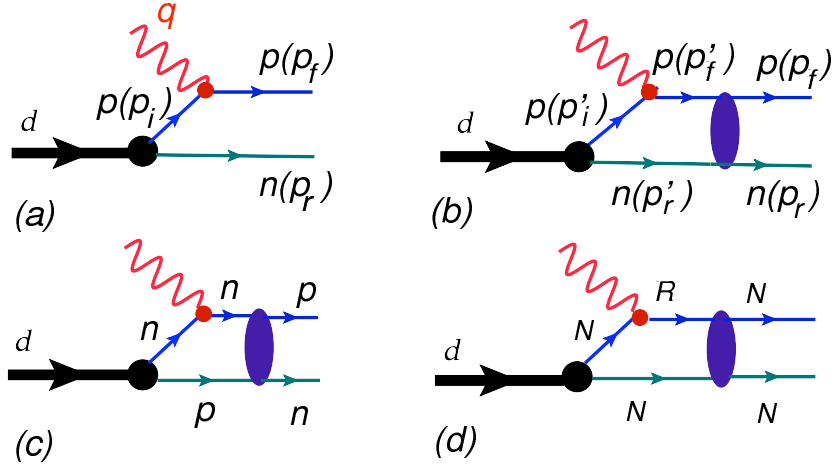


Figure 12: Impulse approximation (a), diagonal (b) and change-exchange (c) final state interactions and intermediate resonance contributions (d) to the $D(e,e'p)n$ reaction. Figure reprinted with permission from Ref. [100]

scattering from nucleons in the narrow momentum region δy between y_2 and y_1 . Thus, the momentum distribution is connected to the derivative of the scaling function.

Figure 11 shows the deuteron momentum distribution, $n(p)$ as extracted from Eq. (23) out to 900 MeV/c from the more recent measurement at higher energy [64]. While the agreement with the deuteron momentum distribution calculated from the NN potential again suggests that final state interactions are not too large in this region, it is difficult to set precise limits, as other modern NN potential yield predictions that vary by 10–20% for these nucleon momenta above 400 MeV/c. Thus, further studies of FSI contributions for scattering from high-momentum nucleons are still necessary. For inclusive scattering, the FSI contributions are less of a concern than in exclusive reactions, due to the closure approximation which is increasingly well satisfied as Q^2 increases, leading to FSI contributions that largely cancel. When the struck nucleon is extremely close to another nucleon, as in the case of scattering from one nucleon in an SRC, the FSIs are confined within the correlated nucleons. Thus, while the observation of a Q^2 -independent scaling function supports the y -scaling picture in general, the high momentum tails of the distribution may still have contributions from a nearly Q^2 -independent FSI contribution due to rescattering of the struck nucleon from the correlated nucleon in the SRC.

Exclusive $D(e,e'p)n$ measurements can provide additional information, as the initial kinematics of the struck proton can be fully reconstructed within the PWIA. However, while these reactions have the potential to provide a more complete understanding of the high momentum components of the nucleon distribution, they are also more sensitive to the details of the reaction

mechanism. The deuteron, then, provides the best testing ground for both the high momentum wave function and the competing effects including final state interactions, isobar contributions, and reaction dynamics. This is one of the main reasons why these reactions have been so intensively studied by several groups [101, 102, 103, 104, 103, 105, 106, 107, 108, 100].

One important aspect of exclusive $D(e,e'N)N$ reactions is that they provide the possibility to map out the role of intermediate inelastic transitions such as IC contributions and to study the onset of the eikonal regime in the final state interaction of two outgoing nucleons. This is an extremely important issue because, unlike MEC contributions, IC and FSI contributions do not decrease rapidly with increasing Q^2 values⁵. As a result, the most relevant processes contributing to the exclusive $D(e,e'p)n$ reactions at large Q^2 are the PWIA single nucleon knock-out, final state interactions, and intermediate resonance contributions (mainly the Δ -isobar) of Fig. 12.

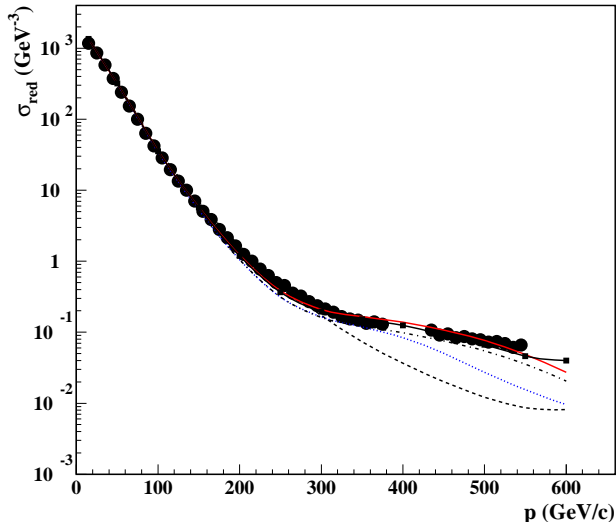


Figure 13: The ratio of the $D(e,e'p)n$ cross section to the elastic ep cross section as a function of p_m , with the ep kinematics taken such that it reduces to the deuteron momentum distribution in the PWIA. The data are from Ref. [109]. Dashed line – PWIA calculation; dotted line – PWIA + FSI term with only on-shell $pn \rightarrow pn$ rescattering included; dash-dotted line – PWIA + FSI with on- and off-shell $pn \rightarrow pn$ rescattering; solid line – PWIA + full FSI ($pn \rightarrow pn$ and charge-exchange $pn \rightarrow np$ rescattering); and solid line with squares – PWIA + full FSI + contribution from the mechanism in which the proton is a spectator and the neutron was struck by the virtual photon. Figure reprinted with permission from Ref. [100].

The first experiments on $D(e,e'p)n$ with the momentum transfer close to

⁵For $Q^2 < 4 \text{ GeV}^2$, the $\gamma^*N \rightarrow \Delta$ transition amplitude is comparable with the elastic $\gamma^*N \rightarrow N$ form factor and the FSI contribution is essentially Q^2 independent, at least up to $Q^2 \approx 8 (\text{GeV}/c)^2$ [76, 49].

the GeV/c region were performed at SLAC [110] and Jefferson Lab [111]. The SLAC measurement covered $1.2 < Q^2 < 6.8 \text{ GeV}^2$, but was limited to p_m values below 300 MeV/c. Even so, the cross section, and in particular the asymmetry between positive and negative p_m values, showed the importance of having detailed relativistic calculations [112, 113]. The Jefferson Lab measurement was performed at $Q^2 \approx 0.7 (\text{GeV}/c)^2$, where data were taken for $x \approx 1$ (on top of the quasi-elastic peak) [111]. The extracted momentum distribution follows the early Saclay results up to $\approx 300 \text{ MeV}/c$, but above this, final state interactions dominate the results [109]. Studies of this experiment [104, 100] demonstrated that FSIs, calculated within the eikonal approximation, can reasonably well describe the absolute cross section of the reaction (see Fig. 13), even when FSI yield 80% of the total cross section. This provides a significant test of the validity of the eikonal approximation, suggesting that the corrections can be reliably applied in kinematics where the contributions can be further suppressed. Another result of these measurements is the observation that kinematical suppression of IC for the low energy transfer region ($x \geq 1$) is effective at these kinematics, with no substantial IC contribution observed in these measurements.

These measurements were followed by a measurement at high- p_m and Q^2 up to $5 (\text{GeV}/c)^2$ [114] where for the first time, the momentum and energy transfer in the reactions exceeded the nucleon mass. The momentum distribution shows a substantial contribution from FSI at large missing momenta ($p_m > 300 \text{ MeV}/c$) when integrated over all recoil neutron angles, as shown in Fig. 14. The main advantage of this experiment was that it provided access to the recoil-nucleon angular dependence of the cross section at large p_m . This is critical for distinguishing the onset of the eikonal regime of FSI which is characterized by a very specific angular distribution, with nuclear screening minima and incoherent rescattering maxima [107, 108].

Figure 15 show the comparison of the generalized eikonal approximation calculations [100] and the data from Ref. [114]. The calculation in the comparison is evaluated over identical kinematic integrations as the experiment. Despite these integrations, which lessen the sensitivity of the cross section to various dynamical details of the process, several important observations can be made:

- First, the angular distribution exhibits the expected eikonal features, with a clear minimum or maximum in the top and bottom plots of Fig. 15, respectively, at nearly transverse kinematics due to the final state interaction. The maximum of the FSI contributions is at recoil angles of 70° , in agreement with the generalized eikonal approximation prediction of Refs. [107, 108], as opposed to the Glauber theory calculations (not shown) which predict peak FSI contributions at 90° .
- The calculation disagrees with the data for $\theta_r > 70^\circ$, which corresponds to the $x < 1$ kinematic range close to the inelastic threshold. This could be due to intermediate isobar contributions. The comparisons also suggest that the relative strength of the Δ -isobar contribution may diminish with increasing Q^2 and for neutron production angles $\theta_r \rightarrow 180^\circ$. If this is

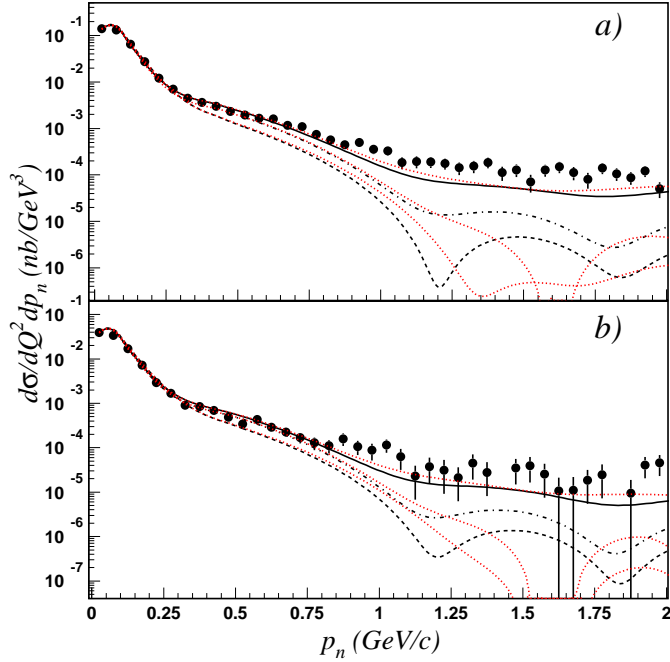


Figure 14: The recoil neutron momentum distribution for (a) $Q^2 = 4 \pm 0.5 \text{ GeV}^2$ and (b) $Q^2 = 5 \pm 0.5 \text{ GeV}^2$. The dashed, dash-dotted and solid curves are calculated [103] using the Paris potential [11] and averaged over the CLAS acceptance for PWIA, PWIA+FSI and PWIA+FSI+MEC+N Δ , respectively. The red dotted curves are calculated using Av18 potential [115]. Figure reprinted with permission from Ref. [114]

confirmed in more precise measurements it will have an important implication for SRCs in deep-inelastic reactions, since in this case fast backward recoil nucleons will not be affected by the final state interaction with the products of DIS scattering.

- The forward direction of the recoil nucleon momentum, being far from the Δ -isobar threshold, exhibits a relatively small contribution from FSI. This indicates that the forward recoil angle region is best suited for studies of PWIA properties of the reaction such as the deuteron wave function and off-shell electromagnetic current.

The results of another related experiment [117, 118] have recently been submitted for publication [116] and are shown in Fig. 16. In this experiment, the reaction is measured at forward recoil angles and for Q^2 up to 3.5 GeV^2 , with extremely high precision. Their data extend to $p_m = 550 \text{ MeV}/c$ and the cross sections are examined as a function of θ_r from 20° to 90° . The results are com-

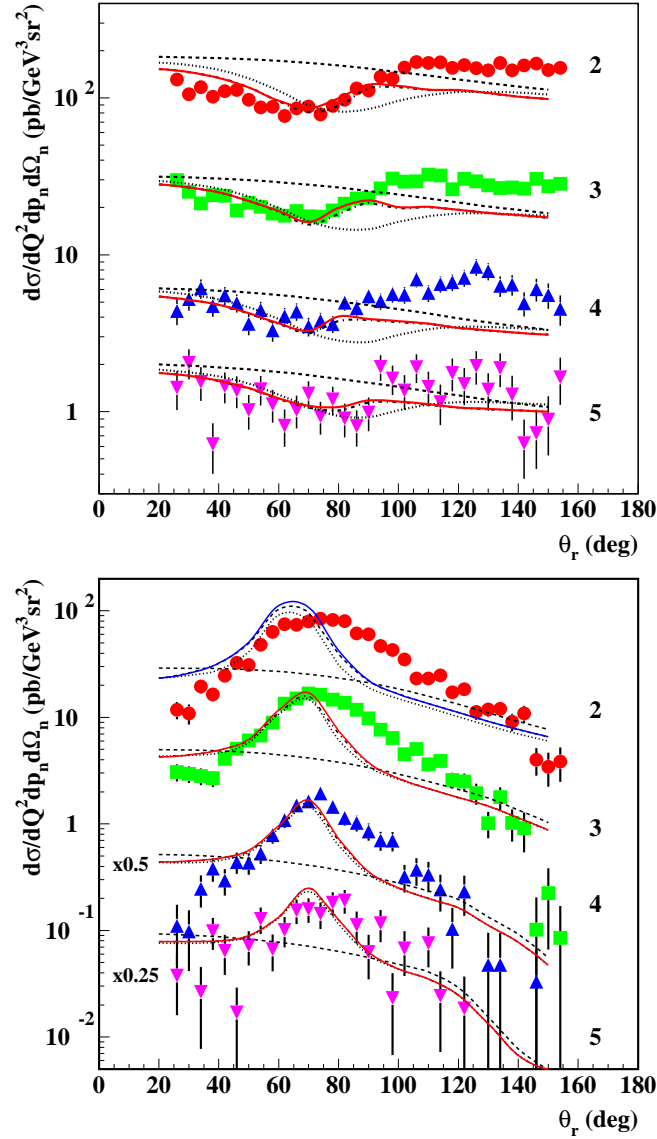


Figure 15: **Top:** Dependence of the differential cross section on the direction of the recoil neutron momentum. The data are from Ref. [114]. Dashed line - PWIA calculation; dotted line - PWIA + FSI term that contains only on-shell part of the $pn \rightarrow pn$ rescattering; dash-dotted line - PWIA+ FSI term that contains both, off- and on- shell parts of the $pn \rightarrow pn$ rescattering; solid line - PWIA + full FSI containing $pn \rightarrow pn$ and charge exchange $pn \rightarrow np$ rescatterings. The momentum of the recoil neutron is restricted to $200 < p_r < 300 \text{ MeV}/c$. The labels 2, 3, 4 and 5 correspond Q^2 bins of $Q^2 = 2 \pm 0.25, 3 \pm 0.5, 4 \pm 0.5, \text{ and } 5 \pm 0.5 \text{ GeV}^2$, respectively. **Bottom:** Same as the top figure, but with the momentum of the recoil neutron is restricted to $400 < p_r < 600 \text{ MeV}/c$. The results for bins “4” and “5” are scaled by factors of 0.5 and 0.25 respectively. Figure reprinted with permission from Ref. [100]

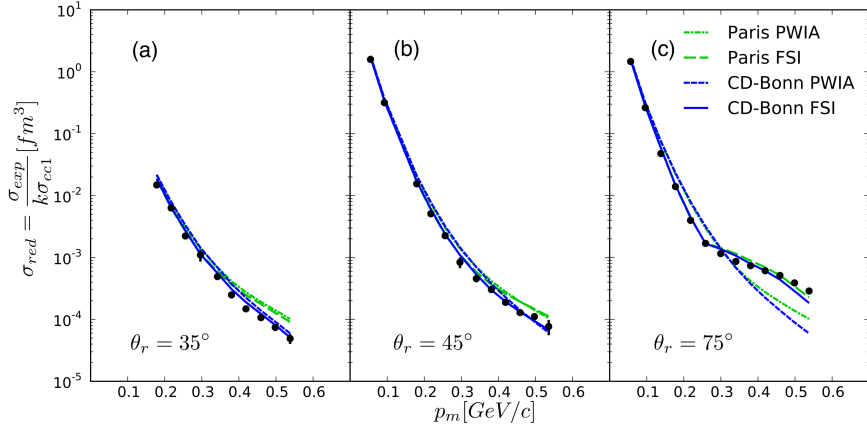


Figure 16: The reduced cross section as function of missing momentum is shown in panels a, b and c for $\theta_r = 35^\circ$; 45° and 75° , respectively. CD-Bonn potential: dashed (blue) lines PWIA, solid (blue) lines FSI. Paris potential: dash-dot (green) lines PWIA, long-dashed (green) lines FSI. The PWIA results are for all angles identical. Figure reprinted with permission from Ref. [116].

pared to three models of scattering from the deuteron, with and without the inclusion of FSI, MEC, and IC, which all yield a reasonable description of the data. These data will allow for more detailed evaluations of the models of the FSI contributions over a range of θ_r and p_m values. In addition, they show that for $\theta_r \approx 40^\circ$, FSI contributions are relatively small and θ_r -independent over the full p_m range of the experiment, suggesting that these kinematics may provide the most direct access to the high-momentum tail of the deuteron momentum distribution.

These high- Q^2 experiments on deuteron electrodisintegration have already shown great potential to resolve several issues related to the exploration of nucleon with high initial momentum and missing energy. This will allow for a clean extraction of the high-momentum components of the deuteron momentum distribution in future measurements focused on kinematic regions where FSI, MEC, and IC are suppressed. Future experiments can also provide further data where these effects are large to provide a more quantitative validation of calculations of these effects in a well understood nucleus. This will be critical in moving to similar detailed studies for heavier nuclei.

6. Inclusive Reactions Beyond the Deuteron

The first high- Q^2 experiments that probed the high-momentum component of the ground state wave functions of more complex nuclei were inclusive measurements performed at SLAC in the 80s [119, 120] and 90s [121, 122, 123, 77, 124], followed by series of measurements at Jefferson Lab [91, 63, 125, 126, 93, 94]. A compilation of the data from the many of these experiments as well as a detailed discussion of quasielastic scattering (with a focus on probing the mean-field structure of the nucleus) can be found in Ref. [127].

To probe SRCs in these experiments, kinematic conditions similar to those discussed for inclusive scattering from the deuteron should be considered. Thus, they require $Q^2 > 1 \text{ GeV}^2$ measurements at $x > 1$, such that the scattering is far from the inelastic pion production threshold and dominated by quasi-elastic scattering from the bound nucleon.

One of the first approaches in probing the momentum distribution of nucleons in heavy nuclei was the framework of y scaling [57] where the y parameter was defined as a solution of the following equation:

$$q_0 + m_A = \sqrt{m_N^2 + (q + y)^2} + \sqrt{m_{A-1}^2 + y^2} . \quad (24)$$

This is a generalization of the case for the deuteron (Eq. (21)), with the assumption that the final state is a two-body system consisting of the struck nucleon and a spectator (A-1) system. Note that the value used for m_{A-1}^2 is related to the excitation of the residual system, and so for the case of an unexcited (A-1) spectator, corresponding to to panel a) of Fig. 17, this is the mass of the ground state (A-1) spectator nucleus. There can also be small excitation of the (A-1) system, yielding a larger effective mass for the A-1 system, while the case of Fig. 17b corresponds to a significantly larger value for m_{A-1}^2 , due to the large kinetic energy of the spectator nucleon from the initial-state SRC.

nucleus in its ground state, corresponding to to panel a) of Fig. 17.

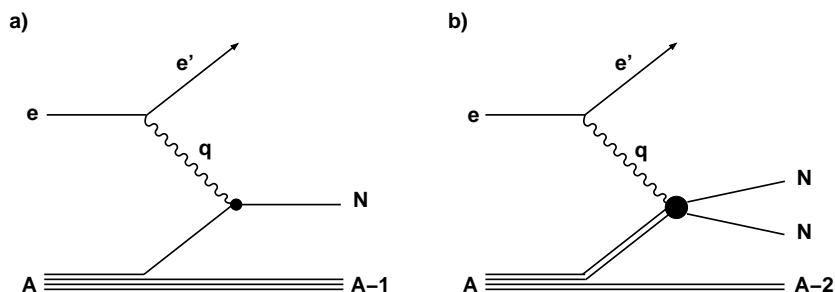


Figure 17: Shown are the dominate diagrams of the $A(e,e')$ reaction for $x > 1$ and $Q^2 > 1(\text{GeV}/c)^2$. Figure a) shows single nucleon scattering while figure b) shows scattering from a correlated initial-state pair.

The requirement that measurements be made for $x > 1$ corresponds to negative values of y . While scattering at large negative y is sensitive to the

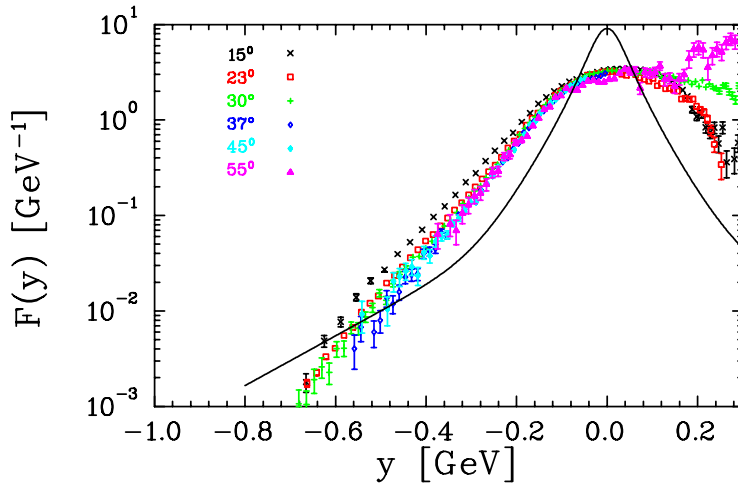


Figure 18: Extracted y -scaling function $F(y)$ for Fe [63, 128], compared to a fit to the deuterium data (solid line). Note that a model of the inelastic contributions which are significant for $y > 0$ has been subtracted to isolate the quasielastic contributions. Figure adapted from Ref. [128]

tails of the momentum distribution, there is an additional complication that arises in applying the y -scaling approach for complex nuclei. The extraction of y from Eq. (24) assumes an unexcited $(A-1)$ spectator nucleus in the final state. This is a reasonable approximation for low values of y , where one is removing a nucleon from one of the nuclear shells, but not for high momentum nucleons which are part of an SRC. In this case, one expects that in addition to the struck nucleon, there will be one high momentum spectator nucleon (the 2nd nucleon from the SRC) along with an unexcited $(A-2)$ spectator, as shown in panel b) of Fig. 17. For large values of y , there is a significant difference in the kinetic energy of the spectator system in these two pictures. This is not an issue for the deuteron, where the two-body final state is well justified if one avoids resonance excitations, but can be very important for heavier nuclei. Figure 18 shows $F(y)$ extracted from the JLab Hall C measurements on Fe [63, 128] at the same kinematics as the deuterium measurement from Fig. 10, and the definition of y from Eq. (24). The result shows two unexpected features. First, the peak is not symmetric about $y = 0$. While the model-dependent subtraction of the inelastic contributions is significant for $y > 0$ and large Q^2 , the agreement among the low Q^2 data sets suggests that the subtraction is not the source of the asymmetry. Second, the tail of the distribution falls off significantly more rapidly for Fe than it does for deuterium, suggesting that Fe has fewer very high momentum nucleons. One would expect both the mean-field and SRC contributions to yield more high-momentum nucleons in Fe than in ^2H . Both of these unexpected features are consequences of treating the spectator system as an unexcited $(A-1)$ nucleus.

This issue can be addressed by adjusting the assumptions that go into defining Eq. (24) or by explicitly calculating corrections to $F(y)$ to account for the modified final state. The first approach was to replace y with y_2 [16, 129]:

$$q_0 + m_A = \sqrt{m_N^2 + (q + y_2)^2} + \sqrt{m_N^2 + y_2^2} + m_{A-2}, \quad (25)$$

which follows from the assumption that scattering from a high momentum nucleon follows the scenario of Fig. 17b in which 2N SRC is factorized from the low momentum residual (A-2) nucleus, assumed to be at rest. This resolves the problem in the high-momentum tail, yielding a falloff similar to that observed in the deuteron, but alters the extracted scaling function $F(y)$ near $y = 0$, where the standard definition of y gives a reasonable approximation.

Later approaches attempted to improve the definition of y by incorporating the impact of SRCs at large values of $|y|$ while maintaining appropriate behavior at small $|y|$ values. One such attempt was the introduction of y_{CW} by Ciofi degli Atti and West [130]:

$$q_0 + m_A = \sqrt{m_N^2 + (q + y_{CW})^2} + E_{A-1}^*, \quad (26)$$

where E_{A-1}^* , the average energy of the residual (A-1) system is taken from a model where the two-nucleon SRC dominates for large values of $|y|$. The model also includes a contribution for the average center-of-mass motion of the SRC and corrections such that at low $|y|$, the excitation energy of the residual nucleus approaches the expected value for the (A-1) spectator nucleus. Note that the calculation of E_{A-1}^* was refined over time (most recently in Ref. [61]) yielding somewhat different definitions of y_{CW} in different works.

Another approach uses a simple convolution of the SRC distribution (taken to be identical to the deuteron momentum distribution) with an estimated center-of-mass motion of the SRC. From this, one can determine the average contribution from both the C.M. motion of the pair and the relative momentum of the nucleons in the SRC to determine the excitation energy of the residual system, neglecting transverse momentum, allowing for the extraction of the initial nucleon momentum, y^* [99]:

$$q_0 + m_A = \sqrt{m_N^2 + (q + y^*)^2} + \sqrt{m_N^2 + (K_{CM}/2 - k_{rel})^2} + \sqrt{(m_{A-2} + K_{CM})^2}, \quad (27)$$

where the initial nucleon momentum, y^* , is broken down into the contributions from the C.M. motion of the SRC and the relative motion within the pair: $y^* = K_{CM}/2 + k_{rel}$. The underlying picture is the same as the y_{CW} approach, but rather than calculating the expected excitation, the motion of the SRC is adjusted so that the convolution reproduces the observed distribution, thus yielding an estimate of average contribution from the C.M. motion as a function of y^* . Figure 19 shows the result of the analysis [99, 128] using the modified y^* scaling variable. The shape of the $F(y^*)$ distribution for heavy nuclei at large negative y^* values is nearly identical to that of the deuteron in the scaling (large Q^2) limit, and also provides a more symmetric peak about $y^* = 0$.

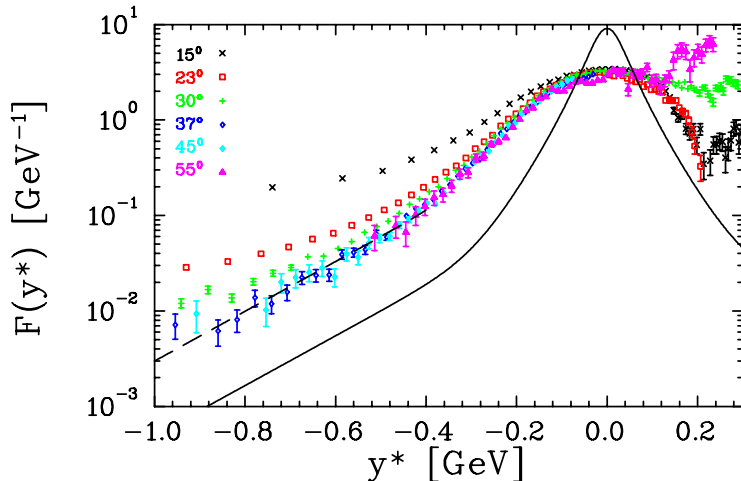


Figure 19: Extracted y^* -scaling function $F(y^*)$ for Fe [128], compared to a fit to the high- Q^2 deuterium data (solid) from Fig. 10 and a scaled up version of the high-momentum tail of the deuterium fit (dashed). Note that a model of the inelastic contributions which are significant for $y > 0$ has been subtracted to try and isolate the quasielastic contributions. Figure adapted from Ref. [128].

This situation confirms the expectation that high momentum tail of the nuclear momentum distribution is generated predominantly by NN short-range correlations. Note that use of the y_{CW} variable yields very similar results, and that for the deuteron, both y^* and y_{CW} reduce to the standard definition of y .

While these modified scaling variables produce results that are consistent with the SRC expectation, they require a model of the excitation of the residual (A-1) system. This is determined in a picture that is consistent with the initial state assumed in the SRC picture, but in both cases the correction is model dependent. This makes it difficult to use this approach to make precise, quantitative extractions. Similarly, there have been attempts to apply corrections to the scaling function, rather the scaling variable, i.e. $F(y, Q^2) = f(y, Q^2) - B(y, Q^2)$, where $F(y, Q^2)$ is the measured scaling function, $B(y, Q^2)$ is the calculated “binding correction” for the target, and $f(y, Q^2)$ is the “corrected” scaling function which can be related to the nucleon momentum distribution in the nucleus [19, 130]. Note that for the deuteron, $B(y, Q^2) = 0$ and $F(y, Q^2) = f(y, Q^2)$.

In spite of the fact that these analyses require a model-dependent correction to either the scaling variable or scaling function, they all yield results consistent with the expectations of Eq. (1), supporting the idea that the high-momentum components have a universal behavior. If this behavior is universal, then the *ratio* of cross sections in the region dominated by 2N SRCs should allow for an extraction of the relative strength of SRCs in heavy nuclei and the deuteron [43, 56, 61]. For a perfectly defined y -scaling variable, the ratio $F^A(y)/F^d(y)$ for

$|y| > k_{Fermi}$ should be constant and yield a measure of the relative contribution of SRCs in nucleus A relative to deuterium, $a_2(A, Z)$ of Eq. (1). However, the fact that a model-dependent correction in the definition of y is required for heavy nuclei may yield a modified value in the extracted ratio or introduce an artificial y dependence. Thus, we would like to compare the high-momentum tails in nuclei in a way that does not require such model-dependent corrections.

To compare the relative strength of the high-momentum tail in various nuclei, it is useful to examine the ratio of cross sections from different nuclei as a function of α_i (Eq. (7)) or, for inclusive scattering, Bjorken x (since $\alpha_i \rightarrow x$ at high Q^2). To isolate two-nucleon SRCs, one wants to be well above $x = 1$, where single nucleons with $k \lesssim k_{Fermi}$ dominate, but below $x = 2$, above which the contributions of 3N SRCs may become significant. In this region, if the underlying SRC distributions are identical, one expects to see the same x dependence in the cross section, with the ratio providing an indication of the relative contribution related to SRCs. In this case one can define the per-nucleon cross section ratio and the “isoscalar” ratio:

$$r(A, {}^2\text{H}) = \frac{\sigma_{eA}/A}{\sigma_{ed}/2}, \quad r_{iso}(A, {}^2\text{H}) = \frac{\sigma_{eA}/(Z\sigma_{ep} + N\sigma_{en})}{\sigma_{ed}/(\sigma_{ep} + \sigma_{en})}, \quad (28)$$

where $r_{iso}(A, {}^2\text{H})$ accounts for the difference between the $e-p$ and $e-n$ elastic scattering cross sections, assuming that the relative contribution of protons and neutrons in the high-momentum tail scales like the total number of protons and neutrons. This was the assumption used in most of the analyses that used the inclusive cross section ratios to extract the relative contribution of the SRCs between heavy nuclei and the deuteron. More recently, two-nucleon knock-out measurements (discussed in Sec. 8), suggested that np SRCs dominate the high-momentum tail, as one expects if the high-momentum tails are dominated by the isospin-dependent tensor interaction. A dominance of iso-singlet np pairs would yield identical proton and neutron contributions to the high-momentum tail, such that the isoscalar correction does not need to be applied, and the relative cross section per nucleon in the tails, $r(A, {}^2\text{H})$, yields a direct measure of the relative strength of the high momentum tails in the nuclei. This will be discussed more at the end of this section where we present results from these extractions.

The simple SRC model predicts that $r(A, {}^2\text{H})$ will be independent of x and Q^2 for $Q^2 \gtrsim 1.5 \text{ GeV}^2$ and $1.5 < x < 2$. The lower limit of x depends on Q^2 , and illustrated in Fig. 3, while the upper limit on x is to ensure the dominance of the 2N SRCs, which would be zero above $x = 2$ for stationary SRCs and die out rapidly above $x = 2$ after accounting for motion of the pair. In the region where scaling is observed, that is to say the ratio is independent of x and Q^2 , Eq. (1) allows us to relate the magnitude of $r(A, {}^2\text{H})$ to $a_2(A)$, the relative (to the deuteron) probability of a nucleon being part of a 2N SRC.

Examination of the ratio of high- x scattering between two nuclei has an additional advantage. As discussed in Sec. 5, if the scattering occurs from one of a pair of nucleons that is very close together, then the final state interactions between the nucleons need not fall rapidly with Q^2 and the cross section

may be sensitive to these final state interactions between nucleons in the SRC. This could lead to a modification of the cross section for both the deuteron and heavier nuclei. However, because these FSIs occur *within* the two-nucleon correlation, it is expected that they will be identical for scattering from a 2N SRC in a heavy nucleus or for scattering from a high-momentum component in the deuteron and should thus cancel in the A/D ratio. This is supported by more detailed evaluations of the space-time properties of final state interaction [58, 44], which demonstrate that the distance the struck nucleon propagates before rescattering shrinks with increasing Q^2 , and is comparable to the size of NN correlations for $Q^2 > 1 \text{ GeV}^2$ and $x > 1.5$, as discussed in Sec. 4.3.

In the PWIA, the momentum distribution in the high-momentum tail of a nucleus relative to the deuteron is $a_2 = n_A(k)/n_2(k) = (2/A)\sigma_A/\sigma_2$ for large enough x values. As discussed in Sec. 1, this reduces to $r(A, ^2\text{H}) = (2/A)\sigma_A/\sigma_{2\text{H}}$ if only isosinglet np pairs contribute, as one would expect if the tensor interaction dominates. This is under the assumption that the deuteron-like pairs in the nucleus are at rest, and thus the high-momentum tails are unaffected by motion of the 2N SRC in the nucleus. The impact of the total SRC momentum will be discussed later.

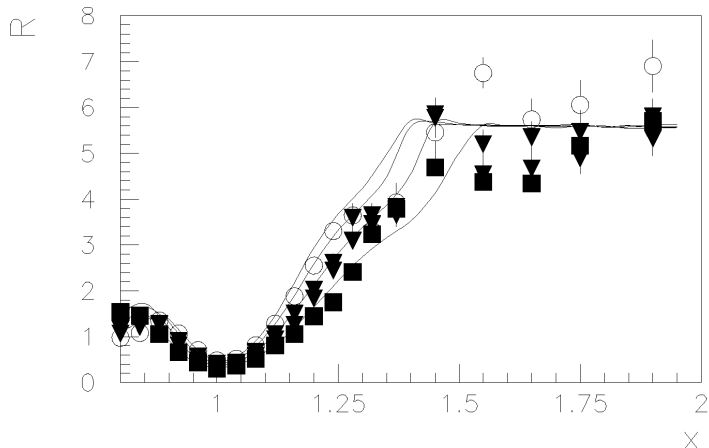


Figure 20: The x dependence of the ratio $r(A, ^2\text{H})$ for Fe nucleus for different values of $Q^2 = 1.2\text{--}2.9 \text{ GeV}^2$. The ratios and calculations are taken from Ref. [58].

One of the first extractions of $r(A, ^2\text{H})$ [58] combined cross sections from multiple SLAC data sets to construct the ratios of Eq. (28). The statistics were rather limited and the deuteron data were measured at different kinematics, so comparisons to the other nuclei required nontrivial extrapolations. The result of these analysis and a comparison with the theoretical prediction based on the 2N SRC model is given in Fig. 20. Note that in their extraction of the ratio, they applied an isoscalar correction to extract $r_{iso}(A, ^2\text{H})$ for ^3He , where the correction is large, but neglected the small correction for iron, for which they

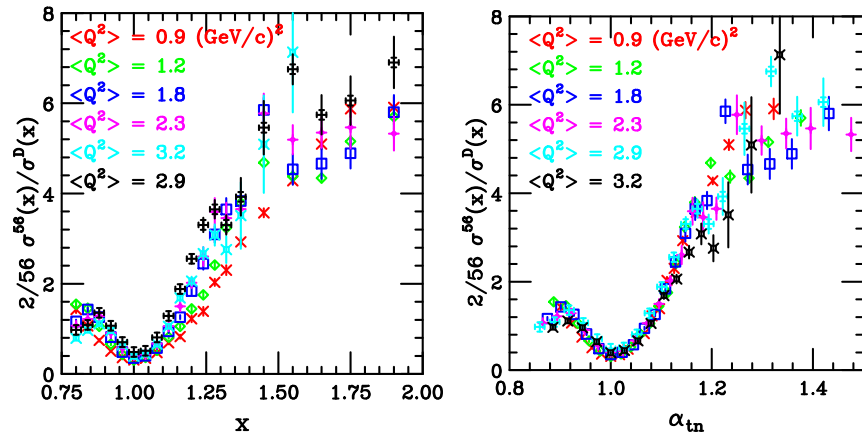


Figure 21: Ratio of Fe to ${}^2\text{H}$ for different Q^2 values, plotted as a function of x (left panel) and α (right panel) [58].

examine the ratio $r(A, {}^2\text{H})$.

As discussed in Sec. 4.2, one expects reduced Q^2 dependence if the ratio is taken as a function of α_{tn} , which is an approximation to the light cone momentum fraction of the struck nucleon based on the assumption of interaction with a nucleon from a 2N SRC. The data are shown as functions of x and α_{tn} in Fig. 21. There is a clear Q^2 dependence when taken as a function of x in the transition region between the QE peak ($x \approx 1$) and the SRC-dominated region, while this is significantly smaller when taken as a function of α_{tn} . Because α_{tn} is an approximation to the real light cone momentum α_i based on the assumption of a pair of nucleons with large relative momentum and zero total momentum, this again supports the picture of scattering from a nearly at-rest SRC.

When the SLAC measurements were published, this comparison provided the strongest indication of the existence of scaling in the ratios $r(A, {}^2\text{H})$. Subsequent experiments at Jefferson Lab [63, 91, 93, 64] provided data for deuterium and a variety of nuclei, extending to higher Q^2 with improved statistics, and confirmed the observation of scaling in the target ratios. These data allowed for further examination of the correlation between Q^2 and the x_{min} value at which scaling of the ratio is observed (Fig. 3).

Because the structure in the 2N SRC scaling region is expected to be universal, one can make similar comparisons between any two nuclei. Measurements using the CEBAF Large Acceptance Spectrometer (CLAS) in Hall B at Jefferson Lab [125, 126] looked at the ratio $r_{iso}(A, {}^3\text{He})$ (Fig. 22). The Q^2 coverage of the data made it possible to examine the onset of scaling in the 2N SRC regime, where a plateau was visible at $x > 1.4$ for Q^2 values above 1.4 GeV^2 .

Examining the ratios of heavy nuclei to ${}^3\text{He}$ also allows for an extension of these measurements out beyond $x = 2$, which may allow for the identification of high-momentum configurations involving three nucleons which share significant

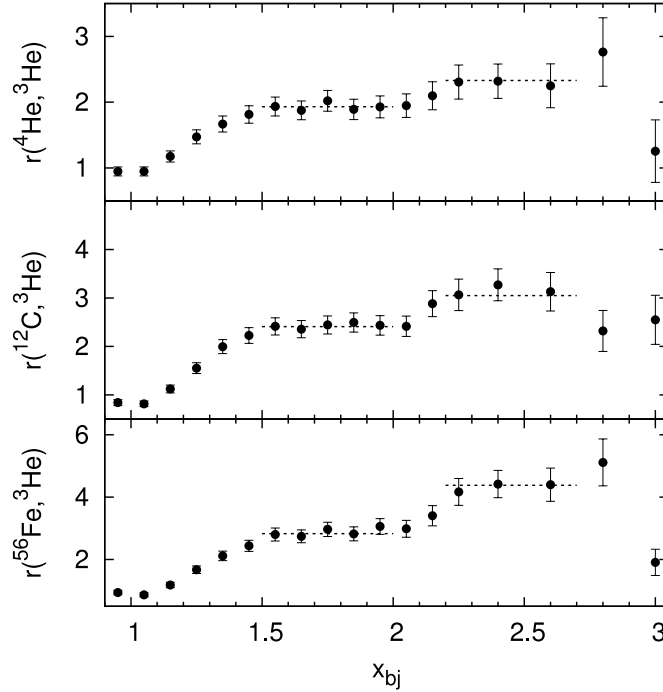


Figure 22: Cross section ratios, r_{iso} (Eq. 28)) for (a) ${}^4\text{He}/{}^3\text{He}$ (b) ${}^{12}\text{C}/{}^3\text{He}$ and (c) $\text{Fe}/{}^3\text{He}$ from Ref. [126] as a function of x_B for $Q^2 > 1.4 \text{ GeV}^2$. The horizontal dashed lines indicate the two-nucleon and three-nucleon scaling regions used to calculate the per-nucleon probabilities for two- and three-nucleon short-range correlations in nucleus A relative to ${}^3\text{He}$.

momentum (3N SRCs). While data for ${}^3\text{He}$ had been taken in previous SLAC measurements, the rapid fall of the cross sections at large x meant that the statistics for $x > 2$ were insufficient to provide a clear extraction of such ratios, although an early extraction based on preliminary cross section results was shown in Figure 8.3 of Ref. [56]. The higher statistics of the second CLAS measurement [126] provided an improved look at scaling in the $x_B > 2$ region for $Q^2 > 1.4 \text{ GeV}^2$. The data above $x = 2.25$ are consistent with a constant value, as shown in Fig. 22, which was interpreted as a dominance of 3N SRCs. Results from the recent measurement from Hall C at JLab (E02-019) [64] are compared to the CLAS data in Fig. 23. The new data are in excellent agreement with the CLAS measurement in the 2N SRC region, and differ slightly near the QE peak due to the lower momentum resolution of the CLAS measurement. Both extractions have limited statistics, but the Hall C data show a significantly larger ratio for $x > 2$. The Hall C data in this region are taken at $Q^2 \approx 2.9 \text{ GeV}^2$, while the CLAS data cover a wide range in Q^2 with an average Q^2 value near 1.6 GeV^2 , suggesting that the CLAS data may be too low in Q^2 to cleanly isolate the signature of 3N SRCs. However, the preliminary results from the

early SLAC measurements (Figure 8.3 of Ref. [56]) show no indication of a Q^2 dependence from 1 to 2.4 GeV², and yield a ratio in between the two JLab measurements.

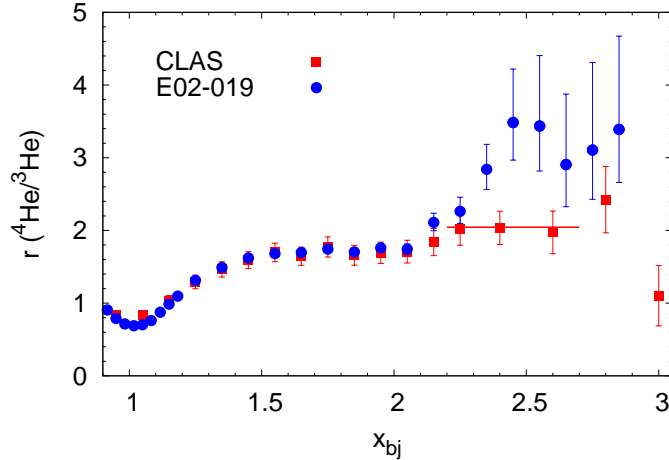


Figure 23: Comparison of the $^4\text{He}/^3\text{He}$ ratios from CLAS [126] and E02-019 [64]. Note that the isoscalar correction has been removed from the CLAS ratios, and both data sets represent the direct ratio of the measured cross section per nucleon.

Unfortunately, none of these measurements have data with sufficient statistics and Q^2 range to precisely determine the kinematics at which scaling sets in. The difference could be related to a true Q^2 dependence in the ratio or an inconsistency between the measurements. While $Q^2 = 1.4$ GeV² is sufficient to observe scaling in the 2N SRC region, it is not as clear what x and Q^2 values are required to isolate 3N SRC contributions. From Fig. 3, we observe that for $Q^2 = 1.5$ and $x > 1.5$, the minimum initial nucleon momentum is above 250 MeV/c, and thus one expects the single-particle contribution to the momentum distribution, dominant at $k < k_{Fermi}$, to be strongly suppressed. So it is not surprising that 2N SRC contributions dominate in this region. However, it is not clear what p_{min} value is required for the 2N SRC contributions to be strongly suppressed, and it may be that a larger Q^2 value is required to isolate 3N SRC contributions. An experiment was recently completed [131] that focused on the $x > 2$ regime with the goal of mapping out the x and Q^2 dependence with sufficient precision to confirm the onset of scaling and determine the scaling threshold in the 3N SRC regime.

As mentioned above, one can use the cross section ratio in the 2N SRC regime to determine the contribution of two-nucleon correlations in heavy nuclei relative to the contribution in the deuteron. In Ref. [126], the probability of a nucleon-nucleon correlation in the deuteron was taken to be the fraction of the deuteron momentum distribution above $k = 275$ MeV/c. These are momenta

that have been shown in $\vec{D}(\vec{e}, e'p)$ asymmetry measurements to be dominated by highly correlated nucleons [85]. Based on a calculation of the deuteron structure [10], they find that $(4.1 \pm 0.8)\%$ of the time, the nucleons in deuterium had $k > 275$ MeV/c, and were thus assumed to be in a short-range, high-momentum configuration. Taking this as a measure of the contribution of 2N SRCs in deuterium, and using the cross section ratios in the plateau region as a measure of the relative contribution of 2N SRCs in heavier nuclei, one can extract the absolute contribution for the nuclei where $r(A, ^2\text{H})$ measurements exist. One can also combine the CLAS $r_{iso}(A, ^3\text{He})$ measurements with a measured or calculated value for $r(^3\text{He}, ^2\text{H})$. The latter was taken to be $r(^3\text{He}, ^2\text{H})=1.97 \pm 0.1$ based on the average of the SLAC extraction [58] (1.7 ± 0.3), and a calculated value [36] (2.0 ± 0.1).

A similar extraction of the contribution of 3N SRCs was also performed, yielding a contribution of less than 1% for carbon or iron [126]. However, as noted above, it is not clear at this point if this measurement was able to isolate the 3N SRC contributions, and the more recent data [64] suggest a larger contribution from 3N SRCs.

In extracting relative contributions of SRCs from the cross section ratios, it is assumed that final state interactions do not modify the ratios in the scaling region. This is expected to be valid for sufficiently high Q^2 , as interactions between the struck nucleon and spectators at large distance scales will fall rapidly with Q^2 , and interactions with nucleons that are very close (i.e. the other nucleon(s) in the SRC) should be identical for SRCs in light or heavy nuclei, and thus cancel in the ratio. While we expect that FSI contributions should not impact these extractions, a more quantitative evaluation, especially for the data at modest Q^2 values, would be worthwhile.

At this point, we reiterate that, except for the recent extraction from the Hall C measurement at 6 GeV [64], these extractions are based on the simple SRC model, where the scattering is assumed to have occurred from a nucleon in a stationary 2N (or 3N) SRC, where the 2N SRCs are assumed to be isospin-independent and thus of equal importance for pp, np, and nn pairs. In reality, the SRCs have small but non-zero total momentum and the NN potential that generates the bulk of the high-momentum pairs is strongly isospin-dependent and accounting for this will modify the results for the extracted 2N and 3N SRC probabilities. These effects require corrections to the standard extraction of the probability of nucleons being found in SRCs in nuclei.

First, these values were obtained from measurements of $r_{iso}(A, ^3\text{He})$, as defined in Eq. (28), which assumes that the contribution of high-momentum protons and neutrons scales with Z and N . For the case of isoscalar dominance, the tensor interaction is the primary source of high momentum nucleons, and so only np SRCs are formed. In this case, the neutron and proton have equal high-momentum distributions and this correction should not be applied. Note that using the raw $r(A, ^3\text{He})$ ratio means assuming total dominance of np pairs, while calculations and the triple-coincidence measurements yield small but non-zero contributions from iso-triplet pairs. Thus, while using the uncorrected ratio is a much better approximation than using $r_{iso}(A, ^2\text{H})$, it is probably a small

underestimate of the more true value.

Table 1 includes values for $r(A, {}^3\text{He})$ as published (with the isoscalar correction), and with the isoscalar correction removed. The raw cross section ratios are 15–18% below the values with the isoscalar correction applied. If the conversion from $A/{}^3\text{He}$ ratios to $A/{}^2\text{H}$ ratios had been done using the measured ${}^3\text{He}/{}^2\text{H}$ ratio from SLAC, which applied the same isoscalar correction to ${}^3\text{He}$, then only the small factor applied to the non-isoscalar Fe target would have to be removed. However, in the analysis of Ref. [126], the value used is $r({}^3\text{He}/{}^2\text{H})=1.97$, which is mainly based on a calculated ratio [36] and which does not include the isoscalar correction factor applied in the $A/{}^3\text{He}$ measurements. Note that the SLAC results quoted for ${}^3\text{He}$, $r_{iso}({}^3\text{He}/{}^2\text{H})=1.7\pm 0.3$ correspond to an uncorrected ratio of $r({}^3\text{He}/{}^2\text{H})=2.0\pm 0.3$, in good agreement with the calculation of Ref. [36].

Table 1: Shown are the average ratios, $r(A/{}^3\text{He})$ for the scaling regions $1.5 < x_B < 2$ from the CLAS data as published [126], and after removing the isoscalar correction that was applied (“raw”). For the CLAS data, the $A/{}^3\text{He}$ cross section ratio is converted to $A/{}^2\text{H}$, taking $r({}^3\text{He}/{}^2\text{H})=2.0$ as extracted from the raw ${}^3\text{He}/{}^2\text{H}$ data from SLAC [58] (no isoscalar correction) or the calculation of Ref. [36]. $R_{2N}(A)$ is extracted from the $r(A, {}^2\text{H})$ by applying a correction for the CM motion of the pair as estimated in Ref. [64], which yields a relative 2N SRC contribution 10–20% lower than the raw cross section ratio.

	$r_{iso}(A/{}^3\text{He})$ (published)	$r(A/{}^3\text{He})$ (raw)	$R_{2N}(A)$ CLAS	$R_{2N}(A)$ SLAC	$R_{2N}(A)$ E02-019
${}^3\text{He}$	-	-	-	1.8 ± 0.3	1.93 ± 0.10
${}^4\text{He}$	1.93 ± 0.17	1.69 ± 0.15	2.85 ± 0.29	2.8 ± 0.4	3.02 ± 0.17
${}^9\text{Be}$	-	-	-	-	3.37 ± 0.17
${}^{12}\text{C}$	2.49 ± 0.15	2.11 ± 0.18	3.55 ± 0.35	4.2 ± 0.5	4.00 ± 0.24
Fe(Cu)	2.98 ± 0.18	2.38 ± 0.19	3.96 ± 0.38	4.3 ± 0.8	(4.33 ± 0.28)
Au	-	-	-	4.0 ± 0.6	4.26 ± 0.29

Once we have removed the isoscalar correction, the results in Table 1 represent the raw $A/{}^3\text{He}$ per-nucleon cross section ratio, which should correspond to the relative strength in the high-momentum tails. If the 2N SRC is at rest, then the relative strength in the high-momentum tails corresponds to the relative probability for a nucleon to be in a 2N SRC. If we relax this constraint, and allow for the pair to have a non-zero total momentum, then the direct connection between the high-momentum contribution and the relative strength of SRCs is broken. The high-momentum tail of the deuteron-like pair can be “smeared” by the pair motion, yielding an overall increase in the high-momentum tails. Note that this is a real enhancement of the high-momentum tails in the nucleus, so the ratio still provides a direct measure of the tail of the momentum distribution. This correction simply separates the enhancement of the high-momentum tail into a relative probability of finding SRCs in the nucleus and an enhancement of the SRC high-momentum tail due to motion of the pair.

The smearing effect was expected to be $\sim 20\%$ for heavy nuclei [10]. While this effect is discussed in Ref. [126], no correction or uncertainty is applied when extracting the relative 2N SRC contribution from the ratios. In the analysis

of the E02-019 data [64], a correction for the impact of the CM motion is applied when extracting the relative contribution of 2N SRCs. Table 1 shows the SLAC, CLAS, and E02-019 data extractions of $R_{2N}(A)$ which is the ratio $r(A, ^2\text{H})$ with the CM correction ($(20\pm 6)\%$ for iron) removed, and is related to the relative number of SRCs, as opposed to their relative contribution to the high-momentum tails. The same correction is applied to all experiments, and the CLAS ratios are converted from $r(A, ^3\text{He})$ to $r(A, ^2\text{H})$ taking $r(^3\text{He}/^2\text{H})=2.0$.

The question of the isospin structure of the 2N SRCs has been examined in recent triple-coincidence reactions, discussed in Sec. 8, and will be further studied in inclusive scattering from nuclei of similar mass but with different N/Z ratios, e.g. recent measurements of ^{40}Ca and ^{48}Ca at Jefferson Lab [131] and future measurements planned for ^3H and ^3He . It is less clear what impact this would have in the $x > 2$ regime, where one is attempting to isolate 3N SRCs.

While there are still some issues to be resolved, the significant body of inclusive data already taken demonstrates that it is feasible to kinematically isolate scattering from 2N SRCs. We have mapped out the strength of the 2N SRCs as a function of A for several nuclei. The inclusion of ^9Be in the most recent measurement [64] demonstrates an anomalous behavior in the A dependence of the strength of the 2N SRC contributions. For non-interacting nucleons, one would expect that the probability for two nucleons to be close enough to interact via the short-range tensor or repulsive core of the NN interaction would be proportional to the nuclear density. However, while ^9Be is a very low density nucleus, comparable to ^3He , the extracted value of $R_{2N}(A)$ is much larger, on par with the significantly denser ^4He and ^{12}C . This is similar to the behavior observed in measurements of the EMC effect in these same light nuclei [132], which was interpreted as an effect of the strong cluster structure in ^9Be . One would expect a similar effect here, where clustering among the nucleons in the nucleus will yield an increase in the fraction of the time that nucleons are close together, even though the average density can be very low if the clusters are spread apart. Thus, this observation reinforces the interpretation of the A dependence of the EMC effects.

While the results from the initial extension of inclusive measurements to the three-nucleon correlation region have yet to demonstrate a clear sensitivity to 3N SRC, a recently completed experiment [131] will address this question in detail. Future inclusive measurements will map out the strength of 2N and 3N SRCs in a large set of light and medium nuclei [133]. These data may also be able to provide information on the isospin structure of three-nucleon configurations by comparing ^3H to ^3He [134]. While the isospin structure of the 3N SRC is well defined for these nuclei, if the momentum sharing is not identical for the singly- and doubly-occurring nuclei, one will see a modified ratio in the 3N SRC region.

However, while we have learned a great deal from these inclusive measurements, more complex reactions, in which one or more nucleons from the SRC are detected, are important for providing more detail on the structure of the hadrons and additional information on questions such as the center-of-mass motion and isospin structure of the SRCs. These issues will be discussed in the

next sections.

7. Semi-Inclusive A(e,e'N) Knock-out Reactions beyond the Deuteron

Semi-inclusive A(e,e'N) reactions on nuclei, in which the struck nucleon is detected in coincidence with the scattered electron, provides the next highest level of complexity along with new details of the SRC structure. The conditions required for isolation of the structure of SRCs are discussed in Sec. 4.4. While inclusive reactions within the PWIA framework can provide some information about the momentum distribution of the nucleon, semi-inclusive reactions can, in principle, fully probe the nuclear spectral function. In the PWIA, the spectral function is related to the measured cross section as follows [98]:

$$\frac{d\sigma}{d\Omega_{e'}dE_{e'}d^3p_NdE_m} = \frac{F_N}{F_A}\sigma_{eN} \cdot S_A(p_m, E_m) , \quad (29)$$

where F_A is the nuclear flux factor and F_N is the flux factor calculated for moving bound nucleon with momentum $\vec{p}_i = -\vec{p}_m$, and σ_{eN} is the cross section for scattering from the bound nucleon. Within the PWIA, the nuclear spectral function, $S(p_m, E_m)$, can be related to the ground state (ψ_A) and residual (ϕ_{A-1}) nuclear wave functions as follows:

$$S_A(p_m, E_m) = | \langle \psi_{A-1} | \delta(H_{A-1} - E_m) a(p_i) | \psi_A \rangle |^2 , \quad (30)$$

where $a(k)$ is an annihilation operator for the nucleon with momentum k . Several remarkable properties of the spectral function define the specific utility of the semi-inclusive reactions:

- The cross section is sensitive to the composition of the (A-1) residual state through the reconstruction of the missing energy, E_m . This provides a measure of the excitation of the residual system, allowing us to separate a one-body spectator system consisting of an (A-1) nucleus (ground state or excited state) or a multi-body final state.
- For the case of the coherent (A-1) state, the parameter E_m represents the nucleon removal energy of the particular nuclear shell.
- At a fixed value of E_m associated with a specific nuclear shell, the p_m dependence of the spectral function is related to the momentum distribution of the nucleon in the given nuclear shell.
- The occupation number of the given shell (labeled α) can be extracted:

$$n_\alpha = \int_{\Delta E_m} \int S(p_m, E_m) d^3p_m dE_m , \quad (31)$$

where integration over the E_m covers the missing energy width of the given nuclear shell.

Historically the measurements of the occupation number in Eq. (31) [8, 9] gave the first glimpse of the role that correlations play in the redistribution of probabilities in the ground state nuclear wave functions. Namely the experimental measurements revealed a substantial missing strength in the values of n_α for all shells over a range of nuclei, which was attributed in part to the short-range interaction of the nucleon at the given shell.

Probing SRCs directly in high- Q^2 A(e,e'N) reactions requires of taking the spectral function to large values of missing momentum ($p_m > k_{Fermi}$) and energy ($E_m > 100$ MeV). In this case, E_m characterizes the nucleon removal energy in the continuum (rather than particular nuclear shell). From the practical point of view, the more relevant quantity will be the nuclear recoil energy E_R defined in Sec. 4.4. The advantage of considering E_R is that the most prominent and new signature of SRCs in coincidence reactions (as compared to the inclusive scattering) is the correlation relation between E_R and missing momentum p_m according to Eq. (17):

$$E_R \approx \sqrt{m_N^2 + p_m^2} - m_N . \quad (32)$$

Note however that this is merely a kinematical correlation and its observation only indicates the dominance of the two-body currents, but not necessarily 2N SRCs. Such a correlation was observed for example in ${}^4\text{He}(e,e'p)$ data at NIKHEF [135, 136] at $Q^2 = 0.34$ GeV². However, the theoretical analysis demonstrated that the strength of the cross section was dominated by the long range two-body currents such as MEC and IC.

To go beyond the correlation relation of Eq. (32) and probe the part of the spectral function dominated by SRC, the factorized relation between the electron-nucleon cross section and the spectral function must be valid. For A(e,e'p) scattering, this factorization was studied in Ref. [137, 138] and it was demonstrated that in the limit of $Q^2 \gg p_i^2$, Eq. (29) is valid, even when including final state interactions within the eikonal approximation. The FSI do not become negligible, even at very large Q^2 , and so detailed experimental and theoretical studies, such as the deuteron measurements discussed in Sec. 5 are critical. While significant FSI always remain, their implementation is simplified at high energy. In this case the spectral function is defined within the distorted wave impulse approximation (DWIA) ($S_A^{DWIA}(p_m, E_m, q)$) and depends strongly on the relative angle of \vec{p}_m and \vec{q} (see e.g. Ref. [137] and Figs. 15 and 16). The advantage of the DWIA is that if its application is justified, then one can use the knowledge of σ_{eN} obtained from the studies of exclusive D(e,e'N)N reaction (Sec. 5) at given virtuality of the bound nucleon to extract $S_A^{DWIA}(p_m, E_m, q)$ from Eq. (29).

The first measurement of high- Q^2 semi-inclusive reactions at p_m values corresponding to probing SRCs was performed at Jefferson Lab using a ${}^3\text{He}$ target. Measurements of the ${}^3\text{He}(e,e'p)D$ and ${}^3\text{He}(e,e'p)pn$ reactions were taken in Hall A with a beam energy of 4.8 GeV, for $Q^2 = 1.5$ (GeV/c)² and $x_B \approx 1$. When this experiment was proposed, it was expected that these kinematics would cleanly isolate short-range correlations at missing momenta greater than 300 MeV/c.

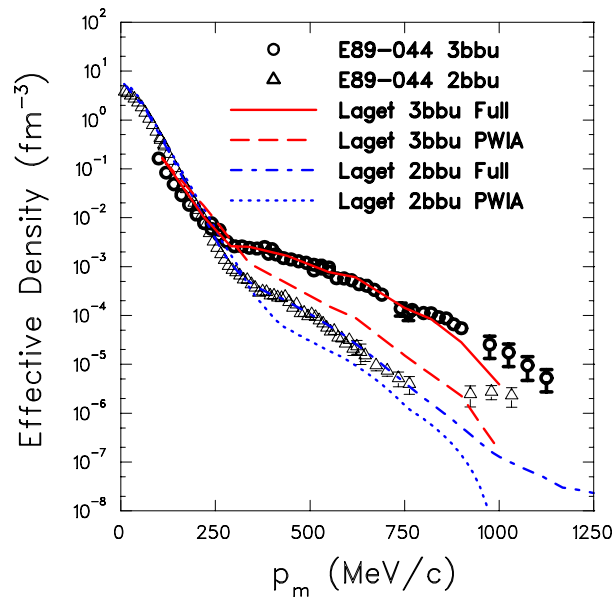


Figure 24: Proton effective momentum density distributions extracted from ${}^3\text{He}(e,e'p)pn$ three-body break-up (3bbu - open black circles) and the ${}^3\text{He}(e,e'p)D$ two-body break-up (2bbu - open black triangles) [139]. The 3bbu integration covers E_M from threshold to 140 MeV. The curves are calculations from J.-M. Laget [103] which show dominance of the continuum cross section at large missing momentum, along with strong FSI contributions. Figure reprinted with permission from Ref. [139]

What was observed was a much greater strength in the high missing momentum region than expected [139, 140] as shown in Fig. 24. In this figure, the three-body break-up (3bbu) has been integrated over missing energy so that it could be plotted together with the two-body break-up (2bbu) and the strengths of the two reactions compared. The measurements clearly demonstrated the dominance of the three-body break-up channel at high p_m , as expected in the SRC picture.

One important result of this measurement was that it demonstrated the validity of the eikonal approximation in calculating the final state interaction, which provides the dominant contribution at high p_m . The enhanced cross section was explained as an interference between correlations in the initial state and final-state interaction [103], where neither effect alone could explain the observed cross section. Subsequently, calculations within the generalized eikonal approximation (GEA) [141, 142, 143, 144] which used the realistic spectral function of Ref. [115], in which correlations are included in a self-consistent fashion, achieved a parameter-free description of the data.

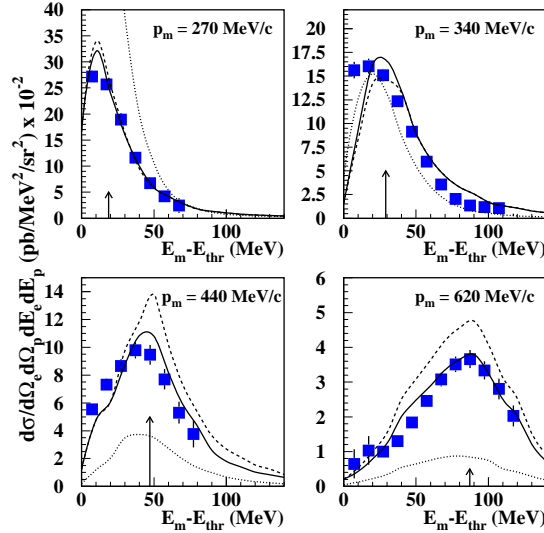


Figure 25: The dependence of the differential cross section on the missing energy for ${}^3\text{He}$ three-body break-up reactions at different values of initial nucleon momenta (p_i from Eq. (15)). Dotted, dashed and solid curves corresponds to PWIA, PWIA + single rescattering and PWIA + single + double rescatterings [138, 137]. Data are from Ref. [139]. Arrows define the correlation according to Eq. (32). Similar description of the data is achieved in Refs. [142, 103]. Figure reprinted with permission from Ref. [44]

Another important result of the above mentioned measurements is that in the three-body break-up channel, the clear correlation between E_R and p_m of Eq. (32) is observed, as seen in Fig. 25. The comparison of theoretical calcula-

tions based on generalized eikonal approximation within DWIA [138, 137] with the data of Ref. [139] demonstrated that the large contribution from final state re-interaction not only preserves the pattern of the correlation of Eq. (32) but actually reinforces it. This indicates a rather new phenomenon, that in high energy kinematics sensitive to SRC, FSI is dominated by single rescattering of the struck nucleon with a spectator nucleon from the SRC. As a result, this rescattering does not destroy the correlation structure of the spectral function, as it is related to 2-body interactions contained within the SRC. The validity of this assertion is crucial for understanding the role of the FSI in the x -scaling of the inclusive cross section ratios at $x > 1$ (Sec. 6). If FSI is confined within the SRC, then it will cancel out in the ratios of Eq. (28) without distorting the factorization of the 2N SRC from the (A-2) residual nuclear system.

The fact that the eikonal approximation provides a satisfactory description of the data for Q^2 as low as 1.5 GeV^2 demonstrates the feasibility of working in a well understood kinematic region with experimentally feasible kinematic restrictions. To suppress the absolute magnitude of FSI in the semi-inclusive cross section, one requires similar kinematic restrictions to those discussed in Sec. 4.4 (see also Refs. [145, 146]). The study of the issue of the suppression in the final state interaction at $x > 1$ kinematics within generalized eikonal approximation [108, 46] demonstrated that an additional restriction needs to be imposed on measured magnitudes of missing momentum and recoil energy E_R such that:

$$|p_m| - \frac{q_0}{|q|} E_R > k_{Fermi} . \quad (33)$$

Thus it will be very important to extend the $^3\text{H}(e,e'p)$ experiments to the $x > 1$ domain, which will allow us to verify the prediction of FSI suppression. Equation (33) is a consequence of the eikonal regime of FSI, and no such condition exists for FSI at low energy. In the high- Q^2 region where the eikonal regime is established, A($e,e'p$) experiments will be able to verify that this condition is sufficient. If so, then it should be possible to extract the spectral function in a region where FSI are small and can be reliably calculated.

In Jefferson Lab's Hall C, A($e,e'p$) measurements done in parallel kinematics determined the strength of the high momentum region instead of simply inferring it from the absence of the strength seen in the low missing momentum region. This was the first proton knock-out measurement aimed at extracting the high-momentum component at kinematics where the corrections to the PWIA appear to be small. However, because of the $x < 1$ kinematics probed in this reaction, the large missing energy range was restricted due to inelastic contributions (as seen in Fig. 3 of Ref. [147]). Nonetheless, the observed strength at large p_m in the region that was free of large contributions from other reactions was found to be in reasonable agreement with the theoretical expectation [148, 149]

Comprehensive studies of semi-inclusive reactions on light nuclei at $x > 1$ kinematics are crucial for extending such measurements reliably to medium to heavy nuclei. At present, there are two approaches being used to further these measurements. Some experiments have been performed in kinematics

which minimize the reaction mechanism effects in order to focus on probing the structure of the SRCs, while others are aimed at better understanding the FSI, MEC, and IC, so that models of these contributions can be constrained well enough to reliably correct for such effects in kinematics optimized to reduce their impact. To date, the studies focused on more fully understanding the reaction mechanism have focused on the deuteron [109, 114, 116], with some additional measurements on ^3He [139, 140].

8. Triple-coincidence Reactions

A newer approach to resolving the detailed structure of short-range correlations involves making nucleon-knockout measurements in which two outgoing nucleons are detected, either in photo-nuclear reactions [150] or in coincidence with the scattered electron in electroproduction reactions [151, 152, 153, 154]. For most of these initial measurements, two protons were detected so as to minimize meson exchange effects, since only neutral mesons can be exchanged between two protons. However, since the energy and momentum transfer were only few hundred MeV, it was practically impossible to distinguish the struck and recoil nucleons. Theoretical studies of these reactions demonstrated that in fact the dominant contribution comes from a two-step processes where there is an electromagnetic interaction with one proton, with the second proton knock-out coming from IC or FSI effects [155, 156, 157]. Even though these reactions demonstrated sensitivity to high momentum component of the nuclear wave function [158], the SRC evidence was indirect and the dominant mechanisms were final state interactions and long-range nucleon correlations [159]. It is interesting to note that two-nucleon knock-out reactions in which the outgoing nucleons carry approximately same momenta are produced mainly due to the final state interactions, even in the large momentum transfer region [160, 161, 162].

Thus, the kinematics which can maximize the contributions from SRC should correspond to the “asymmetric” situation in which one nucleon (final momentum p_N) can be identified as a struck nucleon with momentum close to the large (few GeV/c) momentum transfer and the another (final momentum p_r) identified as the recoil (spectator) nucleon from within the SRC, with momentum exceeding characteristic Fermi momentum of the nucleus, but well below the scale of the momentum transfer, as discussed in Sec. 4.5.

In this case, one can characterize the $A(e,e'N_N N_r)$ cross section in the PWIA as follows:

$$\frac{d\sigma}{d\Omega_{e'} dE_{e'} d^3p_N dd^3p_r} = \frac{F_N}{F_A} \sigma_{eN} \cdot D_A(p_i, p_r, E_r) , \quad (34)$$

where the decay function $D_A(p_i, p_r, E_r)$ [56, 137, 44] :

$$D_A(p_i, p_r, E_R) = | \langle \psi_{A-1} a^\dagger(p_r) | \delta(H_{A-1} - (E_R - T_{A-1})a(p_i) | \psi_A \rangle |^2 , \quad (35)$$

describes the probability that after a nucleon with momentum p_i is instantaneously removed from the nucleus, the residual (A-1) nucleon system will have excitation energy $E_m = E_R - T_{A-1}$ and contain a nucleon with momentum

p_r . The integration of this function by d^3p_r represents the part of the nuclear spectral function (Eq. (30)) corresponding to the case of the break-up of (A-1) residual nucleus with at least one nucleon in the continuum. Note that, as in the case of A(e,e'N) reactions, if factorization of the nucleon electromagnetic current is justified then the decay function can be generalized within the DWIA to account for the final state interaction effects.

If a 2N SRC is probed, one of the prominent signatures will be that the decay function will exhibit strong correlation between p_i and p_r , peaking at

$$\vec{p}_i \approx -\vec{p}_r, \quad (36)$$

as discussed in Sec. 4.5. The first attempt to probe such angular correlation was made in the two-proton knockout experiment of Ref. [152] in which the $^{12}\text{C}(e,pp)X$ cross section was measured as a function of relative angle of two outgoing protons for parallel kinematics. Even though theoretical calculations showed sensitivity of the angular function to the SRCs, no clear correlation signature was observed due to impossibility of separating struck and spectator proton in low momentum transfer kinematics.

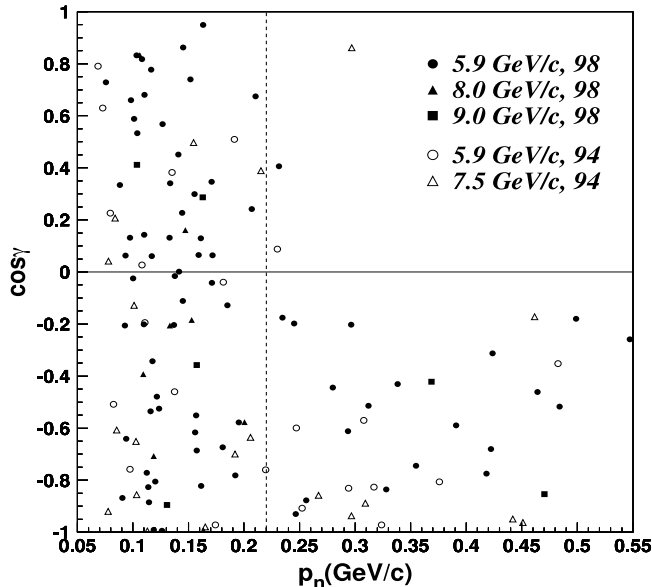


Figure 26: The correlation between the magnitude of the recoil neutron momentum p_n and its direction γ relative to \vec{p}_i . The legend gives the initial proton beam momentum and year of the run, with hollow points (labeled 94) from Ref. [163] and solid points (labeled 98) from Ref. [164]. In all cases, no angular correlation is observed for neutron momenta less than k_{Fermi} , while neutrons with larger momentum are produced preferably in the backward hemisphere of the reaction.

The first time such an angular correlation was observed unambiguously in the high momentum transfer regime was the $p + ^{12}\text{C} \rightarrow p + p + n + X$ measure-

ment of E850 at Brookhaven National Lab [163, 164]. The experiment looked for recoil neutrons produced in coincidence with single proton knockout, and the results are shown in Figure 26. Neutrons with momenta p_n below the Fermi momentum were uniformly distributed in $\cos\gamma$, where γ is the angle between the neutron momentum and the reconstructed initial momentum of the struck proton, p_i . Neutrons above the Fermi momentum were almost exclusively observed for $\cos\gamma < 0$, i.e. opposite to the direction of \vec{p}_i . This is consistent with the assumption that high-momentum nucleons are the results of SRCs, in which the two nucleons have large relative momenta but a small total momentum, and thus have initial momenta that are large and back-to-back. Using the data from Ref. [164], they extracted the probability that a neutron with $p_n > 220$ MeV/c $\approx k_{Fermi}$ is found in association with a proton with $p_i > 220$ MeV/c, after correcting for acceptance and efficiency. They determined that $(49 \pm 13)\%$ of events with a fast proton had an associated backwards-going fast neutron.

This is essentially the probability that the fast recoil neutron is observed in coincidence with the fast proton. However, a pn pair with large relative momenta may not yield a high-momentum neutron in the final state; the neutron could be reabsorbed as it passes through the nucleus or the pn pair might be moving in the mean field of the (A-2) nucleus such that the final neutron momentum in the rest frame of the nucleus is below k_{Fermi} . A more detailed analysis of the above experiment was made in Ref. [165], which was based on the modeling of the spectral and decay functions of the reaction within the light-cone approximation [166]. This analysis allowed for an extraction of the quantity $P_{pn/pX}$, which represents the underlying probability of finding a pn correlation in the "pX" configuration that is defined by the presence of at least one proton with $p_i > k_{Fermi}$. The analysis was similar to that of Ref [164], except that only events with nucleons above 275 MeV/c were examined, to be more clearly in the region where SRC are expected to dominate, and corrections were applied to account for the possibility that the high-momentum nucleons might not be observed in the final state, yielding

$$P_{pn/pX} = 0.92_{-0.18}^{+0.28}, \quad (37)$$

This result indicates that the removal of a proton from the nucleus with initial momentum 275 – 550 MeV/c is accompanied by the emission of a correlated neutron that carries momentum roughly equal and opposite to the initial proton momentum $92_{-18}^{+8}\%$ of the time (where the upper limit is simply truncated to ensure that the maximum value for this quantity is 100%).

Even though no recoil protons were measured in the experiments of Ref. [163, 164], it was possible to estimate the upper limit for the ratio of probabilities of pp and pn SRCs [165], using the relationship $2P_{pp} + P_{pn} \leq P_{pX}$, where P_{pp} has an additional factor of two in the weight as it will yield a "pX" configuration with a high momentum proton if either of the protons is initially at the appropriate kinematics to be detected when struck by the beam proton. This leads to:

$$P_{pp/pX} \leq \frac{1}{2}(1 - P_{pn/pX}) = 0.04_{-0.04}^{+0.09}, \quad (38)$$

where the upper limit occurs if all configurations with a detected high-momentum proton are associated with a high-momentum spectator nucleon and the lower limit corresponds to no pp pairs⁶. Note that $P_{pp/pX}$ does *not* correspond to the probability that an observed high-momentum proton would have an associated high-momentum recoil proton because it applies the factor of two weighting to pp pairs based on the assumption that for a finite acceptance experiment, you will “double count” the pp SRCs since either proton can be the high- p_m proton. Therefore, $P_{pp/pX}$ is half of what would be observed in a direct measurement, and has an upper limit of $P_{pp/pX} = 0.5$ if only pp SRCs are present.

By making triple-coincidence measurements where both recoil proton and neutrons are detected, one can more directly probe probability that a high-momentum nucleon is associated with an SRC and extract the isospin structure of SRCs in the nucleus. Such measurements were carried out for the first time in at Jefferson Lab [167, 168] where scattered electrons and knocked-out protons were detected in coincidence, with a large acceptance detector used to look for an associated recoil proton or neutron in $^{12}\text{C}(e,e'pN)$ reactions.

The Hall A triple-coincidence experiment used an incident electron beam of 4.627 GeV and the two Hall A high-resolution spectrometers (HRS) [169] to identify the $^{12}\text{C}(e,e'p)$ reaction. The $^{12}\text{C}(e,e'p)$ kinematics were chosen such that the measurement was at $Q^2 \approx 2 \text{ GeV}^2$ and $x \approx 1.2$, with missing momenta from 300–600 MeV/c. The BigBite [170] large-acceptance spectrometer was used to detect recoil protons with $\vec{p}_r \approx -\vec{p}_m$ from $^{12}\text{C}(e,e'pp)$ events, while a neutron detector placed behind BigBite was simultaneously used to detect recoil neutrons from $^{12}\text{C}(e,e'pn)$ reactions.

Reaching sufficiently large values of Q^2 and Bjorken- x was required to reduce MEC and IC contributions as well as moderating the effect of the FSI (see discussion in Sec. 7), while the p_m range was chosen to map out the region of 2N SRC dominance. A cut was applied to the missing energy reconstructed from the $^{12}\text{C}(e,e'p)$ kinematics which significantly suppressed the contribution associated with the excitation of an intermediate Δ resonance [167].

The first signature of SRCs was the correlation between strength of the cross section and the relative angle (γ) between initial momentum of the struck nucleon p_i and momentum of the recoil nucleon p_r . Figure 27 shows the distribution of events in $\cos\gamma$ for the highest p_m setting of 550 MeV/c [167], which is strongly peaked near $\cos\gamma = -1$, corresponding to the back-to-back initial momenta of the struck and recoil protons. The solid curve is the simulated distribution for scattering from a moving pair, with the pair center-of-mass momentum taken to be a gaussian distribution with a width of 0.136 GeV/c. That width was varied to best reproduce the data, but is also consistent with the width deduced from the (p,ppn) experiment at Brookhaven National Lab [164] as well as a theoretical calculation based on the convolution of two independent single particle momentum distributions [10]. Also shown in Fig. 27 is the

⁶In Ref. [165], this expression was assigned to P_{pp}/P_{pn} rather than $P_{pp/pX}$, but these quantities differ only by a factor of $P_{pn/pX}$, which is close to unity in this case.

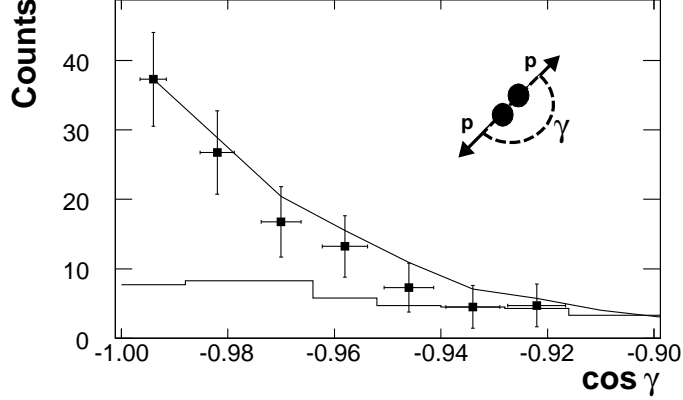


Figure 27: For the $^{12}\text{C}(e,e'\text{pp})$ reaction at $Q^2 > 1$ $(\text{GeV}/c)^2$, the distribution of the cosine of the opening angle between the \vec{p}_{miss} and \vec{p}_{rec} for the $p_m = 0.55$ GeV/c setting. The curve is a simulation of the scattering off a moving pair with a width of 0.136 GeV/c for the pair center-of-mass momentum and the histogram shows the distribution of random events. Figure reprinted with permission from Ref. [167]

angular correlation for the random background as defined by a time window offset from the coincidence peak, which shows the effect of the acceptance of the spectator proton detector.

The other main quantity of interest for the two-proton knockout case is the fraction of high- p_m events in which there is a high-momentum, backward-angle correlated proton, i.e. the ratio of $^{12}\text{C}(e,e'\text{pp})$ to $^{12}\text{C}(e,e'\text{p})$ events. The measured ratio must be corrected to account for the finite acceptance of BigBite. This is done using a PWIA simulation of events for scattering from a pp SRC with a total pair momentum distribution obtained from the measured angular correlation. The raw and acceptance-corrected $^{12}\text{C}(e,e'\text{pp}) / ^{12}\text{C}(e,e'\text{p})$ ratios are shown in Fig. 28. It was observed that for $300 < p_m < 600$ MeV/c , approximately 9% of the $^{12}\text{C}(e,e'\text{p})$ events had a high-momentum recoil proton with $\vec{p}_r \approx -\vec{p}_m$, independent of the value of p_m within this region. The shaded region indicates the range of results obtained by varying the width of the pair momentum distribution within the $\pm 2\sigma$ range on the extracted width. Averaged over the entire p_m range and accounting for the experimental uncertainties and impact of the pair motion yields $^{12}\text{C}(e,e'\text{pp})/^{12}\text{C}(e,e'\text{p})=(9.5\pm 2)\%$ [167]. Note that absorption of the second proton as it exits the nucleus was estimated to decrease this ratio by 15–20%, while the effect of charge-exchange FSI were estimated to yield a similar increase due to the more common pn SRCs yielding a pair of protons in the final state. Because these effects were estimated to be similar in magnitude but of opposite sign, no correction (or uncertainty) was applied for these effects.

The experiment also extracted the ratio of $A(e,e'\text{pn})$ to $A(e,e'\text{p})$ yields using

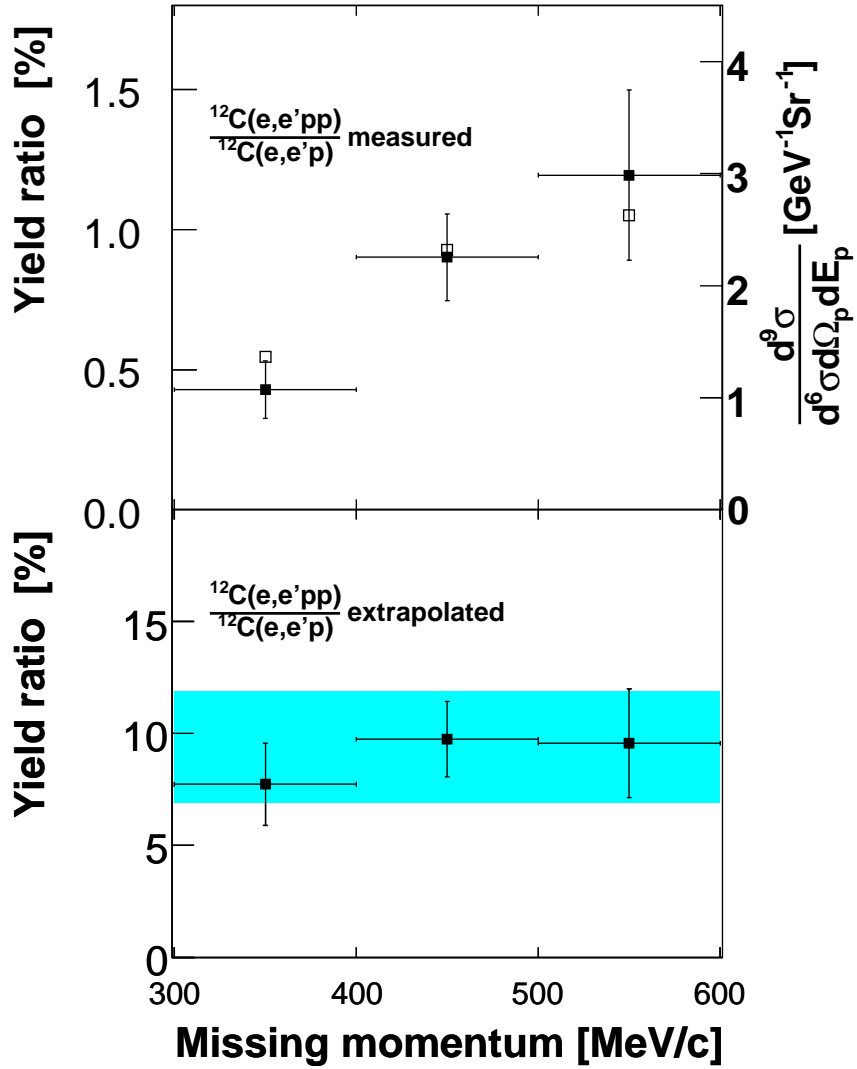


Figure 28: The measured and extrapolated ratios of yields for the $^{12}\text{C}(e,e'pp)$ and the $^{12}\text{C}(e,e'p)$ reactions. The solid squares indicate the raw yield ratio, while the hollow squares show the ratio of the extracted cross section. The shaded area represents the range of results associated with varying the gaussian width of the pair momentum distribution over the range 0.136 ± 0.040 GeV/c (corresponding to the 2σ range in the extracted value of this width). Figure reprinted with permission from Ref. [167]

a similar procedure [168]. Taking into account the finite acceptance of the neutron detector and the $\sim 40\%$ neutron detection efficiency, it was found that $96 \pm 22\%$ of the $A(e,e'p)$ events with a missing momentum above 300 MeV/c had a recoiling neutron. This is in agreement with the $(p, 2pn)/(p, 2p)$ ratio [165] (Eq. (37)) extracted from the Brookhaven proton beam measurement [164].

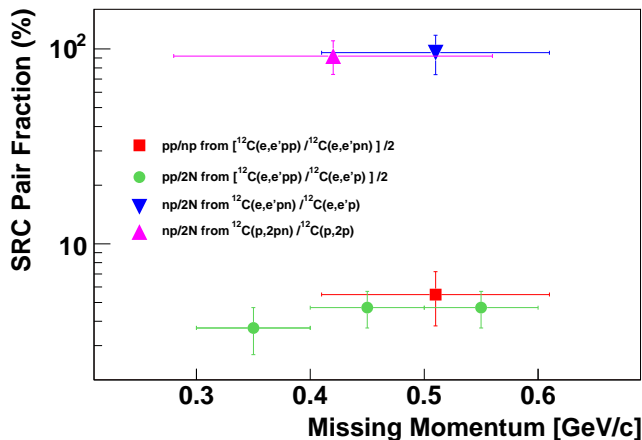


Figure 29: The fraction of correlated pair combinations in carbon as obtained from the $A(e,e'pp)$ to $A(e,e'pn)$ reactions [168], as well as from previous $(p, 2pn)$ data [165]. Note that the pp/np ratio has been corrected for charge-exchange FSI, but the other ratios have not. Figure reprinted with permission from Ref. [168]

The largest advantage of the Jefferson Lab triple-coincidence experiment was that both pp and pn pairs were measured, whereas for the Brookhaven result, only an upper limit on the rate of pp correlations could be deduced. Since the $^{12}\text{C}(e,e'pp)$ and $^{12}\text{C}(e,e'pn)$ data were collected simultaneously with detectors covering nearly identical solid angles, the $^{12}\text{C}(e,e'pn) / ^{12}\text{C}(e,e'pp)$ ratio could be determined with reduced systematic and theoretical uncertainties, e.g. the acceptance correction associated with the total momentum of the pair. Correcting only for detector efficiencies, a ratio of 8.1 ± 2.2 was obtained. The acceptance and attenuation of the recoiling protons and neutrons was assumed to be equal, and the only correction related to final-state interactions of the measured $^{12}\text{C}(e,e'pn)$ to $^{12}\text{C}(e,e'pp)$ ratio is due to single charge exchange interactions. Because the $(e,e'pn)$ cross section is much larger than the $(e,e'pp)$ cross section, the main impact of the charge exchange FSI will be the leakage of $(e,e'pn)$ events into the observed $(e,e'pp)$ sample. A Glauber approximation calculation [171] estimated this yields an 11% decrease in the $^{12}\text{C}(e,e'pn)/^{12}\text{C}(e,e'pp)$ ratio, thus implying an initial pn/pp ratio of 9.0 ± 2.5 .

Since the experiment triggered only on forward $^{12}\text{C}(e,e'p)$ events, the probability of detecting pp pairs was twice that of pn pairs; thus, we conclude that the ratio of pn/pp pairs in the ^{12}C ground state is 18 ± 5 . This result translates

to the following ratio of the pp to pn two-nucleons SRCs:

$$\frac{P_{pp}}{P_{pn}} = 0.056^{+0.021}_{-0.012}, \quad (39)$$

in agreement with Eq. (38). Since these two experiments yield consistent results at very different kinematics, it furthers the interpretation of the process as being due to scattering off a correlated pair of nucleons [172].

Note that the pn/pp ratio quoted in [168] is not calculated using the quoted value for the pp/pX ratio from the analysis of [167]. The pp/pX and pn/pX extractions apply different cuts and corrections, so cannot be used to extract the pn/pp ratio. The original extraction of pp/pX used the combined result from all p_m settings, while the pn/pX ratio was extracted using only the high- p_m data, and thus required different corrections for acceptance, efficiency, etc.... Therefore, a new extraction of pp/pX was performed [173] using only the largest p_m setting to match the kinematics of the pn/pX measurement. No correction was applied for nuclear transparency or charge-exchange FSI, as the transparency was assumed to cancel in the pn/pp ratio and the charge-exchange FSI is applied to the ratio as a separate correction. This analysis yielded $pp/pX = (11.8 \pm 1.8)\%$ for the high- p_m data set, larger than the $(9.5 \pm 2)\%$ quoted in Ref. [167] and with a smaller uncertainty, as the uncertainty due to the total pair momentum is neglected because it is assumed to cancel in the pn/pp ratio.

In both the BNL and Jefferson Lab experiments, SRCs are identified kinematically, by looking for two nucleons which, in the PWIA, reconstruct to a pair of nucleons with a large relative but a small total momenta. As with the p_m-E_r correlation (Fig. 25), the kinematics only tell us that the reaction involves a two-body process with low total momentum; one can obtain the same final state in a two-step process where one low-momentum nucleon is struck and a secondary interaction leads to a second high-momentum nucleon in the final state. Thus, one must consider the possibility of FSI in both cases. In the BNL measurement, the hard elastic $pp \rightarrow pp$ cross section falls as s^{-10} . Therefore, there is a strong enhancement in the cross section for events at lower s , i.e. where the struck proton has a large momentum in the direction of the proton beam, which amplifies the signal from pre-existing SRCs relative to scattering from a low-momentum nucleon with a subsequent reinteraction [166, 174]. For the Jefferson Lab experiment, the electron kinematics are chosen to suppress the contribution of FSI by taking data at $x = 1.2$ and $Q^2 = 2 \text{ GeV}^2$ which, in the PWIA, corresponds to a minimal longitudinal momentum of $\sim 200 \text{ MeV}/c$. The hadron rescattering cross section does not go away at high Q^2 , but a rescattering of the struck proton will not modify x , reconstructed from only the electron kinematics, unless the rescattering takes place within a short distance of the initial interaction, $\sim 1 \text{ fm}$ for this experiment. Thus, the measurement is expected to be sensitive only to scattering from short-range configurations.

While we normally associate such short-range configurations with high-momentum components, the triple-coincidence reactions demonstrate that only short-range iso-singlet np configurations yield high momentum. While the short timescale relevant for FSI at $x > 1$ limits the effects to rescattering between nucleons that

are already very close together, it does not require that these nucleons be in what we call a short-range correlation, i.e. they do not have to be in a high relative momentum state. Iso-singlet np pairs feel a strong tensor interaction when are close together, generating high-momentum states, while nn, pp, and iso-triplet np pairs can be close together without interacting strongly, at least until they are close enough to interact via the short-range repulsive core. There are also pp pairs at short distance, but which are not in a high relative momentum configuration because they do not have a strong tensor interaction at short distances. Scattering from such a low-momentum nucleon which rescatters from another close-by low-momentum nucleon would be indistinguishable from PWIA scattering from an initial-state high-momentum pair, and thus the measurement will potentially be sensitive to a combination scattering from SRCs and scattering from low-momentum pairs which are close enough together that they can undergo final-state interactions.

This raises some interesting questions which may make the triple-coincidence results even more significant. The analysis of the $^{12}\text{C}(e,e'p)$ events at high p_m [175] suggests that the FSI contributions are small when the final state is reconstructed to be a ^{11}B nucleus, but dominate the cross section for more inelastic scattering. Because the experiment reconstructs that nearly 100% of these high- p_m $^{12}\text{C}(e,e'p)$ events are associated with a high-momentum recoil nucleon corresponding to an initial SRC (in the PWIA), the majority of the triple-coincidence events must also involve a final-state interaction. Had the measurements observed np pairs and pp pairs in equal numbers, then it could mean that both iso-singlet and iso-triplet pairs occur frequently or else it could mean that there is a significant contribution coming from scattering from low relative momentum iso-triplet pairs with a significant final state interaction generating two high-momentum nucleons which reconstruct to a small total momentum and a large relative momentum.

The fact that FSI contributions dominate the triple-coincidence channel combined with the observed dominance of np pairs demonstrates that FSI between low-momentum pp pairs with small relative separation does not contribute significantly. This would appear to imply one of the following options: few short-distance pp pairs in the initial state, some suppression of FSI when scattering from such pp pairs, or an isospin-dependent FSI where low momentum pairs (pp, np, or nn) have rescattering which mimics an initial state SRC at these kinematics only for np pairs. This opens up the possibility that a comparison of the isospin structure in the triple-coincidence measurement, which has large FSI contributions, and the inclusive measurements on nuclei with different N/Z ratios could provide a way to determine the role of short-distance nucleon pairs that do not generate high momentum states. However, a more detailed examination of the role of final-state interactions in the triple-coincidence measurements is needed to more fully understand the implications of these measurements.

The startlingly small ratio of proton-proton to neutron-proton SRCs was explained by several groups [137, 37, 32] to be a consequence of the dominance of the tensor interaction in this p_m range. In Ref. [137], the triple-coincidence reaction was studied for $^3\text{He}(e,e'NN)N$ reactions at high Q^2 . These reactions

are the most simple from the point of view of triple-coincidence measurements and allow the calculation of the above defined decay function through the realistic wave function of ${}^3\text{He}$ nucleus. The decay function was calculated in the distorted wave impulse approximation with FSI implemented within the generalized eikonal approximation. The result of the calculations for ${}^3\text{He}(e,e'pp)n$ and ${}^3\text{He}(e,e'pn)p$ reactions in the kinematics that maximize the contribution from 2N SRCs are presented in Fig. 30. One can see that for recoil momenta of 300–600 MeV/c, the pp correlations are suppressed by an order of magnitude or more compared to pn correlations.

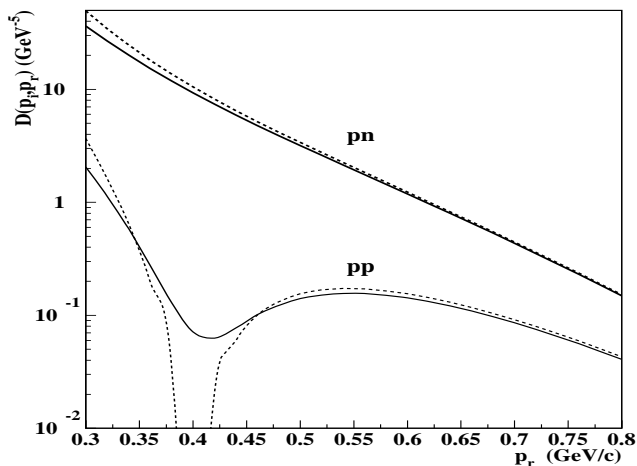


Figure 30: Recoil nucleon momentum dependence of the decay function calculated for ${}^3\text{He}(e,e'N_N N_r)N$ reaction for 2N SRC kinematics in which initial and recoil nucleons are correlated back-to-back, i.e. for NN pairs with zero total momentum. Dashed line PWIA, solid line DWIA calculations of Ref. [137]. Labels “pp” and “pn” mark the results for pp and pn 2N SRCs respectively.

Very similar results are obtained also for other nuclei [37, 176] in calculations of the two-nucleon relative momentum distributions (shown in Fig. 31) for the ground states of light nuclei ($A < 8$) using variational-Monte-Carlo wave functions derived from a realistic Hamiltonian with two- and three-nucleon potentials. Their calculation for the relative nucleon momentum distribution for at-rest nucleon pairs shows the same large proton-neutron to proton-proton ratio in the relative momentum range of 300–600 MeV/c. Note that within PWIA, the two-nucleon relative momentum distribution with the pair at rest in the center-of-mass is related to the decay functions that enter into the cross section of triple-coincidence reactions.

The universality of the above two results is based on the fact that in the momentum range of 300–600 GeV/c, the NN interaction is dominated by the tensor force which means that the iso-triplet pp, pn, and nn channels are strongly sup-

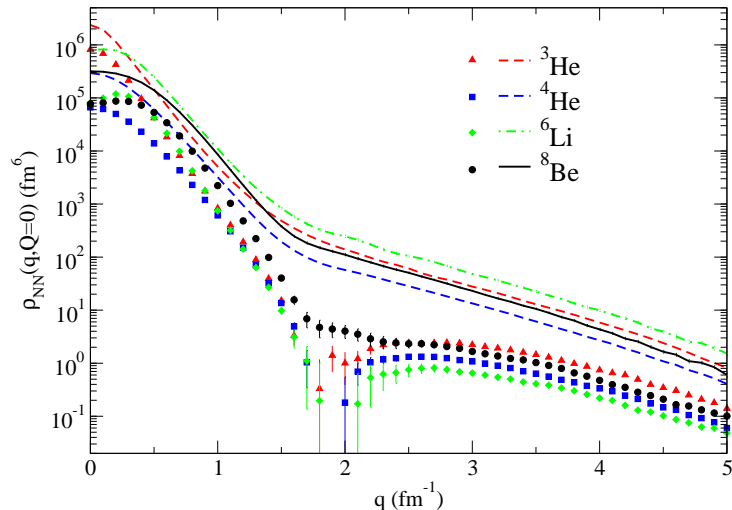


Figure 31: The momentum distribution for neutron-proton pairs (lines) and proton-proton pairs (symbols) are shown for various nuclei. The calculations assume pairs at rest as a function of the relative momentum of the nucleons in the pair. The dip in the proton-proton pair momentum distribution around 2 fm^{-1} ($400 \text{ MeV}/c$) is due to nucleon-nucleon tensor correlations. Figure reprinted with permission from Ref. [37]

pressed relative to the iso-singlet pn channel. These theoretical conclusions are in agreement with earlier studies of nuclear spectral functions for large momenta that also indicated the dominance of tensor correlations [177, 10]. Note that in the inclusive measurements, the cross section is sensitive to a range of momenta with $p > p_{min}$ (Fig. 3). While this includes very large momenta, where iso-triplet pairs are not as strongly suppressed, the contribution to the inclusive cross section from this region is small because there are so few of these extremely high momentum nucleons. So the cross section is dominated by scattering from nucleons in the 300–500 MeV/c range, where there is a strong suppression of iso-triplet SRCs.

Finally, studies of two-nucleon knockout in ^3He are a special case, as the measurement of the scattered electron in coincidence with two of the nucleons provides for a complete kinematic reconstruction of the final three-body system, provided that particle production can be suppressed. This affords the possibility to study a two-nucleon SRC in a unique way, namely by interacting with the third nucleon which is not part of the SRC. After the fast removal of the spectator nucleon, one expects the residual $(A-1)$ system, i.e. the 2N SRC, to decay into two nucleons, allowing one to directly measure the momenta of both correlated nucleons in the absence of FSI.

Such a strategy was realized in the Jefferson Lab experiment of Ref. [181] in which the $^3\text{He}(e, e'pp)n$ reaction was studied using 2.2 and 4.4 GeV electron beams and detecting the scattered electron and ejected protons in CLAS over a

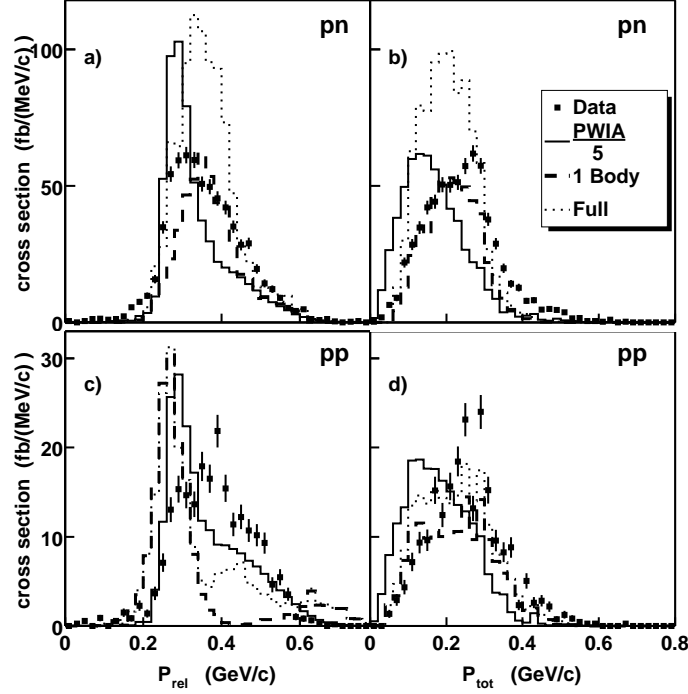


Figure 32: Figure a) shows lab frame cross section versus pn pair relative momentum. Points show the data, solid histogram shows the PWIA calculation multiplied by a factor 0.2, dashed histogram shows Laget’s one-body calculation [178, 179, 180], dotted histogram shows Laget’s full calculation; b) the same for total momentum of the pair; c), d) the same for pp pairs. Figure reprinted with permission from Ref. [181]

wide kinematic range. In the PWIA, interacting with a nucleon inside of an SRC would yield a high-momentum struck nucleon, a recoil nucleon from the SRC with $k > k_{Fermi}$, and a low momentum spectator with $k < k_{Fermi}$. However, if the nucleon that is not in the SRC is struck, there will be three high-momentum nucleons in the final state. The struck nucleon will have a momentum close to q , while the two nucleons in the SRC will come out with large, back-to-back momentum of $k > k_{Fermi}$. The experiment observed that when all three final state nucleons have momenta greater than 250 MeV/c, the reaction is dominated by events where two nucleons each have less than 20% of the transferred energy and the third ‘leading’ nucleon has the remainder. Final state interactions of the leading nucleon are suppressed by requiring that it has perpendicular momentum with respect to \vec{q} of less than 300 MeV/c. In these cases the two other nucleons (the pn or pp pair) are found to be predominantly back-to-back and to have very little total momentum in the direction of the momentum transfer. The relative pair momentum is then almost isotropic with respect to

\vec{q} , suggesting that the nucleon-nucleon pair is correlated and is a spectator to the virtual photon absorption. In this case, the measured relative and total pair momenta, $\vec{p}_{rel} = (\vec{p}_1 - \vec{p}_2)/2$ and $\vec{p}_{tot} = \vec{p}_1 + \vec{p}_2$ are closely related to the initial momenta of the correlated pair. As shown in Fig. 32, the pair relative momentum peaks at about 300–400 MeV/c and the pair total momentum peaks at about 300 MeV/c. The pp and pn momentum distributions are very similar. The advantage of this approach is that there are no contributions from meson exchange currents or isobar configurations since the virtual photon does not interact with the correlated pair. However, because the continuum interaction of the correlated pair is very strong and reduces the calculated cross section by a factor of about ten, this reaction is very difficult to calculate precisely. Diagrammatic calculations [178, 179, 180], are in qualitative agreement with the measured momentum distributions, but only after including the effects of the continuum interaction.

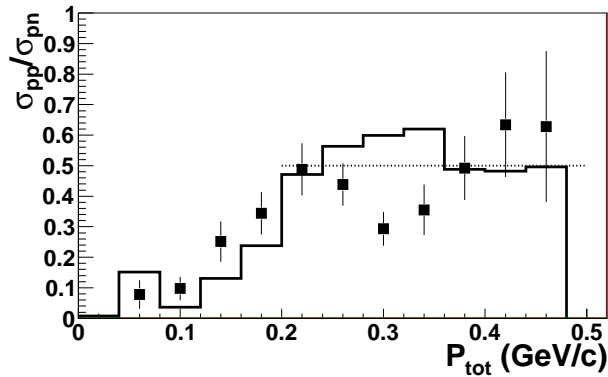


Figure 33: The ratio of cross sections with pp or pn SRC spectators (with relative momentum from 300–500 MeV/c) as a function of the pair total momentum [182] for ${}^3\text{He}$. The histogram is the Golak one-body calculation [183], and the dotted line shows the expectation based on simple pair-counting, assuming isospin-independent pairing. The ratios (data and calculation) are multiplied by 1.5 to approximately account for the difference in the ep and en elastic cross sections associated with np and pp spectators. At low pair momentum, they see strong pn dominance, consistent with the triple-coincidence measurement on Carbon [168], while at high total momentum, they find equal contributions from pp and pn pairs. Figure adapted from Ref. [182]

The measurements were also able to examine the contribution from pn and pp pairs as a function of the total pair momentum [182], as shown in Fig. 33. They observed a smaller difference in the fraction of high-momentum pn to pp pairs, which were observed in a ratio of approximately 4:1. However, when taken as a function of the total momentum of the pair, the ratio becomes much larger at small total momentum, in agreement with the observation of strong np dominance in the triple-coincidence measurement on ${}^{12}\text{C}$. They observe a much smaller difference for the case where there is a large total momentum of

the pair, which for ${}^3\text{He}$ corresponds to the case where all three nucleons appear to have large momenta in the final state. This is taken as further indication of tensor dominance, as $T=1$ pairs are most likely to be in a spin-0 state, which yields a minimum in the distribution for large relative momentum and small total pair momentum. With increasing pair momentum, this minimum is filled in, increasing the pn/pp ratio [182, 176].

9. Summary and Outlook

We have reviewed the physics importance of studying short-range, high-momentum nucleon configurations in nuclei. We then presented in some detail the necessary experimental requirements for measurements that can provide reliable information on these SRCs, and discussed the main results of a new generation of high energy and high momentum transfer measurements aimed at verifying the presence and probing the nature of these correlations.

We emphasized the special role of high Q^2 studies of the deuteron in advancing the field of the short-range nucleon correlations by means of studying reaction mechanisms, off-shell nucleon effects and relativistic dynamics of strongly bound nucleon systems. Going beyond the deuteron, we categorized the experimental program by the reaction mechanism, discussing programs of inclusive, semi-inclusive and triple-coincidence measurements. We reviewed the first high Q^2 experiments in these categories and demonstrated how these experiments advanced our understanding the structure of the short range correlations in the nuclei. Further experimental details on the Jefferson Lab program can be found in Ref. [184], with future plans, including some which go beyond hadronic degrees of freedom to look at non-nucleonic components or medium modification within SRCs, presented in Ref. [49].

The kinematic domain probed and the knowledge obtained from these experiments can be summarized as follows:

- The deuteron momentum distribution has been probed up to 500 MeV/c internal momenta and Q^2 up to about 3.5 GeV². The observation is that MEC and IC contributions can be well controlled by making measurements at large Q^2 and $x > 1$. In this region, FSI can be relatively well calculated within the eikonal approximation, reproducing data taken in kinematic regimes where FSI contributions dominate. This allows for further studies in regions where $A(e,e'p)$ measurements are most sensitive to the reaction mechanism, in particular off-shell effects and relativistic dynamics, to provide the last data needed to fully validate our understanding of the reaction in the deuteron, thus allowing us to extend detailed and quantitative studies to heavier nuclei.
- For inclusive scattering from light-to-heavy nuclei, measurements at high Q^2 and $x > 1$ probe the momentum distribution of the nucleons in nuclei. A clear signature of scaling associated with interaction from 2N SRCs is

observed in the σ_{eA}/σ_{eD} ratios. These ratios allow us to estimate the contribution of 2N SRCs in heavy nuclei relative to the contributions in the deuteron. Moving to similar studies for $x > 2$, initial measurements have seen some indication of the dominance of 3N correlations in these kinematics, although a recent measurement [131] as well as more quantitative studies are required to verify and understand this.

- Semi-inclusive knock-out $A(e,e'N)$ reactions established the clear correlation signature between missing-momentum and missing-energy of the reaction. For the first time, evidence has been acquired that in the SRC domain the final state interaction is localized within the short-range configuration.
- Triple-coincidence experiments gave new insight into the dynamics of 2N SRCs. They probed relative internal momenta up to 600 MeV/c and gave unambiguous evidence that the dynamics of 2N SRC in this domain are dominantly controlled by the tensor component of the NN force. An extension to higher internal momenta was recently completed [185] and the data are currently being analyzed.
- Theoretical analysis of all these experiments allows us to conclude that for up to 600 MeV/c relative momenta, nucleons represent the relevant degrees of freedom in the dynamics of two nucleon short-range correlations.

The knowledge of SRCs obtained so far sets up the main directions which in our opinion the new generation of high Q^2 experiments should follow:

- Extension of the deuteron studies beyond 500 MeV/c. One may expect especially interesting new physics beyond 750 MeV/c, when the threshold of inelastic excitation in the iso-singlet NN system is passed and the role of the non-nucleonic degrees of freedom may be increasingly important. This region also will be defined by the core of the NN interaction, by far the least well understood part of the NN interaction. A $D(e,e'p)$ measurement is planned for Jefferson Lab [186] with the goal of precisely mapping out the high-momentum tail up to 1 GeV/c in the deuteron by making measurements at $x > 1$ and $Q^2 = 4.25 \text{ GeV}^2$.
- The next generation of inclusive measurements will pursue several important issues. One is the detailed studies of $x > 2$ region in probing the onset of 3N correlations. Jefferson Lab experiment E08-014 [131] recently completed data taking which should be able to clearly map out the onset of scaling in the target ratios for $x > 2$. This experiment will also compare scattering from ^{40}Ca and ^{48}Ca to provide another test of the dominance of iso-singlet (np) pairs in SRCs, free from the large FSIs associated with the triple-coincidence measurements. In addition, measurements planned for the 12 GeV upgrade will extend the 2N and 3N SRC measurements to many additional light and heavy nuclei [133], as well as comparing ^3H and ^3He [134] to better study the isospin structure of SRCs.

- For knock-out and triple-coincidence experiments the challenge will be to go beyond 600 MeV/c (beyond the domain of the tensor-forces). It is clear from Figs. 30 and 31 that for larger nucleon momenta, > 600 MeV/c, the ratio of neutron-proton to proton-proton pairs should become smaller as the reaction become dominated by the short-range repulsive core of the nucleon-nucleon interaction. The recently completed triple-coincidence experiment E07-006 [185] will extend the previous measurements beyond 600 MeV/c, and should be able to test this prediction.
- Recent measurements of the EMC effect in light nuclei [132] yield a non-trivial A dependence in the modification of the nuclear structure function in deep-inelastic scattering. These data suggest that the nuclear structure function depends on the local, microscopic structure of the nucleus. As the question of local, high-density structure is the primary focus of SRC measurements, it was natural to compare the two measurements, and a quantitative correlation between the size of the EMC effect and the strength of SRCs in nuclei was observed [187]. Extensions of both SRC [133] and EMC effect [188] measurements after the Jefferson Lab 12 GeV upgrade, including several light nuclei, some of which have significant cluster structure, will help extend these comparisons which may relate both the structure functions and the SRCs to the microscopic nuclear structure.
- Finally, moving to the realm of scattering from quarks in nuclei provides access to short-range structure in a region where non-hadronic degrees of freedom may become important [49, 189, 128]. Recent measurements suggest that even with 6 GeV electrons, we may be able to reliably extract the distribution of “super-fast” quarks at $x > 1$. The distribution of these super-fast quarks is sensitive to the short-range structure of the nucleus which drives the high-momentum components of the nuclear wave function. While the present data [94] suggest that the high-momentum contributions can be explained by SRCs, without the need for any non-hadronic contributions, the range of this data is still somewhat limited. Measurements planned for 11 GeV will move into a region with dramatically increased sensitivity to non-hadronic components in nuclei [133, 49, 128].

Acknowledgments

This work was supported by the U.S. Department of Energy, Office of Nuclear Physics, under contracts DE-AC02-06CH11357, DE-AC05-06OR23177, and DE-FG02-01ER-41172. We thank our colleagues who assisted in the preparation of this work, including Werner Boeglin, Donal Day, Nadia Fomin, Roy Holt, Ushma Kriplani, Eli Piasetzky, Mark Strikman, and Larry Weinstein for useful comments and discussions, including preliminary results from recent measurements, and providing figures.

References

- [1] E. J. Moniz, et al., Nuclear fermi momenta from quasielastic electron scattering, *Phys. Rev. Lett.* 26 (1971) 445–448.
- [2] H. A. Bethe, Theory of nuclear matter, *Ann. Rev. Nucl. Part. Sci.* 21 (1971) 93–244.
- [3] M. G. Mayer, J. H. D. Jensen, Elementary Theory of Nuclear Shell Structure , Elementary Theory of Nuclear Shell Structure New York, USA: John Wiley and Sons, Inc.
- [4] D. Koltun, Total Binding Energies of Nuclei, and Particle-Removal Experiments, *Phys.Rev.Lett.* 28 (1972) 182–185.
- [5] M. Bernheim, A. Bussière, A. Gillebert, J. Mougey, P. X. Ho, M. Priou, D. Royer, I. Sick, G. J. Wagner, C12(e,e'p) Results as a Critical Test of an Energy Sum Rule, *Phys. Rev.Lett* 32 (1974) 898–901.
- [6] A. Faessler, S. Krewald, G. J. Wagner, Is there evidence of three-body forces from violation of the Koltun energy sum rule?, *Phys.Rev.* C11 (1975) 2069–2072.
- [7] D. Royer, J. Mougey, M. Priou, M. Bernheim, A. Bussiere, et al., Influence of short range correlations on (e,e'p) cross sections, *Phys.Rev.* C12 (1975) 327–329.
- [8] J. J. Kelly, Nucleon knockout by intermediate-energy electrons, *Adv. Nucl. Phys.* 23 (1996) 75–294.
- [9] L. Lapikas, Quasi-elastic electron scattering off nuclei, *Nucl. Phys.* A553 (1993) 297–308.
- [10] C. Ciofi degli Atti, S. Simula, Realistic model of the nucleon spectral function in few and many nucleon systems, *Phys. Rev.* C53 (1996) 1689.
- [11] M. Lacombe, et al., Parametrization of the Paris n n Potential, *Phys. Rev.* C21 (1980) 861–873.
- [12] C. Ciofi degli Atti, E. Pace, G. Salm, Analysis of the proton momentum distribution in ^3He , *Physics Letters B* 141 (1984) 14 – 18.
- [13] R. Schiavilla, V. R. Pandharipande, R. B. Wiringa, Momentum distributions in a $A = 3$ and 4 nuclei, *Nucl. Phys.* A449 (1986) 219–242.
- [14] O. Benhar, C. Ciofi Degli Atti, S. Liuti, G. Salm, Realistic many-body wave functions and nucleon momentum distributions in finite nuclei, *Physics Letters B* 177 (1986) 135 – 140.
- [15] S. C. Pieper, R. B. Wiringa, V. R. Pandharipande, Variational calculation of the ground state of ^{16}O , *Phys. Rev.* C46 (1992) 1741–1756.

- [16] X.-D. Ji, J. Engel, High momentum nucleons in finite nuclei and y-scaling, *Phys. Rev. C* 40 (1989) 497–501.
- [17] M. Jaminon, C. Mahaux, H. Ng, Effect of correlations on the momentum distribution of protons in ^{208}Pb , *Nuclear Physics A* 452 (1986) 445 – 461.
- [18] S. Fantoni, V. R. Pandharipande, Momentum distribution of nucleons in nuclear matter, *Nucl. Phys. A* 427 (1984) 473 – 492.
- [19] C. Ciofi degli Atti, E. Pace, G. Salme, y-scaling analysis of quasielastic electron scattering and nucleon momentum distributions in few body systems, complex nuclei and nuclear matter, *Phys. Rev. C* 43 (1991) 1155–1176.
- [20] M. Bernheim, et al., Momentum distribution of nucleons in the deuteron from the $d(e,e'p)n$ reaction, *Nucl. Phys. A* 365 (1981) 349–370.
- [21] S. Turck-Chieze, et al., Exclusive deuteron electrodisintegration at high neutron recoil momentum, *Phys. Lett. B* 142 (1984) 145–148.
- [22] E. Jans, et al., Quasifree $(e, e' p)$ reaction on He-3, *Phys. Rev. Lett.* 49 (1982) 974–978.
- [23] E. Jans, et al., The quasifree ^3He $(e,e'p)$ reaction, *Nucl. Phys. A* 475 (1987) 687–719.
- [24] C. Marchand, M. Bernheim, A. Gerard, J. Laget, A. Magnon, et al., High proton momenta and short range nucleon-nucleon correlations in a He-3 $(e,e'p)$ experiment, *Phys.Rev.Lett.* 60 (1988) 1703.
- [25] J. F. J. Van Den Brand, et al., Electrodisintegration of He-4 studied with the reaction $^4\text{He}(e,e'p)^3\text{H}$, *Phys. Rev. Lett.* 60 (1988) 2006–2009.
- [26] J. Le Goff, M. Bernheim, M. Brussel, G. Capitani, J. Danel, et al., Short range interaction of nucleons inside the nucleus via He-4 $(e,e'p)$ R reaction, *Phys.Rev. C* 50 (1994) 2278–2287.
- [27] S. Frullani, J. Mougey, Single Particle Properties of Nuclei Through $(e, e' p)$ Reactions, *Adv. Nucl. Phys.* 14 (1984) 1–283.
- [28] H. Muther, A. Polls, Two-body correlations in nuclear systems, *Prog.Part.Nucl.Phys.* 45 (2000) 243–334.
- [29] A. Fabrocini, F. Aria de Saavedra, G. Co, Ground state correlations in ^{16}O and ^{40}Ca , *Phys.Rev. C* 61 (2000) 044302.
- [30] W. Dickhoff, C. Barbieri, Self consistent Green's function method for nuclei and nuclear matter, *Prog.Part.Nucl.Phys.* 52 (2004) 377–496.

- [31] M. Alvioli, C. Ciofi degli Atti, H. Morita, Ground-state energies, densities and momentum distributions in closed-shell nuclei calculated within a cluster expansion approach and realistic interactions, *Phys.Rev. C* 72 (2005) 054310.
- [32] M. Alvioli, C. Ciofi degli Atti, H. Morita, Proton-neutron and proton-proton correlations in medium-weight nuclei and the role of the tensor force, *Phys. Rev. Lett.* 100 (2008) 162503.
- [33] Y. Suzuki, W. Horiuchi, Significance and properties of internucleon correlation functions, *Nucl.Phys. A* 818 (2009) 188–207.
- [34] M. Vanhalst, W. Cosyn, J. Ryckebusch, Counting the amount of correlated pairs in a nucleus, *Phys.Rev. C* 84 (2011) 031302.
- [35] H. Feldmeier, W. Horiuchi, T. Neff, Y. Suzuki, Universality of short-range nucleon-nucleon correlations, *Phys. Rev. C* 84, 054003.
- [36] J. L. Forest, et al., Femtometer Toroidal Structures in Nuclei, *Phys. Rev. C* 54 (1996) 646–667.
- [37] R. Schiavilla, R. B. Wiringa, S. C. Pieper, J. Carlson, Tensor Forces and the Ground-State Structure of Nuclei, *Phys. Rev. Lett.* 98 (2007) 132501.
- [38] R. B. Wiringa, R. Schiavilla, S. C. Pieper, J. Carlson, Dependence of two-nucleon momentum densities on total pair momentum, *Phys. Rev. C* 78 (2008) 021001.
- [39] H. Muther, W. Dickhoff, Single-particle spectral function of O-16, *Phys.Rev. C* 49 (1994) R17–R20.
- [40] J. Levinger, The High-energy nuclear photoeffect, *Phys.Rev.* 84 (1951) 43–51.
- [41] K. Gottfried, On the determination of the nuclear pair correlation function from the high energy photo-effect, *Nucl.Phys.* 5 (1958) 557–587.
- [42] G. Brown, A. Jackson, *The nucleon-nucleon interaction*, North-Holland, 1976.
URL <http://books.google.com/books?id=9uDvAAAAMAAJ>
- [43] L. L. Frankfurt, M. I. Strikman, High-Energy Phenomena, Short Range Nuclear Structure and QCD, *Phys. Rept.* 76 (1981) 215–347.
- [44] L. Frankfurt, M. Sargsian, M. Strikman, Recent observation of short range nucleon correlations in nuclei and their implications for the structure of nuclei and neutron stars, *Int. J. Mod. Phys. A* 23 (2008) 2991–3055.
- [45] A. Nogga, et al., The three-nucleon bound state using realistic potential models, *Phys. Rev. C* 67 (2003) 034004.

- [46] M. M. Sargsian, Selected topics in high energy semi-exclusive electro-nuclear reactions, *Int. J. Mod. Phys. E10* (2001) 405–458.
- [47] J. Van Orden, N. Devine, F. Gross, Elastic electron scattering from the deuteron using the gross equation, *Phys.Rev.Lett.* 75 (1995) 4369–4372.
- [48] S. Brodsky, L. Frankfurt, R. A. Gilman, J. Hiller, G. Miller, et al., Hard photodisintegration of a proton pair in He-3, *Phys.Lett.* B578 (2004) 69–77.
- [49] M. M. Sargsian, et al., Hadrons in the nuclear medium., *J. Phys. G29* (2003) R1.
- [50] P. Stoler, Baryon form-factors at high Q^2 and the transition to perturbative QCD, *Phys. Rept.* 226 (1993) 103–171.
- [51] M. Ungaro, et al., Measurement of the N, $\Delta^+(1232)$ transition at high momentum transfer by π^0 electroproduction, *Phys.Rev.Lett.* 97 (2006) 112003.
- [52] J. B. Kogut, D. E. Soper, Quantum Electrodynamics in the Infinite Momentum Frame, *Phys. Rev. D1* (1970) 2901–2913.
- [53] J. D. Bjorken, J. B. Kogut, D. E. Soper, Quantum Electrodynamics at Infinite Momentum: Scattering from an External Field, *Phys. Rev. D3* (1971) 1382.
- [54] R. Feynman, Photon-hadron interactions.
- [55] D. B. Day, et al., y-scaling in electron nucleus scattering, *Phys. Rev. Lett.* 59 (1987) 427–430.
- [56] L. L. Frankfurt, M. I. Strikman, Hard Nuclear Processes and Microscopic Nuclear Structure, *Phys. Rept.* 160 (1988) 235–427.
- [57] D. B. Day, J. S. McCarthy, T. W. Donnelly, I. Sick, Scaling in inclusive electron - nucleus scattering, *Ann. Rev. Nucl. Part. Sci.* 40 (1990) 357–410.
- [58] L. L. Frankfurt, M. I. Strikman, D. B. Day, M. Sargsian, Evidence for short range correlations from high Q^2 (e,e') reactions, *Phys. Rev. C48* (1993) 2451–2461.
- [59] T. Uchiyama, A. Dieperink, O. Scholten, Final state interactions and y-scaling in inclusive electron scattering, *Phys.Lett.* B233 (1989) 31–36.
- [60] O. Benhar, S. Liuti, Can a highly virtual nucleon experience final state interactions in electron nucleus scattering?, *Phys.Lett.* B389 (1996) 649–654.
- [61] C. Ciofi degli Atti, C. B. Mezzetti, Obtaining information on Short Range Correlations from inclusive electron scattering, *Phys. Rev. C79* (2009) 051302.

- [62] C. B. Mezzetti, C. Ciofi degli Atti, A Novel analysis of the effects of short range correlations in inclusive lepton scattering off nuclei. [arXiv:0906.5564](#).
- [63] J. Arrington, et al., Inclusive electron nucleus scattering at large momentum transfer, *Phys. Rev. Lett.* 82 (1999) 2056–2059.
- [64] N. Fomin, J. Arrington, R. Asaturyan, F. Benmokhtar, W. Boeglin, et al., New measurements of high-momentum nucleons and short-range structures in nuclei., *Phys. Rev. Lett.* 108 (2012) 092502.
- [65] C. Ciofi degli Atti, S. Simula, Nucleon-nucleon correlations and final state interactions in inclusive quasielastic electron scattering off nuclei at $x > 1$, *Phys.Lett.* B325 (1994) 276–282.
- [66] S. Gurvitz, A. Rinat, y -scaling in inclusive scattering, *Phys.Rev.* C35 (1987) 696.
- [67] S. Gurvitz, A. Rinat, R. Rosenfelder, y -scaling and hard core potentials, *Phys.Rev.* C40 (1989) 1363–1375.
- [68] S. Gurvitz, A. Rinat, Relativistic approaches to structure functions of nuclei, *Phys.Rev.* C65 (2002) 024310.
- [69] O. Benhar, A. Fabrocini, S. Fantoni, G. Miller, V. Pandharipande, et al., Scattering of GeV electrons by nuclear matter, *Phys.Rev.* C44 (1991) 2328–2342.
- [70] O. Benhar, V. Pandharipande, Scattering of GeV electrons by light nuclei, *Phys.Rev.* C47 (1993) 2218–2227.
- [71] O. Benhar, A. Fabrocini, S. Fantoni, S. Pieper, V. Pandharipande, et al., Higher order effects in inclusive electron nucleus scattering, *Phys.Lett.* B359 (1995) 8–12.
- [72] O. Benhar, A. Fabrocini, S. Fantoni, I. Sick, Inclusive cross-section ratios at $x > 1$, *Phys.Lett.* B343 (1995) 47–52.
- [73] N. Makins, R. Ent, M. Chapman, J. Hansen, K. Lee, et al., Momentum transfer dependence of nuclear transparency from the quasielastic C-12 ($e, e'p$) reaction, *Phys.Rev.Lett.* 72 (1994) 1986–1989.
- [74] T. G. O’Neill, et al., A-dependence of nuclear transparency in quasielastic $A(e, e'p)$ at high Q^2 , *Phys. Lett.* B351 (1995) 87–92.
- [75] D. Abbott, et al., Quasifree ($e, e'p$) reactions and proton propagation in nuclei, *Phys. Rev. Lett.* 80 (1998) 5072–5076.
- [76] K. Garrow, et al., Nuclear transparency from quasielastic $A(e, e'p)$ reactions up to $Q^2 = 8.1 - (\text{GeV}/c)^2$, *Phys. Rev.* C66 (2002) 044613.

- [77] D. B. Day, et al., Inclusive electron nucleus scattering at high momentum transfer, *Phys. Rev. C* 48 (1993) 1849–1863.
- [78] L. Frankfurt, M. Sargsian, M. Strikman, Future directions for probing two and three nucleon short-range correlations at high energies, *AIP Conf.Proc.* 1056 (2008) 322–329.
- [79] V. Abramovsky, V. Gribov, O. Kancheli, Character of inclusive spectra and fluctuations produced in inelastic processes by multi-pomeron exchange, *Yad.Fiz.* 18 (1973) 595–616.
- [80] L. Bertocchi, D. Treleani, Glauber Theory, Unitarity, and the AGK Cancellation, *J.Phys. G* 3 (1977) 147.
- [81] W. Cosyn, M. Sargsian, work in progress.
- [82] D. Allasia, C. Angelini, A. Baldini, F. Bobisut, A. Borg, et al., Search for a delta (1236) - delta (1236) structure of the deuteron, *Phys.Lett.* B174 (1986) 450–452.
- [83] K. I. Blomqvist, et al., Large recoil momenta in the $D(e,e'p)n$ reaction, *Phys. Lett.* B424 (1998) 33–38.
- [84] H. Arenhovel, W. Leidemann, E. L. Tomusiak, Nucleon polarization in exclusive deuteron electrodisintegration with polarized electrons and a polarized target, *Phys. Rev. C* 52 (1995) 1232–1253.
- [85] I. Passchier, et al., Spin-momentum correlations in quasi-elastic electron scattering from deuterium, *Phys. Rev. Lett.* 88 (2002) 102302.
- [86] F. Ritz, H. Arenhovel, T. Wilbois, Relativistic effects and the role of heavy meson exchange in deuteron photodisintegration, *Few Body Syst.* 24 (1998) 123–138.
- [87] W. Leidemann, E. L. Tomusiak, H. Arenhoevel, Polarization observables in deuteron electrodisintegration, *Few Body Syst. Suppl.* 6 (1992) 236.
- [88] W. P. Schutz, et al., Inelastic electron Deuteron Scattering in the Threshold Region at High Momentum Transfer, *Phys. Rev. Lett.* 38 (1977) 259.
- [89] S. Rock, et al., Measurement of Elastic electron - Neutron Cross-Sections Up to $Q^2 = 10-(\text{GeV}/c)^2$, *Phys. Rev. Lett.* 49 (1982) 1139.
- [90] A. Lung, et al., Measurements of the electric and magnetic form-factors of the neutron from $Q^2 = 1.75 (\text{GeV}/c)^2$ to $4 (\text{GeV}/c)^2$, *Phys. Rev. Lett.* 70 (1993) 718–721.
- [91] J. R. Arrington, Inclusive electron scattering from nuclei at $x > 1$ and high Q^2 . Ph. D. Thesis, California Institute of Technology (1998). [arXiv:nuc1-ex/0608013](https://arxiv.org/abs/nuc1-ex/0608013).

- [92] J. Arrington, et al., x and ξ scaling of the nuclear structure function at large x , Phys. Rev. C64 (2001) 014602.
- [93] N. Fomin, Inclusive electron scattering from nuclei in the quasielastic region at large momentum transfer Ph.D. Thesis, University of Virginia (2007). [arXiv:0812.2144](#).
- [94] N. Fomin, et al., Scaling of the F_2 structure function in nuclei and quark distributions at $x > 1$, Phys. Rev. Lett. 105 (2010) 212502.
- [95] G. B. West, Electron Scattering from Atoms, Nuclei and Nucleons, Phys.Rept. 18 (1975) 263–323.
- [96] I. Sick, D. Day, J. Mccarthy, Nuclear high momentum components and y -scaling in electron scattering, Phys.Rev.Lett. 45 (1980) 871–874.
- [97] E. Pace, G. Salme, Nuclear scaling function and quasielastic electron scattering by nuclei, Phys.Lett. B110 (1982) 411.
- [98] O. Benhar, D. Day, I. Sick, Inclusive quasi-elastic electron-nucleus scattering, Rev. Mod. Phys. 80 (2008) 189–224.
- [99] J. Arrington, Nucleon momentum distributions from a modified scaling analysis of inclusive electron nucleus scattering. [arXiv:nucl-ex/0306016](#).
- [100] M. M. Sargsian, Large Q² Electrodisintegration of the Deuteron in Virtual Nucleon Approximation, Phys. Rev. C82 (2010) 014612.
- [101] S. Jeschonnek, Unfactorized versus factorized calculations for H-2(e, e' p) reactions at GeV energies, Phys. Rev. C63 (2001) 034609.
- [102] C. Ciofi degli Atti, L. P. Kaptari, D. Treleani, On the effects of the final state interaction in the electro-disintegration of the deuteron at intermediate and high energies, Phys. Rev. C63 (2001) 044601.
- [103] J. M. Laget, The electro-disintegration of few body systems revisited, Phys. Lett. B609 (2005) 49–56.
- [104] S. Jeschonnek, J. W. Van Orden, A new calculation for D(e, e' p)n at GeV energies, Phys. Rev. C78 (2008) 014007.
- [105] S. Jeschonnek, J. W. Van Orden, Target Polarization for ${}^2\vec{H}(e, e'p)n$ at GeV energies, Phys. Rev. C80 (2009) 054001.
- [106] S. Jeschonnek, J. W. Van Orden, Ejectile Polarization for ${}^2H(e, e'\vec{p})n$ at GeV energies, Phys. Rev. C81 (2010) 014008.
- [107] L. L. Frankfurt, W. R. Greenberg, G. A. Miller, M. M. Sargsian, M. I. Strikman, Color transparency effects in electron deuteron interactions at intermediate Q², Z. Phys. A352 (1995) 97–113.

- [108] L. L. Frankfurt, M. M. Sargsian, M. I. Strikman, Feynman graphs and generalized eikonal approach to high energy knock-out processes, Phys. Rev. C56 (1997) 1124–1137.
- [109] P. E. Ulmer, et al., H-2(e,e'p)n reaction at high recoil momenta, Phys. Rev. Lett. 89 (2002) 062301.
- [110] H. Bulten, P. Anthony, R. Arnold, J. Arrington, E. Beise, et al., Exclusive electron scattering from deuterium at high momentum transfer, Phys.Rev.Lett. 74 (1995) 4775–4778.
- [111] M. Jones, P. Ulmer, et al., In-plane separations and high momentum structure in d(e,e'p)n, Jefferson Lab Experiment Proposal E94-004 (1994).
- [112] J. Tjon, Relativistic analysis of electron deuteron scattering, Few Body Syst.Suppl. 5 (1992) 5–16.
- [113] G. Beck, H. Arenhovel, Relativistic corrections in quasi-free electrodisintegration of the deuteron, Few Body Syst. 13 (1992) 165–188.
- [114] K. S. Egiyan, et al., Experimental study of exclusive H-2(e,e'p)n reaction mechanisms at high Q^2 , Phys. Rev. Lett. 98 (2007) 262502.
- [115] R. B. Wiringa, V. G. J. Stoks, R. Schiavilla, An Accurate nucleon-nucleon potential with charge independence breaking, Phys. Rev. C51 (1995) 38–51.
- [116] W. Boeglin, et al., Probing the high momentum component of the deuteron at high Q^2 , Phys.Rev.Lett. 107 (2011) 262501.
- [117] W. Boeglin, et al., Jefferson Lab Experiment Proposal E01-020 (2001).
- [118] J. Coman, $^2H(e, e'p)$ Studies of the Deuteron at High Q^2 , PhD. Thesis, FIU (2008).
- [119] S. Rock, et al., Inelastic electron scattering from He-3 AND He-4 in the threshold region at high momentum transfer, Phys. Rev. C26 (1982) 1592.
- [120] P. E. Bosted, R. G. Arnold, S. Rock, Z. M. Szalata, Nuclear scaling in inelastic electron scattering from d, He-3 and He-4, Phys. Rev. Lett. 49 (1982) 1380.
- [121] Z. E. Meziani, et al., High momentum transfer R(T,L) inclusive response functions for He-3, He-4. SLAC-NE-9 experiment, Phys. Rev. Lett. 69 (1992) 41–44.
- [122] B. W. Filippone, et al., Nuclear structure functions at $x > 1$, Phys. Rev. C45 (1992) 1582–1585.
- [123] P. E. Bosted, et al., Measurements of νW_2 and $R = \sigma_L/\sigma_T$ from inelastic electron - aluminum scattering near $x = 1$, Phys. Rev. C46 (1992) 2505–2515.

- [124] J. Arrington, et al., Inclusive electron scattering from nuclei at $x \approx 1$, Phys. Rev. C53 (1996) 2248–2251.
- [125] K. S. Egiyan, et al., Observation of Nuclear Scaling in the $A(e,e')$ Reaction at $x_B > 1$, Phys. Rev. C68 (2003) 014313.
- [126] K. S. Egiyan, et al., Measurement of 2- and 3-Nucleon Short Range Correlation Probabilities in Nuclei, Phys. Rev. Lett. 96 (2006) 082501.
- [127] O. Benhar, D. Day, I. Sick, An Archive for quasi-elastic electron-nucleus scattering data. [arXiv:nuc1-ex/0603032](https://arxiv.org/abs/nuc1-ex/0603032).
- [128] J. Arrington, Hadrons in the nuclear medium - quarks, nucleons, or a bit of both? [arXiv:nuc1-ex/0602007](https://arxiv.org/abs/nuc1-ex/0602007).
- [129] C. Ciofi degli Atti, G. B. West, Old and new facets of y -scaling: The universal features of nuclear structure functions and nucleon momentum distributions. [arXiv:nuc1-th/9702009](https://arxiv.org/abs/nuc1-th/9702009).
- [130] C. Ciofi degli Atti, G. B. West, A new approach to y -scaling and the universal features of scaling functions and nucleon momentum distributions, Phys. Lett. B458 (1999) 447–453.
- [131] J. Arrington, D. Day, D. W. Higinbotham, P. Solvignon, et al., Three-nucleon short range correlations studies in inclusive scattering for $0.8 < Q^2 < 2.8$ (GeV/c)², Jefferson Lab Experiment Proposal E08-014 (2008).
- [132] J. Seely, et al., New measurements of the EMC effect in very light nuclei, Phys. Rev. Lett. 103 (2009) 202301.
- [133] J. Arrington, D. Day, N. Fomin, P. Solvignon, et al., Inclusive scattering from nuclei at $x > 1$ in the quasielastic and deeply inelastic regimes, Jefferson Lab Experiment Proposal E12-06-105 (2006).
- [134] J. Arrington, D. Day, D. W. Higinbotham, P. Solvignon, et al., Precision measurement of the isospin dependence in the 2N and 3N short range correlation region, Jefferson Lab Experiment Proposal E12-11-112 (2011).
- [135] J. van Leeuwe, W. Hesselink, E. Jans, W. Kasdorp, J. Laget, et al., The He-4(e,e'p) cross-section at high missing energies, Phys.Lett. B523 (2001) 6–12.
- [136] J. van Leeuwe, H. Blok, J. van den Brand, H. Bulten, G. Dodge, et al., The ⁴He (e,e'p) cross-section at large missing energy, Nucl.Phys. A631 (1998) 593–596.
- [137] M. M. Sargsian, T. V. Abrahamyan, M. I. Strikman, L. L. Frankfurt, Exclusive electro-disintegration of He-3 at high Q^2 . II: Decay function formalism, Phys. Rev. C71 (2005) 044615.

- [138] M. Sargsian, T. Abrahamyan, M. Strikman, L. Frankfurt, Exclusive electrodisintegration of He-3 at high Q^2 . I. Generalized eikonal approximation, Phys.Rev. C71 (2005) 044614.
- [139] F. Benmokhtar, et al., Measurement of the He-3(e,e'p)pn reaction at high missing energies and momenta, Phys. Rev. Lett. 94 (2005) 082305.
- [140] M. M. Rvachev, et al., The quasielastic He-3(e,e'p)d reaction at $Q^2 = 1.5$ - GeV^2 for recoil momenta up to 1- GeV/c , Phys. Rev. Lett. 94 (2005) 192302.
- [141] C. Ciofi degli Atti, L. P. Kaptari, Calculations of the exclusive processes $2\text{H}(e,e'p)n$, $3\text{He}(e,e'p)2\text{H}$, and $3\text{He}(e,e'p)(pn)$ within a generalized eikonal approximation, Phys. Rev. C71 (2005) 024005.
- [142] C. Ciofi degli Atti, L. P. Kaptari, On the interpretation of the processes He-3(e,e'p)H-2 and He-3(e,e'p)(p n) at high missing momenta, Phys. Rev. Lett. 95 (2005) 052502.
- [143] C. Ciofi delgi Atti, L. P. Kaptari, A non factorized calculation of the process $3\text{He}(e,e'p)2\text{H}$ at medium energies, Phys. Rev. Lett. 100 (2008) 122301.
- [144] M. Alvioli, C. Ciofi degli Atti, L. P. Kaptari, Calculation of the cross section and the transverse- longitudinal asymmetry of the process ${}^3\text{He}(e,e'p)pn$ at medium energies within the unfactorized generalized Glauber approach, Phys. Rev. C81 (2010) 021001.
- [145] D. Rohe, et al., Nuclear transparency from quasielastic $12\text{C}(e,e'p)$, Phys. Rev. C72 (2005) 054602.
- [146] C. Barbieri, D. Rohe, I. Sick, L. Lapikas, Effect of kinematics on final state interactions in (e,e'p) reactions, Phys. Lett. B608 (2005) 47–52.
- [147] D. Rohe, et al., Correlated Strength in Nuclear Spectral Function, Phys. Rev. Lett. 93 (2004) 182501.
- [148] O. Benhar, A. Fabrocini, S. Fantoni, The nucleon spectral function in nuclear matter, Nucl.Phys. A505 (1989) 267–299.
- [149] H. Muther, G. Knehr, A. Polls, Momentum distribution in nuclear matter and finite nuclei, Phys.Rev. C52 (1995) 2955–2968.
- [150] T. Hehl, Study of ($\gamma, N N$) reactions at MAMI, Prog. Part. Nucl. Phys. 34 (1995) 385–386.
- [151] L. J. H. M. Kester, et al., Short-Range Nucleon-Nucleon Correlations Investigated with the Reaction $\text{C-12}(e,e'pp)$, Phys. Rev. Lett. 74 (1995) 1712–1715.

- [152] K. I. Blomqvist, et al., Investigation of short-range nucleon nucleon correlations using the reaction C-12(e,e'pp) in close to 4π geometry, Phys. Lett. B421 (1998) 71–78.
- [153] C. J. G. Onderwater, et al., Signatures for Short-Range Correlations in O-16 Observed in the Reaction O-16 (e,e'pp) C-14, Phys. Rev. Lett. 81 (1998) 2213–2216.
- [154] D. L. Groep, et al., Investigation of the exclusive He-3(e,e'pp)n reaction, Phys. Rev. C63 (2001) 014005.
- [155] J. Rycebusch, M. Vanderhaeghen, L. Machenil, M. Waroquier, Effects of the final state interaction in (γ ,pn) and (γ ,pp) processes, Nucl. Phys. A568 (1994) 828–854.
- [156] J. Rycebusch, L. Machenil, M. Vanderhaeghen, V. Van der Sluys, M. Waroquier, Multinucleon mechanisms in (γ , N) and (γ , NN) reactions, Phys.Rev. C49 (1994) 2704–2715.
- [157] C. Giusti, F. D. Pacati, M. Schwamb, S. Boffi, Electromagnetic proton-neutron knockout off ^{16}O : new achievements in theory, Eur. Phys. J. A33 (2007) 29–38.
- [158] J. Rycebusch, M. Vanderhaeghen, K. Heyde, M. Waroquier, Short range correlations in (e,e'p) and (e,e'pp) reactions on complex nuclei, Phys. Lett. B350 (1995) 1–7.
- [159] J. Rycebusch, K. Heyde, D. Van Neck, M. Waroquier, Aspects of the final state interaction and long range correlations in quasielastic (e,e'p) and (e,e'n) reactions, Nucl. Phys. A503 (1989) 694–722.
- [160] L. L. Frankfurt, G. A. Miller, M. M. Sargsian, M. I. Strikman, QCD rescattering and high-energy two-body photodisintegration of the deuteron, Phys.Rev.Lett. 84 (2000) 3045–3048.
- [161] M. M. Sargsian, C. Granados, Hard Break-Up of Two-Nucleons from the He-3 Nucleus, Phys.Rev. C80 (2009) 014612.
- [162] I. Pomerantz, et al., Hard Photodisintegration of a Proton Pair, Phys. Lett. B684 (2010) 106–109.
- [163] J. L. Aclander, J. Alster, D. Barton, G. Bunce, A. Carroll, et al., The large momentum transfer reaction $^{12}\text{C}(p,2p+n)$ as a new method for measuring short range NN correlations in nuclei, Phys.Lett. B453 (1999) 211–216.
- [164] A. Tang, et al., np short-range correlations from (p,2p+n) measurements, Phys. Rev. Lett. 90 (2003) 042301.
- [165] E. Piassetzky, M. Sargsian, L. Frankfurt, M. Strikman, J. W. Watson, Evidence for the Strong Dominance of Proton-Neutron Correlations in Nuclei, Phys. Rev. Lett. 97 (2006) 162504.

- [166] I. Yaron, et al., Investigation of the high momentum component of nuclear wave function using hard quasielastic $A(p,2p)X$ reactions, *Phys. Rev. C* **66** (2002) 024601.
- [167] R. Shneor, et al., Investigation of Proton-Proton Short-Range Correlations via the $^{12}\text{C}(e,e'pp)$ Reaction, *Phys. Rev. Lett.* **99** (2007) 072501.
- [168] R. Subedi, et al., Probing Cold Dense Nuclear Matter, *Science* **320** (2008) 1476–1478.
- [169] J. Alcorn, et al., Basic Instrumentation for Hall A at Jefferson Lab, *Nucl. Instrum. Meth.* **A522** (2004) 294–346.
- [170] D. J. J. de Lange, et al., The optical properties of the BigBite spectrometer at NIKHEF, *Nucl. Instrum. Meth.* **A412** (1998) 254–264.
- [171] I. Mardor, Y. Mardor, E. Piassetzky, J. Alster, M. M. Sargsian, Effect of multiple scattering on the measurement of nuclear transparency, *Phys. Rev. C* **46** (1992) 761–767.
- [172] D. Higinbotham, E. Piassetzky, M. Strikman, Protons and neutrons cosy up in nuclei and neutron stars, *CERN Cour.* **49N1** (2009) 22–24.
- [173] R. Raj Subedi, Studying short-range correlations with the $^{12}\text{C}(e, e' p n)$ reaction. Ph.D. Thesis (Advisors: John Watson and Douglas Higinbotham).
- [174] G. Farrar, H. Liu, L. Frankfurt, M. Strikman, Study of Bound Nucleons by Quasi-Exclusive Scattering with Large Momentum Transfer, *Phys.Rev.Lett.* **62** (1989) 1095–1098.
- [175] P. Monaghan, Study of the $^{12}\text{C}(e,e'p)$ reaction in a correlations dominant regime with $Q^2 = 2.0$ (GeV/c) 2 and $x_B > 1$. Ph.D. Thesis.
- [176] M. Alvioli, C. Ciofi degli Atti, L. Kaptari, C. Mezzetti, H. Morita, et al., Universality of nucleon-nucleon short-range correlations: two-nucleon momentum distributions in few-body systems, *Phys.Rev.* **C85** (2012) 021001.
- [177] R. Roth, T. Neff, H. Hergert, H. Feldmeier, Nuclear Structure based on Correlated Realistic Nucleon- Nucleon Potentials, *Nucl. Phys.* **A745** (2004) 3–33.
- [178] J. M. Laget, Three-body exchange currents. 1. the He-3 (γ , 2p) n Reaction, *J. Phys.* **G14** (1988) 1445–1451.
- [179] G. Audit, et al., Study of three nucleon mechanisms in the photodisintegration of He-3, *Nucl. Phys.* **A614** (1997) 461–471.
- [180] J.-M. Laget, Role of correlations in the $(e,e'2p)$ n reaction, *Phys. Rev.* **C35** (1987) 832–835.

- [181] R. A. Niyazov, et al., Two nucleon momentum distributions measured in He-3(e,e'pp)n, Phys. Rev. Lett. 92 (2004) 052303.
- [182] H. Baghdasaryan, et al., Tensor Correlations Measured in 3He(e,e'pp)n, Phys. Rev. Lett. 105 (2010) 222501.
- [183] J. Golak, H. Kamada, H. Witala, W. Gloeckle, S. Ishikawa, Electron induced p d and p p n breakup of He-3 with full inclusion of final-state interactions, Phys.Rev. C51 (1995) 1638–1647.
- [184] D. Higinbotham, E. Piassetzky, S. Wood, Short-Distance Structure of Nuclei, J.Phys.Conf.Ser. 299 (2011) 012010.
- [185] S. Gilad, D. W. Higinbotham, E. Piassetzky, V. Sulkosky, J. Watson, et al., Studying short-range correlations in nuclei at the repulsive core limit via the triple coincidence (e,e'pn) reaction, Jefferson Lab Experiment Proposal E07-006 (2007).
- [186] W. Boeglin, M. K. Jones, et al., Deuteron electro-disintegration at very high missing momenta, Jefferson Lab Experiment Proposal E12-10-003 (2010).
- [187] L. Weinstein, E. Piassetzky, D. Higinbotham, J. Gomez, O. Hen, et al., Short Range Correlations and the EMC Effect, Phys.Rev.Lett. 106 (2011) 052301.
- [188] J. Arrington, A. Daniel, D. G. Gaskell, et al., Detailed studies of the nuclear dependence of F₂ in light nuclei, Jefferson Lab Experiment Proposal E12-10-008 (2010).
- [189] J. Arrington, Do ordinary nuclei contain exotic states of matter?, Heavy Ion Phys. 21 (2004) 295–300. [arXiv:hep-ph/0304213](https://arxiv.org/abs/hep-ph/0304213).